KOLLSMAN INSTRUMENT CORPORATION
CORPORATE TECHNOLOGY CENTER
80-08 45TH AVENUE
ELMHURST, NEW YORK 11373

BI-MONTHLY TECHNICAL REPORT
NO. KIC-RD-000162-2

STUDY OF LASER POINTING PROBLEMS

Report Period: 1 October 1964- 30 November 1964

NASA Contract No. NASW-929

Prepared for
NATIONAL AERONAUTICS AND SPACE ADMINISTRATION
Washington, D.C. 20546

Prepared By:

Aaron Wallace
Project Director

Approved:

Dr. Nathan Kaplan
Director of Center

ABSTRACT

16811

The remarkable potential of deep space laser communications based on low power transmitters in deep space vehicles, extremely narrow beamwidths (0.01-1.0 arc seconds), and very wide-band frequency channels can be fully exploited only when the laser beam pointing problem is solved. Of particular interest is the mission of communication from a deep space vehicle directly to Earth.

This second Bi-Monthly Technical Report describes the progress made in the major technical areas of systems analysis and synthesis, establishment of reference axes, and techniques for measuring and positioning the laser beam. The presence of the Earth's atmosphere in the communication link with its random turbulence phenomena profoundly affects the system design, and introduces additional requirements for system synthesis beyond those associated with the extraordinary optical precision due to the narrow beamwidths and the dynamics of closed loop operation with transit time effects and target-observer motions.

During this period, attention has been concentrated on the "In Vacuo" case space vehicle and Earth station system configurations, closed loop system analysis, the dynamics of vehicle trajectories and lead angle computations for observer and target motion compensation and the preliminary aspects of laser beam spreading due to atmospheric differential refraction. These activities correspond to the major technical areas noted above.

The report also includes manpower utilization data and concludes with a bibliography of cited references for the main text, mathematical appendices, and a bibliography for the appendices.

Author

FOREWORD

This Bi-Monthly Technical Report, entitled "Study of Laser Pointing Problems", was prepared in accordance with NASA Contract No. NSAW-929, Article IV B. This second technical report covers the period 1 October-30 November 1964. The work is carried out under the direction of Mr. R. F. Bohling, NASA Headquarters, and Mr. F. R. Morrell, NASA, Langley Research Center. The studies described herein were performed by Aaron Wallace, Project Director, George Strauss, Dr. Sebastian Monaco, George Schuster, Suzanne Winsberg, John Meader and Judah Eichenthal of the Corporate Technology Center, Systems and Space Division staffs of the Kollsman Instrument Corporation.

TABLE OF CONTENTS

Section		Page
I	INTRODUCTION	1
	A. Review of Previous Activities	2
	B. Summary of Progress	3
II	SYSTEMS ANALYSIS	5
	A. Beam Pointing System Block Diagrams	5
	B. Search and Acquisition Process	10
	C. Space Vehicle Tracker Performance	17
	D. Accuracy Requirements for Reference Axes	20
III	REFERENCE AXES	23
	A. Celestial Data	23
	B. Celestial Sensors	29
	C. Atmospheric Beam Spreading Analysis	39
	D. Static Homogeneous Beam Propagation	45
	E. Reference Axes Systems	51
IV	BEAM MEASURING AND POSITIONING	52
	A. Lead Angles and Angular Rates	53
	B. Closed Loop Feedback Analysis	56
	C. Pulsed Signal Gating Noise Reduction	60
	D. Measuring and Positioning Techniques	62
	E. Boresight Maintenance	64
V	CONCLUSIONS	65
VI	PROJECT ACTIVITIES FOR NEXT PERIOD	66
VII	CONFERENCES	66
VIII	MANPOWER UTILIZATION	66
	A. October-November	
	B. December-January	
IX	BIBLIOGRAPHY	67
	APPENDICES	
	A. Trajectories for Mars Fly-By Mission	A-1
	B. Transit Time Corrections	B-1
	C. Transit Time and Aberration Corrections	C-1
	D. Lead Angle, Azimuth and Elevation Rates	D-1
	E. Bibliography for Appendices	E-1

LIST OF ILLUSTRATIONS

Figure		Page
1	Laser Beam Pointing System Block Diagram	6
2	Detailed Laser Beam Pointing System Block Diagram	8
3	Possible Earth Beacon Search Beams	12
4	November, 1964 Mariner/Mars Mission	21
5	Reference Axes' Coordinate System Analysis	22
6	Self-contained Space Vehicle Optical Navigation Techniques	24
7	Summary of Pertinent Characteristics of Stellar Data	26
8	Summary of Pertinent Characteristics of Planetary Data	27
9	Elements of the Orbit	28
10	Reference Coordinate Systems	31
11	Functional Areas of Automatic Celestial Tracker	32
12	Power Density and Visual Magnitude for Celestial Bodies	34
13	Available Power versus Magnitude and Diameter	34
14	Closed Loop Star Tracker "In Vivo"	35
15	High Performance Photomultiplier System S/N with Night Sky Background	35
16	Transfer Characteristic of the Z-Control Axis	37
17	Transfer Characteristic of the Y-Control Axis	37
18	Sensor S/N Ratio vs. Photon Arrival Rate	37
19	Intensity Distribution of a Multi-Mode CW Laser	40
20	Strength of Turbulence Based on Experimental Data	41
21	Turbulon Resulting from Rising Warm Air	43
22	Turbulon Resulting from Cool Descending Air	43
23	N Units versus Elevation for Homogeneous Model	42
24	Homogeneous Model Geometry	46
25	Homogeneous Model Refraction	48
26	Three Homogeneous Layer Refraction	50
27	Earth-Mars Fly-By Mission	54
28	Simplified Servo Model of Closed Loop Tracking	57
29	Phase Shift as a Function of Space Probe Range for Transmitter Lead Angle Servo	59
30	Sampled Data Servo for Electronically Deflected Light Detector	61
31	Synchronization Loop	61

LIST OF TABLES

Table		Page
I	Reference Coordinate Systems	29
II	Homogeneous Model Beam Convergence	47
III	Three Homogeneous Layer Beam Convergence	49
A-I	Trajectory Data	A-13

APPENDICES

TABLE OF CONTENTS

Appendix		Page
A.	TRAJECTORIES FOR MARS FLY-BY MISSION	A-1
	I. Introduction	A-1
	II. Trajectory Parameters	A-1
	III. Vehicle Position Vector in Heliocentric Ecliptic Mean of Launch Date Coordinates	A-6
	IV. Relative Position of Vehicle to Earth	A-8
	V. Relative Velocity of Vehicle and Earth	A-9
B.	TRANSIT TIME CORRECTIONS	B-1
	I. Introduction	B-1
	II. Earth-to-Vehicle to Transmitter	B-1
	III. Vehicle-to-Earth Transmitter	B-5
C.	TRANSIT TIME AND ABBERATION CORRECTIONS	C-1
	I. Introduction	C-1
	II. Relativistic Correction	C-1
	III. Transit Time Correction	C-2
	IV. Total Correction	C-4
D.	LEAD ANGLE, AZIMUTH AND ELEVATION RATES	D-1
	I. Introduction	D-1
	II. Rate of Change of the Lead Angle	D-1
	III. Rate of Change of the Azimuth and Elevation Angles of the Transmitter	D-3
E.	BIBLIOGRAPHY FOR APPENDICES	

APPENDICES

LIST OF ILLUSTRATIONS

Figure		Page
A-1	Heliocentric Ecliptic Coordinates	A-4
A-2	Plane of Transfer Ellipse	A-4
A-3	Transfer Ellipse $\psi < \pi$	A-5
A-4	Transfer Ellipse $\pi < \psi < 2\pi$	A-5
A-5	Ecliptic Geocentric Equatorial Coordinates	A-10
A-6	Ecliptic and Vehicle Coordinates	A-10
B-1	Azimuth and Altitude Angles of Earth to Vehicle Transmitter	B-2
B-2	Orientation of Vehicle to Earth Transmitter	B-6
C-1a	Relativistic Diagram	C-3
C-1b	Non-Relativistic Diagram	C-3
C-2	Azimuth and Elevation Angles of Earth Station Vehicle Receiver and Transmitter	C-5

I. INTRODUCTION

The United States Aerospace investigation and exploration programs under the direction of NASA include families of lunar and near interplanetary missions, far interplanetary and interstellar probes, observatory satellites, and numerous scientific satellites, Ref. (1). From a scientific point of view, the amount of information and data to be generated in the course of these missions is expected to be enormous, as well as of the highest importance for this nation's continued progress in science and space exploration.

It is evident that the successful implementation of these programs will depend upon progress in the propulsion and communication fields. Although a considerable number of advances have already taken place in these areas, it is clear that new communications channels must be developed since the present-day booster-rocket and microwave communications technologies are already approaching ideal performance limitations, Ref. (1), Section II. Optical communications based on the current rapidly expanding laser technology may provide the necessary breakthrough because of the unprecedented space and frequency bandwidths made available as a result of the laser's spatial and temporal coherence, Ref. (1), Sections II, III.

However, the remarkable potential of deep space laser communications based on low power transmitters, extremely narrow beamwidths, and very wideband frequency channels involving high data transmission rates cannot be fully exploited unless the laser beam pointing problem is solved.

Kollsman experience and research activities in the systems synthesis, system analysis, control, and computer fields have led to the conclusion that a systems approach to the Laser Beam Pointing Problem is required in addition to the application of specific technical knowledge to the detailed solution of its component aspects. This systems approach was described in Ref. (1), and the detailed program activities to implement this approach were outlined. Application of systems theory to this problem leads to the major conclusion that the presence of the Earth's atmosphere in the communication link with its random turbulence phenomena profoundly affects the system design. As a result, additional requirements for system synthesis are introduced beyond those associated with the extraordinary optical precision due to the narrow beamwidths and the dynamics of closed-loop operation with transit time effects and target observer motion.

A. REVIEW OF PREVIOUS ACTIVITIES

The present report summarizes the activities of the second bi-monthly period, October-November, whereas the first Bi-Monthly Technical Report, Ref. (1), describes the previous period's investigations. A summary of progress to date is given in the next section, and the previous activities may be briefly described as follows.

A comparison was made of the performance capabilities of deep space radio communications and deep space laser communications "In Vacuo" (without atmosphere). This analysis demonstrated the potential value of laser communications, and established order of magnitude values for some of the major system parameters, Ref. (1), Section IIA, IIB, then a tabulation was made of all the major system variables, errors, and uncertainties, which demonstrated that a simple open cycle system based on conventional astronomical procedures and techniques would encounter insuperable obstacles "In Vivo" (with atmosphere), Ref. (1), Sections IIC, IID. As a result of the analysis of system problems previously set forth, it was concluded that a hybrid open-and-closed loop system utilizing coarse and fine techniques was the most flexible system for the purposes of laser beam pointing, Ref. (1), Section IIE. Analysis of the "In Vivo" conditions (including atmospheric turbulence) in Section III produced the conclusion that a "distributed" type of receiving system at the Earth Station would probably be required to satisfy the constraints imposed by the atmosphere in terms of extraneous radiation interference, angle of arrival fluctuations, and phase coherence degradation, Ref. (1), Section IIF. A preliminary beam pointing acquisition and track sequence was then evolved to implement the hybrid system operation, including the utilization of DSIF data for preliminary open cycle coarse search and acquisition, Ref. (1), Section IIG.

As previously noted, an extensive preliminary analysis was given of the effects of the atmosphere on laser beam propagation, Ref. (1), Sections IIIA-F. In addition, preliminary data was presented on the principles of optical beam deviation for fine beam measuring and positioning, Sections IV A, B, and a detailed discussion of boresight maintenance techniques employed in various Kollsman celestial tracking systems was provided in Section VA. The implications of the hybrid system closed loop tracking on the boresight maintenance subsystem analysis was briefly noted in Section VB.

The subsystem studies on atmospheric propagation, fine beam deflection, and boresight maintenance confirmed the choice of a hybrid system as providing the greatest possibilities for the use of feedback techniques to eliminate or dilute the requirements for extreme precision or accuracy in the subsystems and components.

B. SUMMARY OF PROGRESS

Significant progress has been made in the major technical areas of systems analysis. Reference Axes, Measuring and Positioning Techniques, and Boresight Maintenance, of Ref. (3), Section IA. As a result of the closed loop systems analysis, it has been found possible to relax the accuracy requirements in the Reference Axis needed in addition to the line of sight from the space vehicles to Earth. The analysis also shows that the fine beam deflection system needed for lead angle correction and the boresight maintenance system can be enclosed within the tracking loop, thereby suggesting the possibility of reducing accuracy requirements in these subsystems.

Generalized block diagrams have been evolved to describe the complete Laser Beam Pointing System, both in the space vehicle and the Earth Station for "In Vivo" case (including atmosphere), Section IIA. Provision for utilizing the DSIF network is included, and also, a monitoring system for the Earth Station based on a high flying aircraft to determine the local state of the atmosphere for prediction purposes. Section IIB describes several possible search-acquisition modes based on the use of a one megawatt pulsed laser source for the Earth Station beacon. The use of a pulsed laser bypasses the low power limitation of cw lasers and the practical difficulties of a space borne coherent receiver (due to state-of-the-art limitations). This technique provides adequate signal-to-noise ratios at the space vehicle, further described in Section IIC, wherein by comparison with celestial sensors, it is shown that "In Vacuo" tracking accuracies of 0.001 arc second are feasible. A mathematical analysis of Reference Axes' accuracy requirements is presented in Section IID. It is shown that a two arc second celestial tracker can provide sufficient accuracy for a 0.01 arc second beamwidth system, and lower accuracies are needed for the wider beamwidths (0.1-1.0 arc second).

A survey of celestial data characteristics and some performance attributes for present-day celestial sensors are presented in Sections IIA and IIIB respectively. These sections support the conclusion that present-day celestial data and sensors are adequate for the purposes of laser beam pointing control, and further, that very high closed loop tracking accuracies can be achieved provided that adequate signal-to-noise ratios are available. The analysis of laser beam propagation through the atmosphere in the direction from space to Earth is resumed in Sections IIIC and IIID for static homogeneous single layer and multilayer models. It is shown that for these models, atmospheric effects are negligible, and therefore, turbulence represents the major source of system uncertainty and inaccuracy. Section IIIE

discusses the various types of Reference Axis systems based on other geometrical and analytical techniques, such as gyros, velocity matching, etc., which now become meaningful since the highest order of accuracy is not required.

In order to provide concrete numerical error analysis of system performance, a particular mission has been selected, namely, a Mars Fly-By, similar to the present Mariner/Mars mission. A mathematical analysis of the trajectories has been carried out, and the mathematical details of the lead prediction problem have been determined. These analyses are given in Appendices A-D. Numerical calculations for selected points during the mission are presented in Section IVA which show that the maximum lead angle is of the order of 40 arc seconds, and the associated angular rates are extremely low, of the order of 10^{-5} arc second/second. This data may be compared with the preliminary feedback analysis of the closed loop tracking system presented in Section IVB, and it is concluded that these rates are well below the limitations on the system velocity constant imposed by the transit time transport laps. The use of pulsed time gating techniques to reduce the effects of system internal and external noise in the space vehicle receiver-tracker subsystem is described in Section IVC, taking advantage of the pulsed signal from the Earth Station beacon.

The overall characteristics of the laser beam pointing control system are summarized in Section IVD, and it is shown that for "In Vivo" operation, a distributed type of receiving system is needed for the Earth Station. A preliminary description of a ten by ten array of coherent receivers is given, and the advantages of both spatial and temporal averaging are described in terms of a potential reduction of angle of arrival fluctuations from 1.75 arc seconds r.m.s. to 0.0175 arc second r.m.s. The use of this same array in a pair of three-sensor interferometers to provide error signals to the space vehicle is also described. This loop closure can provide the correction for inaccuracies in the space vehicle laser beam pointing subsystem, thereby diluting the requirement for extremely high precision in the fine beam deflection. The implications of the foregoing for the boresight maintenance system are described in Section IVE, as well as the use of look-through techniques in the space vehicle to correct for slow boresight variations in the cw laser optical system.

Manpower utilization data is given in Section VIII, and a bibliography of cited references may be found in Section IX.

II. SYSTEMS ANALYSIS*

The most flexible Laser Beam Pointing System for "In Vivo" operation is the hybrid (combination open-and-closed loop) system based on the joint use of Reference Axes' data derived from the DSIF and a celestial sensor which provides coarse pointing and initial acquisition information, followed by a cooperative system using successively narrowed fine beam acquisition and tracking modes. In such a system, maximum use of lumped and distributed configurations, coding, correlation and prediction procedures can be employed to optimize data transmission capacities, beam pointing control procedures, propagation conditions, etc.

This section will describe the activities in systems analysis and synthesis, including the development of generalized system block diagrams, a detailed description of the Search and Acquisition process based on the use of DSIF data and a pulsed laser Earth station beacon, and the beam pointing signal-to-noise ratios which can be achieved during the acquisition and track modes. Detailed discussions of the major problem areas of Reference Axes and Beam Measuring and Positioning are given in Sections III and IV.

Inasmuch as the analysis of laser beam atmospheric propagation is still in process, most of the considerations presented in this section apply to the "In Vacuo" case, but the information is capable of being generalized to the "In Vivo" environment, cf. 1 (II E, F).**

A. BEAM POINTING SYSTEM BLOCK DIAGRAMS***

Based on the descriptions of system factors and variables in 1 (II C,D), the arguments leading to the choice of a hybrid open-and-closed cycle system configuration for the Laser Beam Pointing System were presented in 1 (IIE). The similarities and differences between "In Vacuo" and "In Vivo" operation were described in 1 (IIF), leading to the consideration of both "lumped" and "distributed" systems. Thereafter, in 1 (IIG), an operational acquisition and track sequence was presented which precisely covers the "In Vacuo" case, and with modification is suitable for the more realistic "In Vivo" operation. The block diagrams presented in this section are based on the system and operational block diagrams previously given in 1 (Fig. 3) and 1 (Fig. 7) respectively.

The total hybrid open-and-closed cycle system block diagram is shown in Figure 1. Because the "In Vivo" operation is not symmetrical in both directions of propagation as described in 1 (IIF), the

---

* Based on notes prepared by A. Wallace except as noted.
**For convenience, the abbreviation 1(IIE,F) is used to denote Ref., (1), Sects IIE, IIF.
***Based on notes prepared by A. Wallace.

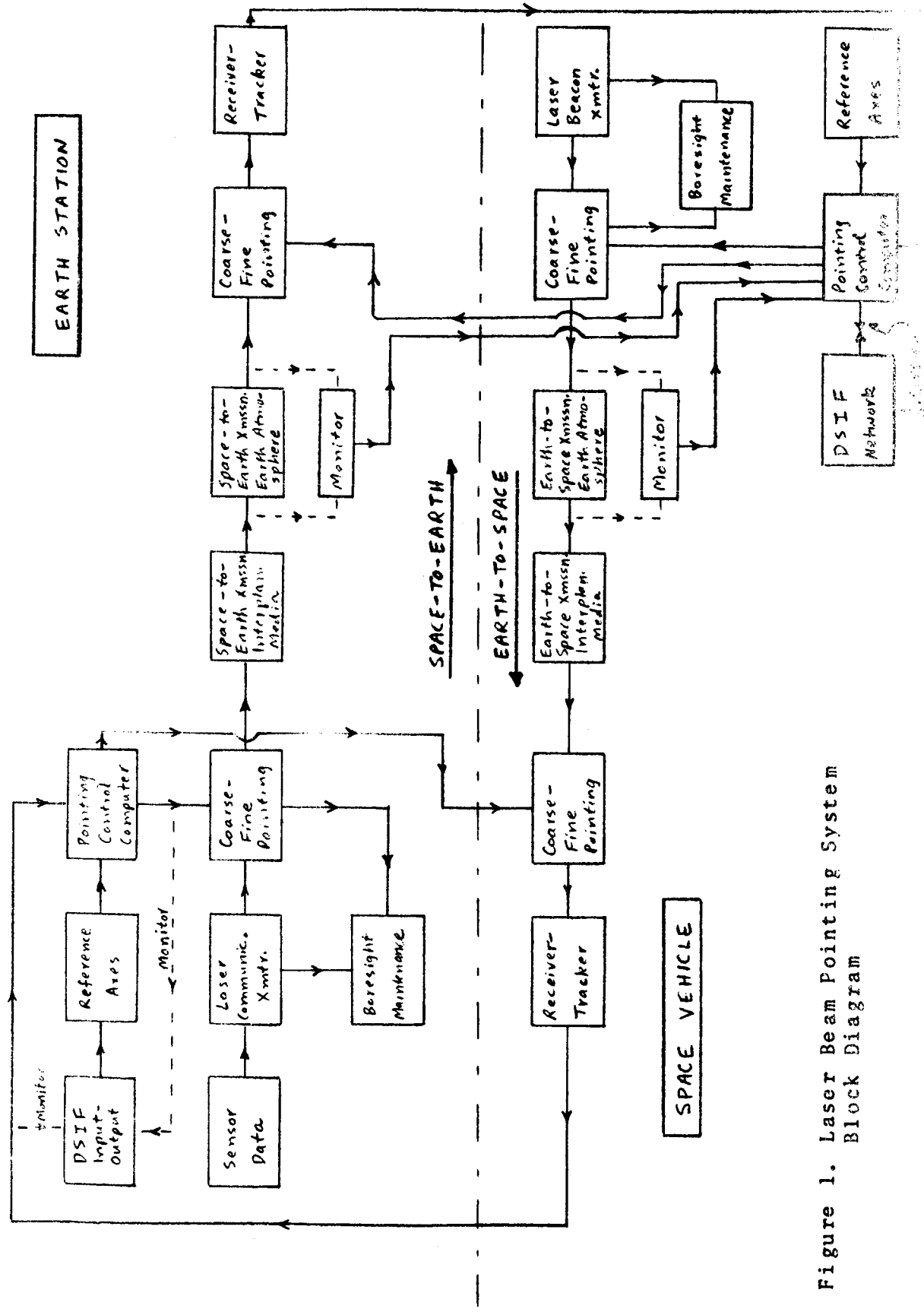

Figure 1. Laser Beam Pointing System Block Diagram

upper part of the block diagram (above the dashed line) shows a separate block for the Space-to-Earth atmospheric transmission (and similarly for the Interplanetary Media). The Earth-to-Space direction of propagation is similarly treated in the lower part of the block diagram. Although the resultant diagram shows a functional symmetry, this is superficial because the effects of atmospheric turbulence and extraneous noise sources have marked influences on the design of the space vehicle and Earth systems, cf.I(IIF). Also, the acquisition and track sequence for both ends of the communications and pointing link is not symmetrical as described in I (IIG).

For example, the space vehicle transmitter will be a low-power modulated cw laser whereas the Earth Station transmitter will probably be a high-power pulsed laser. The space vehicle tracker will be a lumped system using either a parabolic telescope or a phased array, but the Earth Station will probably require a distributed system configuration. Similarly, there will be major differences in the Reference Axes, Boresight Maintenance, etc.

The operation of the system is described by the acquisition and track sequence of 1 (Fig. 7). Together, the two figures provide a first order description, that is, the two figures are complementary in accordance with the precepts of general systems theory, Ref. (2). The block diagram of Fig. (1) is generalized in the sense that it describes all of the classes of systems discussed in 1 (II E, F), that is, "In Vacuo" and "In Vivo", "lumped"and "distributed." In addition, provision is included for DSIF monitoring of the space vehicle and Earth Station detailed performance in accordance with the procedures followed for the Mariner Space vehicles, Ref. (3). Also, provision is made for partially (statistically) closing a loop around the Earth's atmosphere for each direction of propagation by separate monitors. At the time of deep space laser transmission, a high altitude aircraft station-keeping about 40,000 feet above the Earth station can set up a local laser atmospheric measuring system to provide the "pointing control computer" with detailed information on atmospheric propagation for fine pointing control.

A more detailed second order generalized block diagram of the hybrid Laser Beam Pointing System is shown in Figure 2. Comparison with Figure 1 will delineate the main features of the system. Its operation is described by the acquisition and track sequence depicted in 1 (Fig. 7).

It will be noted that the "Pointing Control Computer" has been divided into "Coarse" and "Fine" Sub-computers. This is consistent with the various modes of coarse and fine operation, since both open and closed loop logics are involved which must be worked out separately. Similarly, the actual "pointing" and "optics" are divided into "Coarse" and "Fine" to allow for different modes and

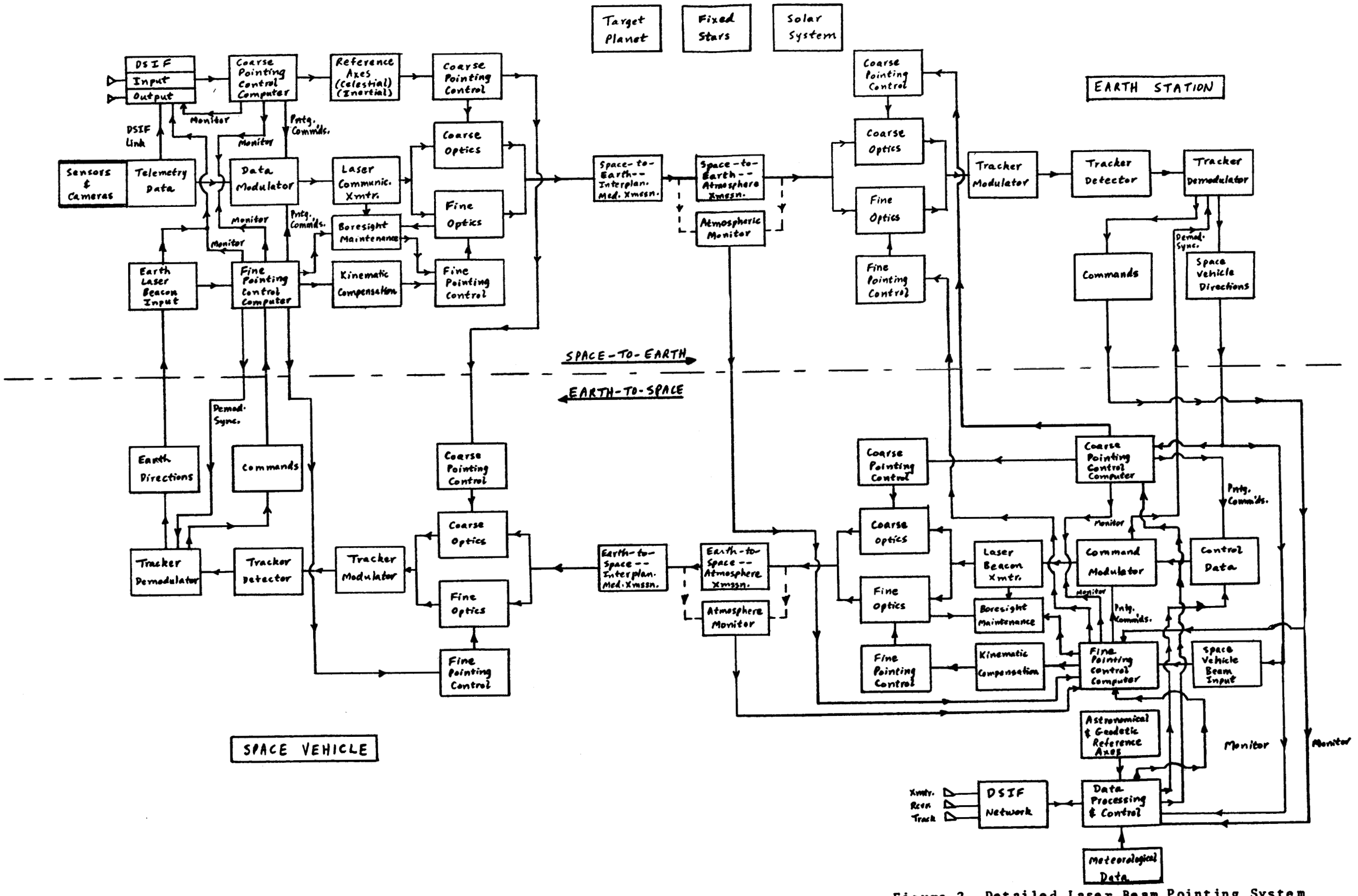

Figure 2. Detailed Laser Beam Pointing System Block Diagram

different hardware implementation. It is assumed that this situation holds both for the space vehicle and the Earth Station, and will cover the spectrum of beamwidths from 0.01 arc second to 1.0 arc second. However, for the wider beamwidths, around 1.0 arc second, some simplification by combination of function will be achievable, that is, tracker coarse-fine pointing, use of single dish for both transmitting and receiving functions in the space vehicle, time-sharing of data-takeoffs, etc.

The space vehicle configuration will be much simpler than that of the Earth Station. By taking advantage of the vehicle's stabilization (sun sensor and canopus tracker), the DSIF command and control, and the inherent advantages of the closed loop configuration used for beam pointing control, the Reference Axes "upstairs" are derived from the Earth Station "downstairs" and "one" directional reference. As described in Section IID later in this report, this reference can be a one or two second accuracy Canopus tracker or Sun Sensor. Other possibilities exist. Because of atmospheric phenomena, the Earth Station configuration will be more complex.

Some of the blocks in Figure 2 are not properly part of the laser beam pointing system, but are shown because they are involved in the total mission, including DSIF control, the laser modulation and data transmission, data processing, etc. Further details concerning possible implementations of the generalized block diagrams of Figures 1 and 2 are given later in this report.

The full impact of the "In Vivo" atmospheric effects on beam pointing accuracy has yet to be evaluated. Preliminary analysis of the laser beam pointing signal-to-noise ratios and the kinematics of lead angle computation for the "In Vacuo" case indicates that the hybrid system can yield laser beam pointing control for the beamwidth spectrum from 0.01 - 1.0 arc second. On the other hand, if the statistics of atmospheric turbulence generate irreducible uncertainties in angle of arrival and received beamwidths of the order of one arc second or greater, the question of the utility of beamwidths smaller than 0.1 arc second becomes a subject for trade-off analysis.

B. SEARCH AND ACQUISITION PROCESS*

Until the start of laser communication, the DSIF constitutes the sole link between Earth Station and space vehicle. The search-acquisition will probably be initially made at a range of some 50 x 10^6 kilometers. It may require periodic repetition since the Earth's rotation requires hand-over of the tracking function from one Earth Station to another. Such re-acquisitions will proceed on the basis of much more precise information than the initial one, and, therefore need not be too time-consuming. There is, however, the possibility of track break at any time, as the result of impact of small space objects strong enough to push the tracking loop beyond its control range, but not strong enough to cause permanent damage, or to interrupt microwave communications. Such track break could occur during the terminal phase of the mission, and new acquisition should not require so much time as to lead to serious loss of real-time information transmission. Acquisition time from any part of the mission must therefore be minimized. This forms the prime criterion for its implementation, and the availability of sufficient laser power at the Earth beacon (within reason) will be assumed.

Tracking information from the microwave system at the Earth Station is quite accurate. A tracking antenna with a 210 foot diameter and 61 db of gain is presently under construction, Ref. (4), and it is expected to furnish space vehicle angle information with error not exceeding 0.02 degree. Actually, the 85-foot,53-db antenna presently in use tracks strong signals with angular errors between 0.01 and 0.02 degree, and signals near threshold with 0.05 degree error. For present purposes, the angular uncertainty at Earth Station with respect to the space vehicle will be taken as 1 minute in each azimuth and elevation. Initial information aboard the space vehicle will be somewhat cruder, angular uncertainty being on the order of 0.50 degree in each direction, and is derived as follows:

Ref. (4) gives the diameter of the spacecraft antenna presently used as four feet, and the gain as 20 db (at L-band). Using the gain as criterion, beamwidth θ is given by

$$\theta_s = (4\pi/G_s)^{1/2} = (4\pi/100)^{1/2} = 0.35 \text{ Radians} = 20^\circ$$

The ground-based station's beamwidth is, by comparison:

$$\theta_g = (4\pi/G_g)^{1/2} = (4\pi/19{,}300)^{1/2} = 0.018 \text{ Radians} = 1^\circ$$

permitting tracking accuracy of 0.02 degree; the lobing technique used thus splits the beam by a factor of 50. Applying the same factor to the space-vehicle antenna yields tracking error of 0.4 degree. The assumed number of 0.5 degree should be readily

achievable, since the space vehicle's angle tracking system has the benefit of the greater transmitter power available from Earth.

The projected S-band system, with the 210-foot ground-based and 10-foot vehicle-borne antenna should yield further improvement.

The space vehicle receiver must therefore search through a somewhat larger volume. While it is possible to break up the scanning process into an Earth-acquisition and a beacon-acquisition phase (the vehicle based laser tracker being used as Earth-acquiring star-tracker during the first phase), and then scanning the angle subtended by Earth for the beacon, it does not readily become apparent what advantage in time and simplicity would be gained by so doing.

In this connection, it may also be noted that the high angular accuracy implied by a 1-second (or less) beam transmission from space does not necessarily apply to the Earth beacon's transmission. This beam could be wider and directed with less precision the major requirement being illumination at the space vehicle. The wider beam would, of course, lead to dilution of power which would have to be made up in order to yield adequate signal at the vehicle.

1. Scanning Approach

Earth Station must locate the space vehicle within a solid angle of 2-by-2 minutes with less than 1-second error in angle. One possible method of search consists of causing a beacon laser beam of about 2-by-2 seconds to scan through the search volume at such speed as to allow the space vehicle receiver to scan its own search volume, 60-by-60 minutes at each element of the beacon scan, Figure 3(a). The vehicle's scan speed is, in an electronically scanned device, limited by signal strength only. By definition, it is assumed that sufficient beacon power can be made available for adequate scan speed. The space vehicle's raster must be scanned through at each of the Earth Station's 3600 beam positions, each of which is identified by a characteristic binary code. This code would, in the case of the 3,600-element raster, require 12 bits. The number of decision elements required for each angular element of the space vehicle's search raster thus depends on the number of angular elements in the Earth Station's raster. The total number of angular elements that may have to be searched is (nm), where n is the number of Earth Station beam positions, and m the number of elements in the space vehicle's search raster.

Assume (for the sake of simplicity)that the values for n which may be chosen increase in binary steps, $n = 2^q$, and the total number of decision elements in the search process is (mnq). If the number of angular elements in the Earth Station's raster is halved ($q' = q-1$, $n' = n/2$), and the power density

Fig. 3(a) Narrow Beam Raster Scan

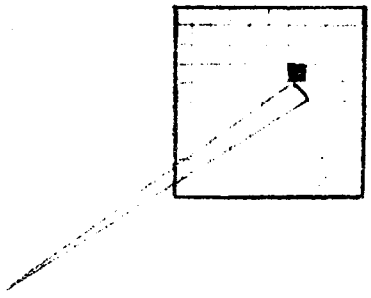

Fig. 3(b) Lobed Wide Beams

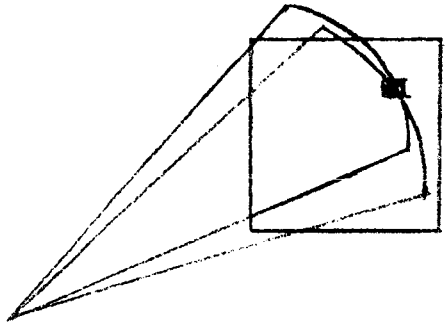

Fig. 3(c) Single Wide Beam

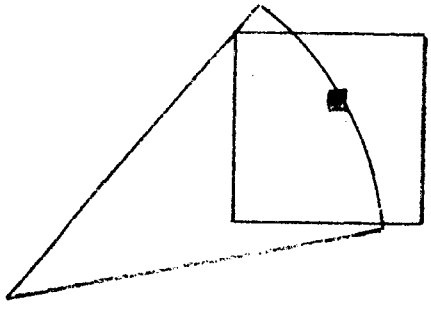

Figure 3. Possible Earth Beacon Search Beams

in the beam incident upon the space vehicle is also halved, requiring T' = 2T (that is, for equal signal-to-noise ratio, twice as much time must be spent on each decision element) then the number of decision elements is m x n' x q' = m x n x (q-1)/2, and the total search time has been reduced by (q-1)/q. This argument would seem to favor breaking the search process up into two or more steps, starting with coarse angles and successively refining them. Actually, however, this would increase the number of required confirmation intervals, each of which may be as long as eight minutes, if re-acquisition at ranges in the order of one AU becomes necessary. This would more than outweigh the slight reduction in frame time, aside from the fact that one or more fine search frames would have to be added. From the point of view of overall efficiency, break-up into coarse and fine search processes probably does not result in much gain.

Once the space vehicle's receiver scan finds the Earth beacon's beam, the characteristic code is sent back. This probably would have to be done via the microwave link, since the Earth Station's light receiver is generally not looking the right way. The Earth Station will then direct its transmitter at the angle element identified by the code retransmitted from the space vehicle and the light receiver at an angle related to the transmitter angle by the computed lead, where it should pick up the space vehicle's laser beam. It is assumed in all the foregoing that the entire search volume is not stationary, but follows the antenna motion of the microwave system, both at the Earth Station and in the space vehicle.

A rough calculation of available signal power indicates that gas-type lasers, capable of providing modulated c-w emission, would be inadequate for the purpose. At a space vehicle range of 0.5 AU, a one-watt Earth Station light transmitter, radiating into a one-second beam will provide a signal strength of, cf. 1(IIB):

$$S_R = \frac{P_T}{\Omega R^2} = \frac{P_T}{\theta^2 R^2} = \frac{1\ W}{(4.85 \times 10\text{-}6)^2 \times (75 \times 10^{11} cm)^2}$$

$$= 7.6 \times 10^{-16}\ \text{Watts-cm}^{-2}$$

This power density is comparable to that from a 6.5 magnitude star, and is judged quite inadequate, particularly in light of the fact that it must be detected against the bright background of sunlight reflected from the Earth. Assuming 58 ergs/(cm^{2}sec.Å), Ref. (5), solar flux outside the Earth's atmosphere, and the space vehicle's light receiver, protected by a filter of one Å bandwidth looking toward a fully illuminated Earth, the incident power density

will be

$$\frac{1\text{Å} \times 58 \text{ ergs} \times 1.27 \times 10^{18} \text{ cm}^2 \times 0.34 \times 10^{-7} \text{ Watt-sec}}{\text{Å} \times \text{cm}^2 \times \text{sec} \times \text{erg} \times 4\pi (75 \times 10^{11} \text{cm})^2}$$

where 1.27×10^{18} is the Earth's area, 0.34 the Earth's albedo, and 75×10^{11} cm the space vehicle range (as before). This amounts to 3.1×10^{-15} watt-cm^{-2}. Even with the Earth's illuminated side partly turned away from the vehicle, the reflected sunlight would be at least comparable to illumination due to the laser beacon.

In order to secure significantly higher beacon power, a pulsed ruby laser may be used, from which powers on the order of one megawatt (peak pulse) can readily be obtained. Such lasers can, however, be presently pulsed at rates only up to about 50 pps. A 12-bit code word would thus require on the order of 0.25 seconds, leading to a totally unacceptable acquisition interval. Even if the space-vehicle's search field of 1.0 by 1.0 degree were broken up into elements of 1.0 by 1.0 minute, a single receiver field would require on the order of 900 seconds. For this reason, an acquisition process based on element-by-element scan appears to be impractial.

2. Lobing Approach

Should the Earth Station transmit at a peak-power level of one megawatt (typically, pulses of 25 nanoseconds width at repetition rates in the range 10 pps to 50 pps) into a beam of one-minute width, the resulting power density at a space vehicle range of 0.5 AU will be

$$S_R = \frac{10^6 \text{ Watts}}{(0.291 \times 10^{-3})^2 \times (75 \times 10^{11} \text{cm})^2} = 2.1 \times 10^{-13} \text{ Watts-cm}^{-2}$$

which compares favorably with the incident illumination from the one-watt laser, despite the greater beamwidth used here. The transmitter beam may be lobed back and forth to either side of the space vehicle's assumed position, Figure 3(b), so that the space vehicle is certain to be illuminated. Each lobe carries a characteristic signature, enabling the space vehicle's light receiver to measure the signal strength received from the two lobes. This information can be transmitted back to Earth, permitting calculation of the actual target angle (assuming well-prescribed beam shape). The process can be performed sequentially for the azimuth and elevation directions. Once angular information is refined on the basis of the relative signal strength due to the two coarse lobes, a finer beam with greater concentration of power can be directed to the space vehicle, permitting more

accurate acquisition and tracking. Lead angle computation for both Earth Station and space vehicle can be performed at the Earth Station. Commands for space vehicle lead can be radioed to the vehicle via the DSIF link.

As an alternative to this angle refinement procedure which depends upon accurate knowledge of the beam shape, the space vehicle can, upon detection and recognition, transmit its own laser beam (based upon the lead-angle command received from the Earth Station. The Earth Station's light receiver can then use conventional beam-splitting techniques to refine the angular measurement, Figure 3(c).

3. Possible Acquisition and Track Sequence

A preliminary description of the hybrid system loop closure process was previously given in 1(IIG), cf. 1(Fig. 7). In partial accordance with the foregoing, the following sequence is proposed as the approach taking best advantage of available time and signal, assuming that Reference Axes have previously been established in the space vehicle.

(a) Earth Station transmits a two-by-two minute, pulsed, one-mw beam, covering the angular uncertainty, thus insuring illumination at the space vehicle, Figure 3(c).

(b) Space vehicle light receiver scans its total field of view (±30 minutes with respect to DSIF antenna axis in both directions), with an instantaneous field of view on the order of one-to-two minutes. The dwell time at each element need not be longer than one PRF interval of the Earth beacon's transmission. Because of the pulse-coded transmission, the threshold may be set so low as to exclude (for practical purposes) the probability of missing the signal if it is there (detection probability almost unity). Logic must be incorporated to increase the dwell time for purposes of code test if a pulse is received. The code test typically consists of counting the number of pulses in a given interval. If the result of the code test is negative, raster scan resumes; if positive, angular information can be refined by use of beam-splitting techniques, resulting in angular error on the order of ±2seconds.

(c) Using the lead-angle command transmitted from the Earth Station, the vehicle transmits a

two-second beam referenced to the coarse line of sight established in (b).

(d) Earth Station receives two-second beam and refines angular information to 0.1 second.

(e) Earth Station transmits a one-second beam to angle established under (d), using appropriate lead correction.

(f) Space vehicle receives fine beam and improves angular tracking accuracy to 0.1 second.

(g) Space vehicle transmits one-second beam, referenced to angle established under (f), with appropriate lead angle.

Further steps of similar type would be used to generate 0.1 and 0.01 arc-second beamwidth closures. Information concerning the generation of Reference Axes and angular tracking techniques is given later in this report, Sects. II, III, IV. Lead angle computations are described in Section IV A and Appendices A-D.

4. Estimate of One Arc Second System Acquisition Period

At a space vehicle range of 0.5 AU, one-way transmission requires approximately four minutes; this is the amount of time needed for (a). Assuming 10 pps coding on the Earth's beacon, the dwell time for each raster element must be a minimum of 0.1 second. If the 60-by-60-minute field of view is broken up into one-by-one-minute elements, the total raster search requires 720 seconds, or 12 minutes. In addition, it may be assumed that with the low threshold setting a few noise pulses will be picked up, necessitating code test intervals of, say, 10 decision elements, or one second each; this is only a trivial addition to the overall search period. The beam-splitting coarse-track operation will, with probable tracking-loop bandwidth upwards of a few cycles per second, require no more than about one second. Retransmission (c) of laser beam from space vehicle to Earth requires about four minutes. Tracking operation (d) at the Earth Station should not add materially to the overall time. Transmission (e) of fine Earth Station beacon beam requires four minutes. Space vehicle fine-track operation needs only a second or less (f). Step (g), which constitutes start of operation of the communications link, requires four minutes. Thus, a total of approximately 28 minutes is required from the inception of search to the start of actual link operation, at a space vehicle range of 0.5 AU. Of this, 16 minutes are due to transmission delay and will increase directly with distance. At a range of one AU, the required period will be 44 minutes. For the very narrow beamwidth systems (0.01, 0.1 arc second), the acquisition process will be longer, depending on the number of additional steps required.

C. SPACE VEHICLE TRACKER PERFORMANCE *

The use of a pulsed laser transmitter for the Earth Station beacon signal offers significant advantages over a low power c-w laser source on the assumption that it will not be possible to provide coherent heterodyne receiver operation in the space vehicle within the next few years for state-of-the-art reasons, 1(II F). Because of the high peak power (one megawatt or more), the beacon signal-to-noise ratio at the space vehicle can be several orders of magnitude greater than the extraneous radiation background limitations usually considered, Ref. (5), cf. Section II B above. For the beam pointing system whose overall tracking bandwidth is small, pulse gating techniques can be used to further decrease the interference due to extraneous radiation sources such as the sunlit Earth, cf. section IV C of this report. If, on the other hand, coherent space vehicle receivers become available, the Earth Station laser transmitter could be derived from a low power c-w source, cf, Refs. (6),(7), since the narrow receiver bandwidths (10 mcps) could be used to filter out the background.

Based on notes prepared by A. Wallace.

The characteristics of celestial data and some performance attributes of celestial sensors are described subsequently in sections III A and III B. In section II D, below, it will be shown that with coarse vehicle stabilization provided by a Sun Sensor and a Canopus Tracker, similar to the Mariner/Mars, the Reference Axes are implemented by the closed loop space vehicle tracking of the Earth Station beacon on the one hand, and a precise (in the order of 1-2 arc seconds) direction to a celestial object (such as Compass) on the other. In other words, because of the closed loop process and the relatively low value of lead angle (up to a maximum of about 40 arc seconds, Section IV A), the need for extreme precision in independent Reference Axes is greatly reduced, and instead, the precision is supplied by the closed loop track process. The situation is analogous to radar tracking in that extreme precision in Reference Axes is replaced by precision in the beam directions implemented by closed loop tracking processes.

Some estimates of potential space vehicle tracker performance can be made by comparison with existing or projected celestial tracker systems. Conventional Earth-based astronomical techniques readily yield precisions of 0.02 arc second, Ref. (8). As described below in Sections III A, B, space vehicle celestial trackers operate on "navigational stars" whose visual magnitudes extend from (+1) to nearly (-2), corresponding to power densities from less than 10^{-13} to 10^{-12} watts/cm.^{2} As for planets, Mars has a visual magnitude close to (-2), Jupiter (-2.4), Venus (-4), (Section III B). The Fine Guidance celestial tracking subsystems of the OAO for the Goddard and Princeton Experiment Packages, as described below, will be able to track stars with magnitude ranges from zero to the seventh with an accuracy of 0.1 arc second.

For comparison, from Ref. (1) Tables III and IV, a one arc second laser communication system generates an "In Vacuo" received signal power of about 10^{-10} watt for the minimum Mars-to-Earth range of 0.524 A U at a visible wavelength of 6328 Å with a receiving telescope diameter of 200 inches, with one watt of transmitter power. For 100 inch diameter, this decreases to 2.5×10^{-11} watt; for 10 inches, 2.5×10^{-13} watt, and for one inch, 2.5×10^{-15} watt. Assume the Earth Station laser beacon transmits a pulsed signal, in the order of one megawatt peak at a prf of 10 pulses per second. For a 10-inch space vehicle telescope, the free space signal becomes 2.5×10^{-7} watts, which is brighter than a minus seventh magnitude ($m_v = -7$) celestial object, Section III D. Hence, a very high signal-to-noise ratio in the track mode is assured, especially since a one or two Angstrom unit filter can be used to eliminate extraneous background radiation.

In the "Coarse Search" mode described above, the Earth Station laser beamwidth could be about one arc minute, assuming a DSIF angular accuracy of about 0.02 degrees. Then, the received space vehicle power for a 10 inch telescope and a one megawatt transmitter power would be about 3600 times smaller, or about 0.7×10^{-10} watt.

This corresponds to the brightness of about a plus one magnitude star (m_V = +1) in the limited spectral region of the laser which provides an adequate signal-to-noise ratio for acquisition. A typical celestial tracker using a high performance photomultiplier system with night sky background can be expected to track a plus four magnitude star (m_V = +4) with about a 20 db signal-to-noise ratio, and the Fine Guidance Tracker for the Princeton OAO Experiment will track a seventh magnitude star (m_V = +7) with about a 17 db (50/1) voltage S/N-ratio and will acquire same with better than a 10 db voltage S/N-ratio, as described in Section III D below.

If the input were the Earth Station one megawatt pulse noted above, then for acquisition, the ideal S/N-ratio for a ten-inch aperture would be better than 27 db with very moderate filtering. For the track mode, the S/N-ratio for a minus seventh magnitude star would be 60 times or 17.8 db larger for an overall S/N-ratio of better than 44 db. Since the angular accuracy of the star tracker is inversely proportional to the S/N-ratio, very high ratios are needed for the greatest accuracy. The values quoted above cover ideal conditions. Actually, allowing for atmospheric attenuation, optical efficiency, etc., S/N-ratio might be 10 db less, that is, 17 db for acquisition and 34 db for track.

Further details on celestial trackers and tracking accuracy analysis are given later (Section III D). From a system point of view, "In Vacuo" tracking accuracy of 0.001 arc second is certainly feasible for a sufficiently high signal-to-noise ratio, especially if the space vehicle telescope aperture is of the order of 30-40 inches. Then, as noted above, this track from space vehicle to Earth together with a one or two arc second celestial reference establishes the space vehicle Reference Axes.

D. ACCURACY REQUIREMENTS FOR REFERENCE AXES*

The mathematical analysis of lead angle computation for aberration and transit time corrections is given in Appendices A-D, and numerical values corresponding to a Mars Fly-By trajectory are given in Section IVA. Typical values range from about 10 arc seconds at the beginning of the mission to about 40 arc seconds at fly-by. The trajectory for the November 28, 1964 Mariner/Mars mission is shown in Figure 4.

The space vehicle is stabilized by means of the Sun Sensor and the Canopus Tracker. Assume that the initial Search-Acquisition process as previously described has been carried out using the DSIF, the Earth Station beacon, and the space vehicle beam pointing system. It is further necessary to use a precision celestial sensor to provide half of the Reference Axes, tracking on Canopus, for example, whose precision is of the order of 1-2 arc seconds, with the other half provided by the space vehicle track to Earth.

A preliminary analysis of the precision needed for the Reference Axes' celestial sensor may be derived as follows, see Figure 5. The space vehicle track to Earth Station coincides with the Y-axis, and the X-Z plane is the plane at right angles to the tracker LOS to Earth (established by the closed loop). The space vehicle transmitter beam is directed along vector $\overline{OP}$ at an azimuth angle α and an elevation angle β (in spherical polar coordinates). These angles represent the components of the space vehicle to Earth transmission lead angle, and for $r = 10^8$ miles, $\alpha \approx 20$ arc second, $\beta \approx 0.2$ arc second, approximately. The Y-axis is also the Reference Axis generated by the closed loop tracking.

The precision celestial sensor is used to determine the X-Y plane (i.e. the Z-axis). This might be the projection of the LOS to Canopus on the X-Z plane perpendicular to the LOS to Earth (Y-axis). It is assumed for this analysis that the LOS to Earth is errorless. A more detailed analysis, now in preparation, will include errors in the closed loop tracking, dynamic errors, etc.

The analysis of Figure 5 shows that a two arc second error in the other Reference Axis (i.e. the Z-axis) is equivalent to a coordinate rotation about the Y-axis. At a range of 100 million miles, the azimuth error is 0.1 mile and the elevation error is 0.001 mile , Eqs. (6), (7). These are small because the lead angles themselves are small, yielding small displacements of the radius vector OP at the Earth, Eqs. (1), (3). The equivalent angular error at the space vehicle is 0.0002 arc second, Eq. (8). These calculations, of course, hold for "In Vacuo"

* Based on notes by A. Wallace, G. Strauss, S. Winsberg, G. Schuster

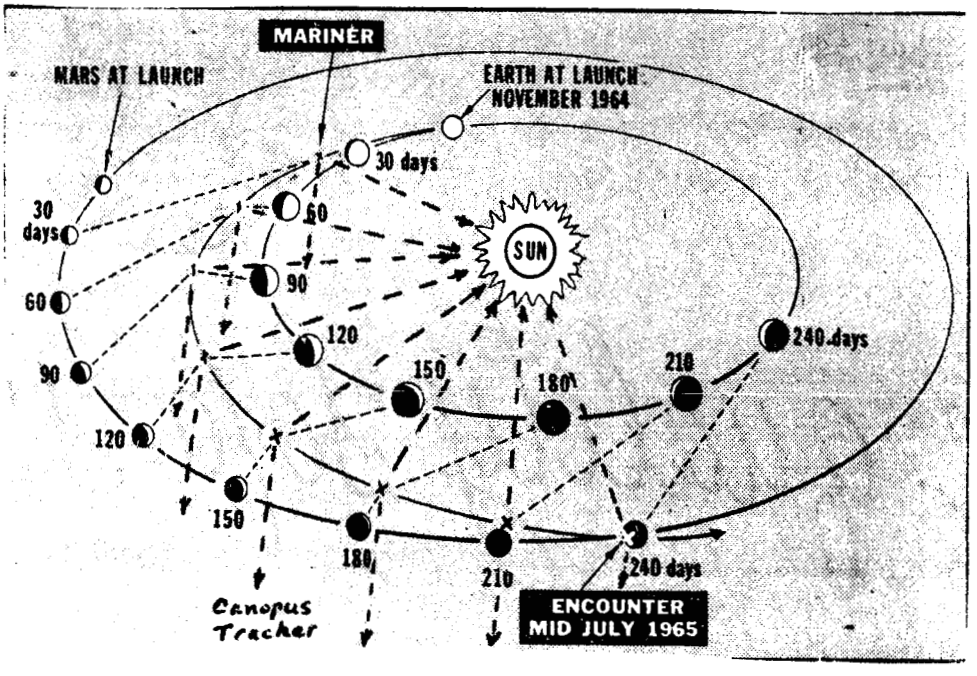

Figure 4. November, 1964 Mariner/Mars Mission

and exclude "In Vivo" anomalies.

For a 0.01 arc second system, a 1-2 second accuracy celestial sensor is adequate when used in conjunction with a closed loop space vehicle-Earth tracking system of 0.001-0.003 arc second accuracy. For a 0.1 arc second system, an order of magnitude greater can be allowed, and so on. It is clear that the geometry of the closed loop tracking to Earth dilutes the requirement for extreme precision in celestial sensors which might otherwise be required for an open-cycle system, cf. 1(IIE). This analysis will eventually be modified to include the effects of "In Vivo" atmospheric propagation in the loop, but is is not expected that the results for the space vehicle configuration will be significantly affected.

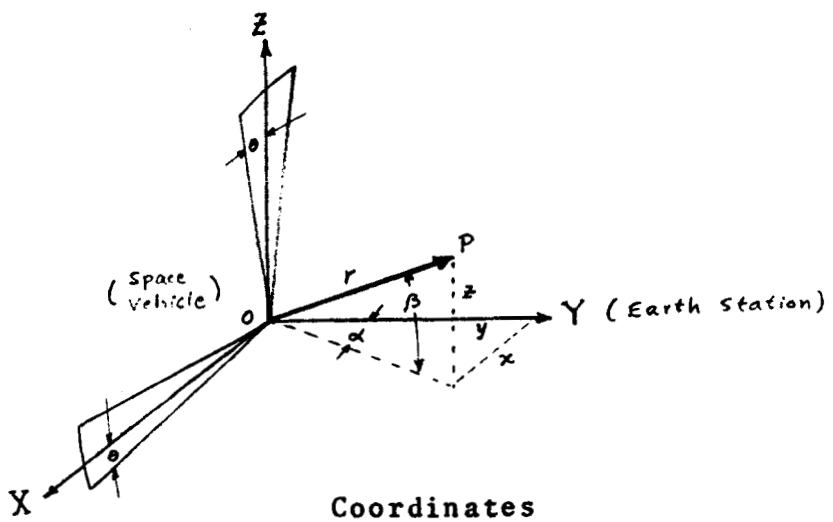

Coordinates

$\Upsilon = 10^8$ miles (Range)

$\alpha = 20 \widehat{\text{sec}} = 10^{-4}$ rad. (Lead angle)

$\beta = 0.2 \widehat{\text{sec}} = 10^{-6}$ rad. (Lead angle)

$\theta = 2 \widehat{\text{sec}} = 10^{-5}$ rad. (Error angle)

$$x = r \cos\beta \sin\alpha = r\alpha = 10^4 \text{ miles} \quad (1)$$
$$y = r \cos\beta \cos\alpha = r = 10^8 \text{ miles} \quad (2)$$
$$z = r \sin\beta = r\beta = 10^2 \text{ miles} \quad (3)$$

Coordinate Rotation

$$z^1 = z \cos\theta - x \sin\theta = z - x\theta \quad (4)$$
$$x^1 = z \sin\theta + x \cos\theta = z\theta + x \quad (5)$$
$$z^1 - z = -x\theta \;; |\Delta z| = |x\theta| = 0.1 \text{ mile} \quad (6)$$
$$x^1 - x = z\theta \;; |\Delta x| = |z\theta| = 0.001 \text{ mile} \quad (7)$$
Note: @ $r = 10^8$ mile, $r d\theta = 0.1$ mile $\Rightarrow d\theta = 10^{-9}$ rad. $= 0.0002 \widehat{\text{sec}}$ (8)

Figure 5. Reference Axes' Coordinate System Analysis

III. REFERENCE AXES

In the preceding section, various systems aspects of the hybrid laser beam pointing system have been discussed, including the Reference Axes. In particular, a simple configuration for these Axes was described for the space vehicle based on the closed loop tracking and a separate precision celestial sensor. However, as previously remarked, the considerations as presented are, strictly speaking, completely valid only for "In Vacuo" analysis, and may require modification for "In Vivo" considerations.

Accordingly, the material presented in this section covers some of the broader aspects of Reference Axes, including the characteristics of celestial data, performance characteristics of conventional celestial sensors, preliminary analyses concerned with atmospheric electromagnetic propagation such as beam refraction and beam spreading, and finally, various possible configurations for the implementation of Reference Axes in the space vehicle.

A. CELESTIAL DATA *

In the "In Vacuo" Case, bilateral symmetry exists between the space vehicle and the Earth station. For practical reasons, however, it is more realistic to concern oneself with the problems of optical measurements in the space platform, utilizing the Earth platform as the basic source of astronomical data.

If the beam pointing system were a pure open-cycle system without DSIF data, a basic set of measurements would be required to determine the distance and the relative velocity of the space vehicle with respect to the fixed stars and/or the Solar System , that is, to several objects whose positions and velocities are known in a given coordinate system, cf, Ref. (1), Fig. 3 and section II E. The vehicle's velocity can be determined from two position measurements separated by a known time interval. For the two-body problem, a minimum of six measurements at a known instant of time is required to determine the six components of the vehicle's position and velocity vectors or the six conventional orbital elements, Ref. (9), sect. 1.2, Chap.6. A general discussion of the instruments that can be used for space navigation is given in Refs. (10), (11), Part III. A schematic presentation of the totality of possible techniques (in principle) including "In Vivo" problems associated with the Earth's atmosphere is shown in Figure 6, cf. Refs. (10), (12).

The next section, III B, will discuss specific implementations of the proven methods of obtaining celestial data accurately. Some of the other possible methods shown in Figure 6 (as well as some not mentioned) will be investigated later in the program. In principle, however, all of the factors and variables listed in Ref. (1), sects. II C, II D, Fig. 3, are also potential sources of observables.

* Based on notes prepared by A. Wallace.

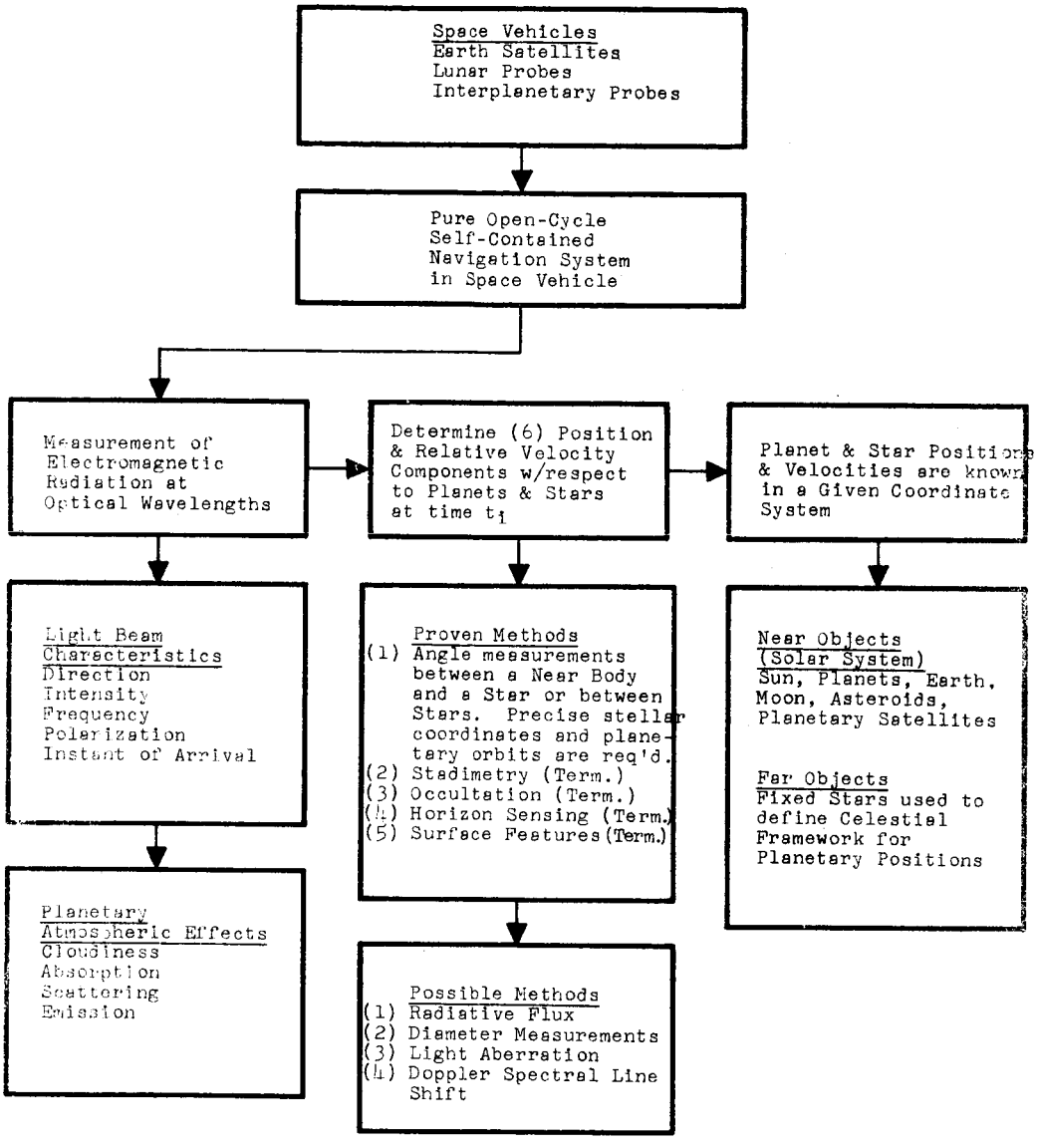

Figure 6. Self-Contained Space Vehicle Optical Navigation Techniques.

1. Stellar Data

By definition, Ref. (12), p. 154, the stars are classified as "far objects" since none of the stellar characteristics (direction, radiative flux, etc.) will change by "measurable" amounts due to movements of an interplanetary vehicle. Solar System objects (Sun, planets, satellites, asteroids) are defined as "near objects" as compared with the "fixed" stars. From a systems point of view, the fixed stars serve to define the geometrical space or absolute coordinate system (with suitable corrections for proper motion, etc.) in which all angular position measurements are made.

Figure 7 summarizes the pertinent characteristics of stellar data as prescribed within the framework of Earth-bound astronomical research. Detailed discussions of these characteristics will be found in Refs. (12), (13), especially on the most important one of the catalogs of positional accuracy of the most prominent stars. Some of the accuracy figures have previously been presented in Ref. (1), Fig. 3 and Table VI.

In accordance with the previous discussions of the Reference Axes for the hybrid system as compared with the pure open loop system, it may be asserted that the presently available stellar data is adequate for laser beam pointing purposes.

Figure 8 summarizes some of the pertinent characteristics of planetary data as prescribed within the framework of Earth-bound astronomical research. Naqvi and Levy, Ref. (12), on which Figure 8 is based, emphasize that the minor planets or asteroids represent a source of potentially great navigational value, because of their small angular diameters (the order of 1 arc second or less at 1 A U) and smallness of errors due to phase.

2. Coordinate Systems

To first order, a typical space vehicle closely approximates a two-body orbit, with deviations separately accounted for by the techniques of perturbation theory, Ref. (9), chaps. 6-9. By the laws of classical mechanics, the position of a body has three degrees of freedom which are described by three second-order differential equations involving six arbitrary constants of integration, Ref. (14). For a particular orbit, these constants or elements are shown in the "equatorial" system in Figure 9, namely: the semi-major axis, a; the eccentricity, e; the time of perifocal passage, T; the angle of inclination, i; the longitude of the ascending node, Ω; and the argument of parifocus, w, Ref. (9), Sect. 1.2. The orientation angles, i, Ω , and w are Eulerian angles, Ref. (14), chap. 1. For analytical purposes, however, rectangular coordinates are preferred.

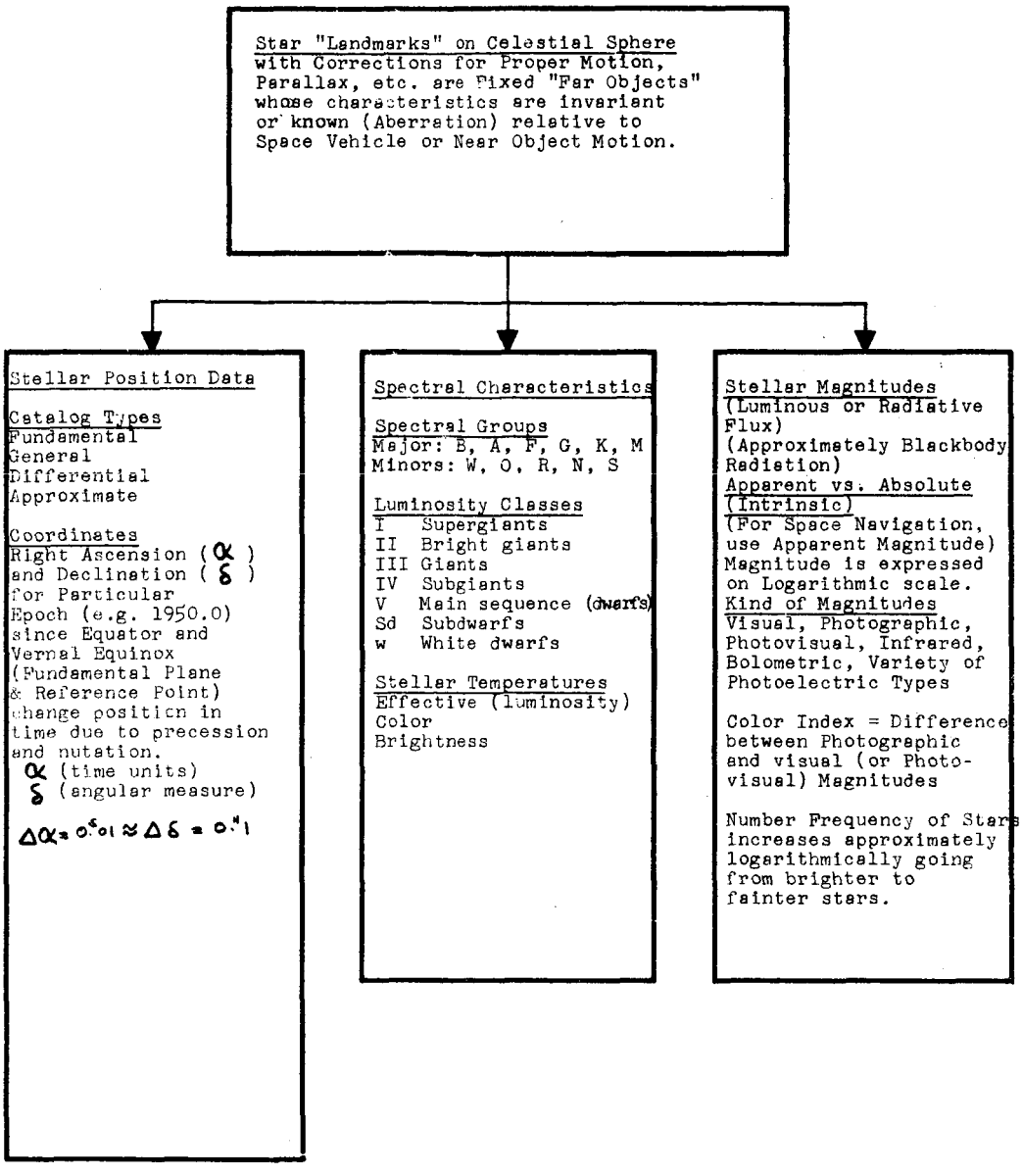

Figure 7. Summary of Pertinent Characteristics of Stellar Data.

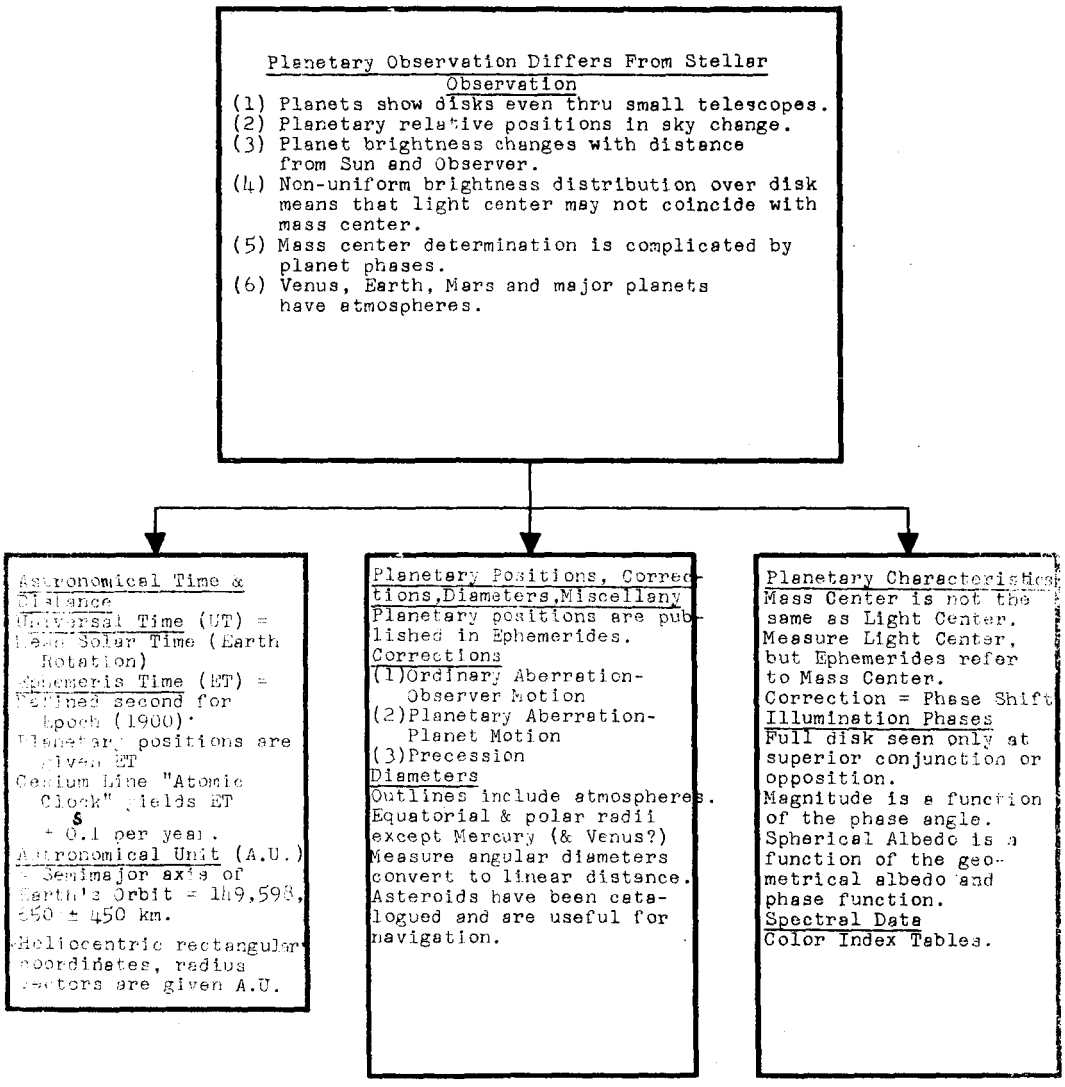

Figure 8. Summary of Pertinent Characteristics of Planetary Data.

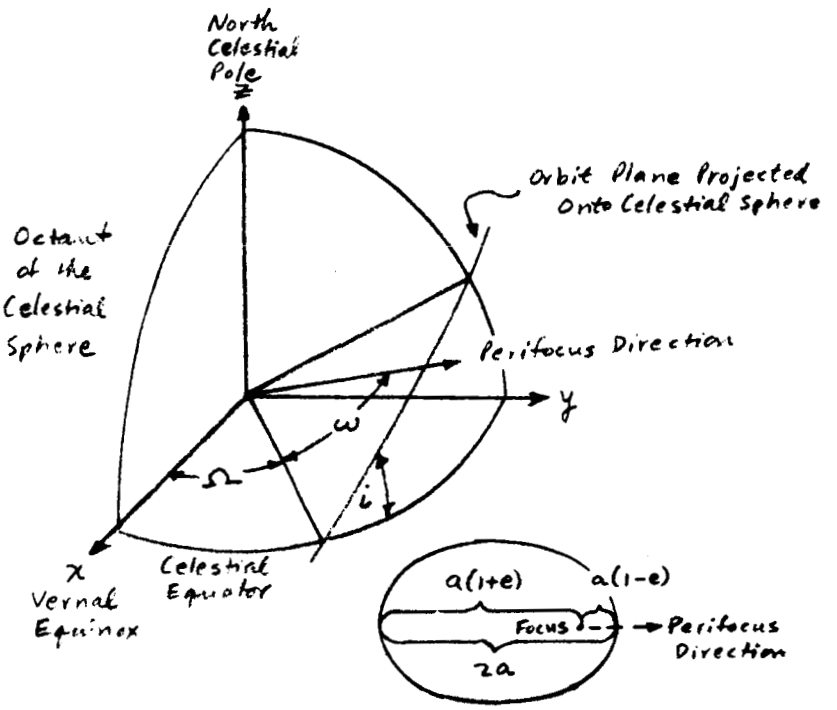

Figure 9. Elements of the Orbit (Reproduced from Ref.(9), Fig.(1))

Orbital analysis for a Mars mission is described in Appendix A, and its application to lead angle determination is presented in Appendices B-D.

The four principal coordinate systems used for analysis are summarized in Table I below and are illustrated in Figure 10. The coordinate systems formulated in terms of the orbit are described in Appendix A, which is concerned with the space vehicle trajectory. The coordinate system used for the Reference Axis accuracy analysis in section II D, Figure 5, was based on spherical-polar coordinates like the other systems shown, and is essentially a topocentric system. In Appendices A-D, the following coordinate systems were used: heliocentric ecliptic, geocentric equatorial, topocentric vehicle coordinates, and topocentric Earth Station coordinates.

TABLE I

Reference Coordinate Systems *

Coordinate System	Origin	Fundamental Plane	Principal Direction
Geographic	Geocenter	Equator	Greenwich Meridian
Topocentric	Topos	Horizon	North
Equatorial	Geocenter Topocenter Heliocenter etc.	Equatorial	Vernal Equinox
Ecliptic	Geocenter Heliocenter	Ecliptic	Vernal Equinox

* Reproduced from Ref. (9), Table III.

Future trade-off and error analyses will be conducted within the framework of these coordinate systems, shown in Figure 9, 10, and Table I, cf. Appendices A-D.

B. CELESTIAL SENSORS *

The previous section presented the basic backgound information on celestial data which can be utilized by the hybrid beam pointing system "Reference Axes" subsystems. The direction-finding techniques currently in use by the various types of celestial

* Based on notes prepared by A. Wallace

sensors now available can also be used by the tracking systems involved in the beam pointing operation. Due to the eccentricities associated with the "In Vivo" operation, it is desirable to consider the whole spectrum of celestial sensors, not only discrete star trackers, since the Earth station may very well turn out to be a "distributed" system as described in Ref. (1), section II F. Further, in a particular mission such as Mars fly-by, it may also be desirable to incorporate during the terminal phase some of the terminal measurement methods listed in Fig. (6).

1. Celestial Sensor Characteristics

Figure 11 illustrates in a general way the functional aspects of an automatic celestial tracker for purposes of position and attitude (including azimuth) determination, Ref. (15). The same functional areas also apply to the beam pointing tracking systems shown in the block diagrams of section II A. The multiplicity of available techniques permits the implementation of a whole family of types of trackers to perform the same or different functions. A family tree of celestial sensors would show subdivisions in terms of target, that is, single and multiple point sources such as stars and small asteroids, contour target sources such as planetary horizons or surface outlines, disk target sources such as the Sun, Moon, and planets, etc. The celestial data utilized by these various types of systems has been previously summarized in Figs. 6,7,8.

By definition, a star of zero visual magnitude ($m_v = 0$) yields a luminous flux density $I_o = 2.1 \times 10^{-10}$ lumens/cm.^{2} or 3.1×10^{-13} watts/cm.^{2} at a point outside of the earth's atmosphere, Ref. (16). Arbitrary visual magnitude (m_v) and flux density (I) are defined by

$$\frac{I}{I_o} = 2.51^{-m_v} \qquad (1)$$

Figure 12 graphically displays Eq. (1) along with brightness data for selected celestial "near" and "far" objects, Ref. (17).

For a circular telescope aperture diameter of D_R, the power collected is

$$P_R = I\, A_R \qquad (2)$$

and

$$A_R = \frac{\pi}{4} D_R^2 = 0.785\, D_R^2 \,, \quad I_o = 1.99 \times 10^{-12} \frac{\text{watts}}{\text{in}^2} \qquad (3)$$

$$\therefore \quad P_R = \frac{1.57 \times 10^{-12} D_R^2}{2.51^{\,m_v}} \text{ watts} \quad (D_R \text{ in inches}) \qquad (4)$$

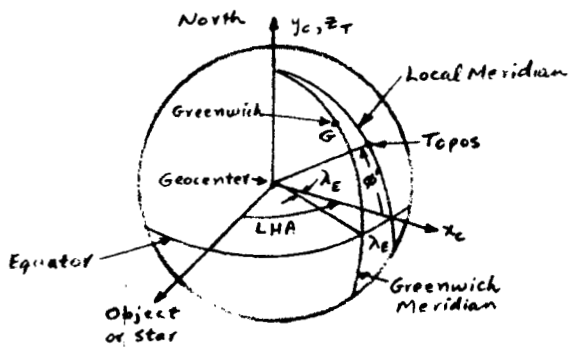

(a) Geographic Coordinates

λ_E: Longitude (East)

ϕ': Latitude (Geocentric)

LHA: Local Hour Angle

Fig. (10a). Geographic System

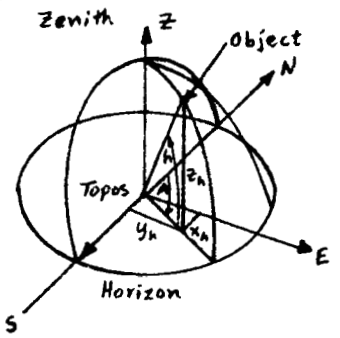

(b) Horizon or Altazimuth Coordinates

Origin at Observers, x_h-axis is directed South; y_h-axis is directed East.

A: Azimuth

h: Altitude

Fig. (10b). Topocentric or Horizon System

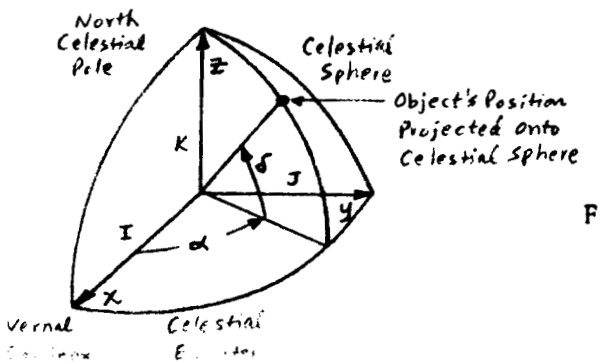

(c) Equatorial Coordinates

α: Right Ascension

δ: Declination

Fig. (10c). Equatorial System

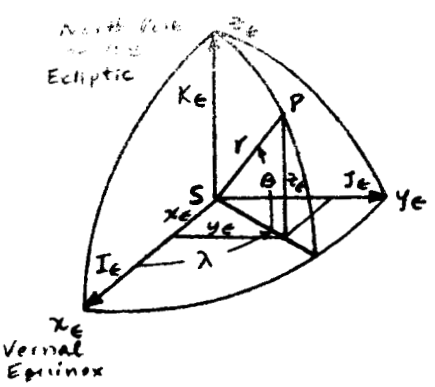

(d) Ecliptic Coordinates

λ: Celestial Longitude

β: Celestial Latitude

Fig. (10d). Ecliptic System

Figure 10. Reference Coordinate Systems
(Reproduced from Ref. (9), Figs. (15, 17-19).)

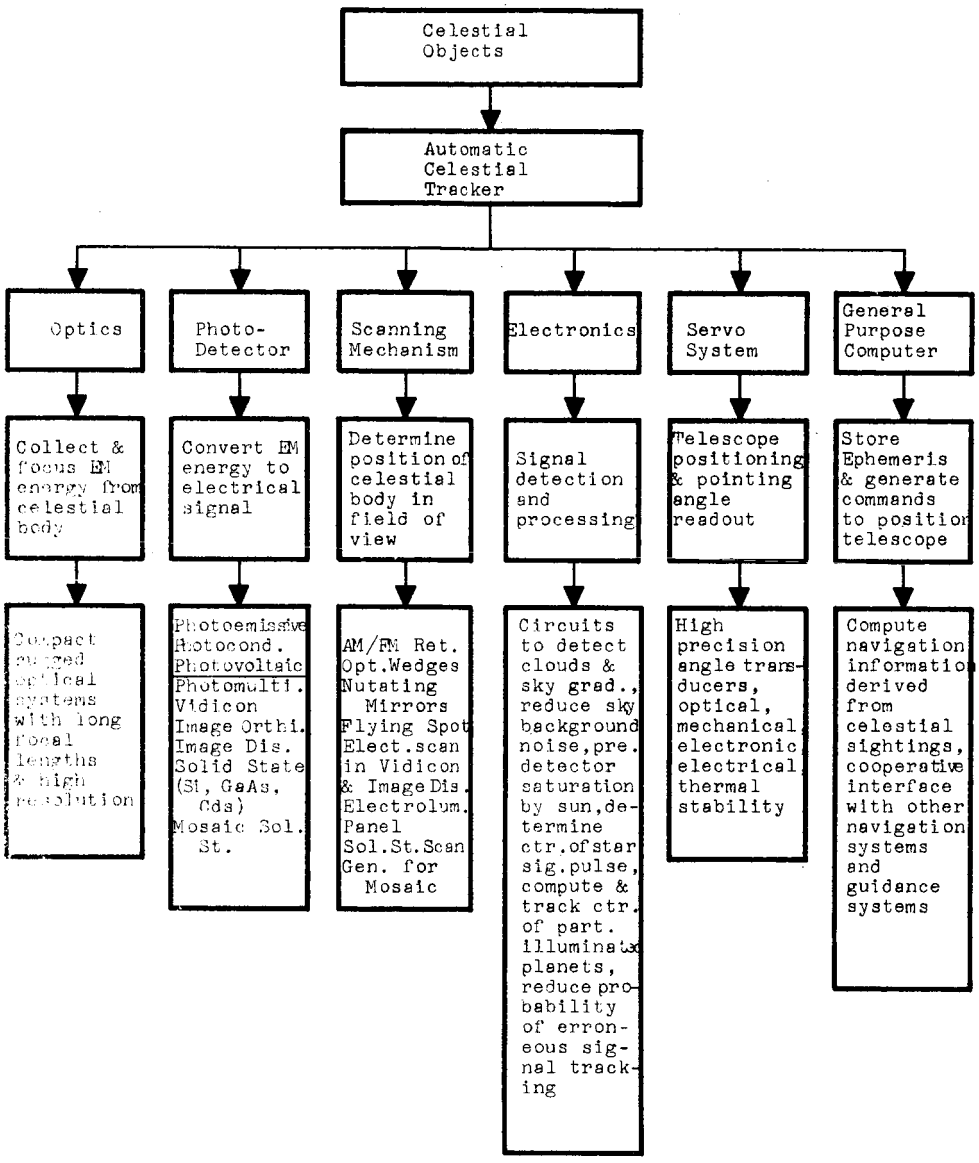

Figure 11. Functional Areas of Automatic Celestial Tracker

Figure 13 graphically displays Eq. (4) for various magnitude values.

A comparison of space vehicle tracker signal powers as a function of equivalent stellar magnitude was previously presented in Section II C. For noncoherent space vehicle tracker receivers, it is evident that the pulsed laser Earth Station beacon offers substantial advantages in the reduction of extraneous interference due to background radiation sources.

A typical closed loop configuration for a star tracker operating in atmosphere (In Vivo) is shown in Figure 14 together with some of the factors determining system performance. The space vehicle celestial sensor operates essentially in the equivalent of a "night sky" and the interplanetary environment which may introduce to a minor extent some of the degradation normally associated with the atmosphere. Figure 15, taken from Ref. (17) shows the ideal signal-to-noise ratio as a function of aperture diameter for a high performance photomultiplier system (η = 1.0, optical efficiency; q = 0.1, quantum efficiency; τ = 0.1 second, observation time) operating with a night sky background and a small field of view.

Comparison with space vehicle tracker performance was previously made in section II C.

2. Accuracy Analysis

A full detailed treatment of tracking accuracy as a function of S/N-ratio and other system parameters will be given in later reports. At the present time, some idea of celestial sensor performance can be gained from a study of the various configurations in use for the Fine Guidance subsystems of the OAO, particularly the Goddard Experiment Package, Ref. (1), sect. V A 5, Ref. (20), and the Princeton Experiment Package, Ref. (18). Both Experiment Packages will have the capability of tracking faint stars to an accuracy of 0.1 arc second. Since the Goddard Package has been partially previously described, Ref. (1), the following analysis pertains to the Princeton Package only.

The optics portion contains a Cassegrain telescope with an 80 cm diameter primary mirror and a high resolution spectrometer. The finer guidance sensor utilizes the star signal falling on the faces of the slit jaws of the spectrometer. The sensor measures the angular error across the slit width by comparing the relative intensities of light energy falling on each side of the slit jaws. The detection system includes an optical chopper and electronic logic circuits in addition to the photo-multipliers. Automatic Gain Control is provided to normalize the error signals since the range in star magnitude is from zero to seventh. Angular tracking is provided in two orthogonal axes, parallel to the slit width (z -axis) and parallel to the slit length (y-axis). The transfer characteristics of the z - and y- control axes are shown in

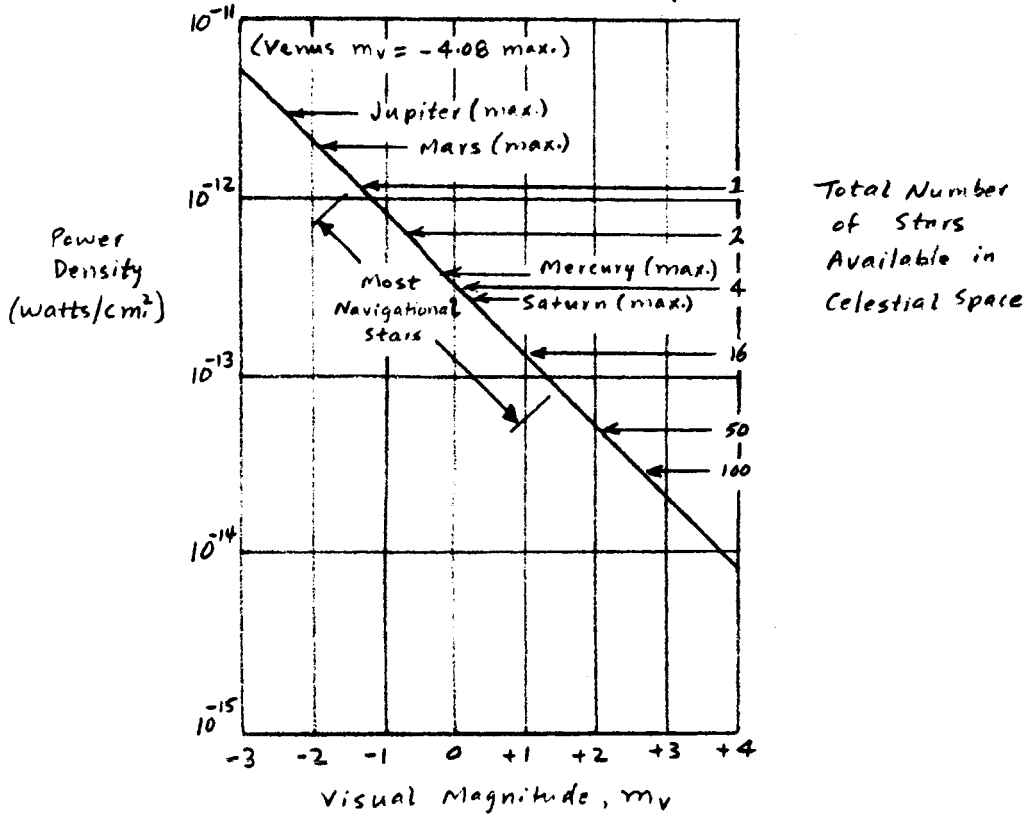

Figure 12. Power Density and Visual Magnitude for Celestial Bodies
(Reproduced from Ref.(17), Fig.(2).)

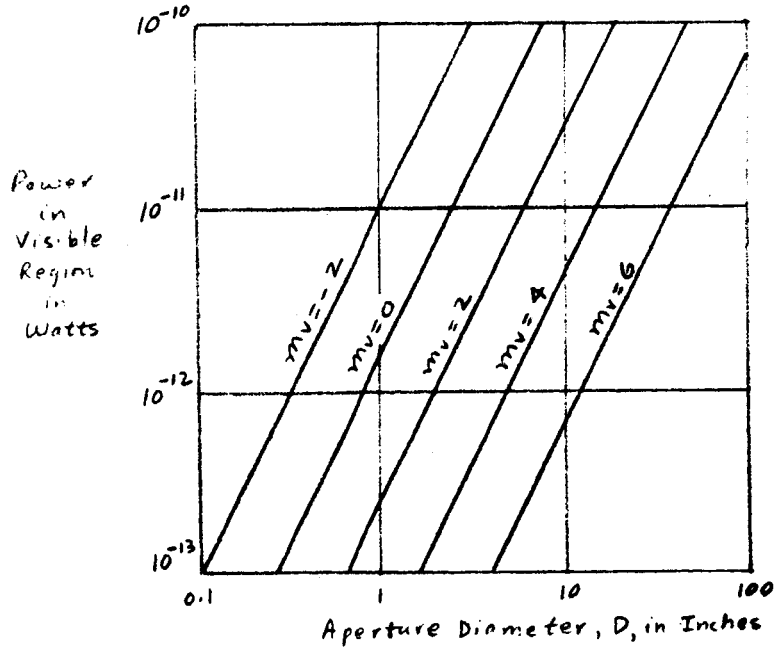

Figure 13. Available Power vs. Magnitude and Diameter
(Reproduced from Ref.(17), Fig.(3).)

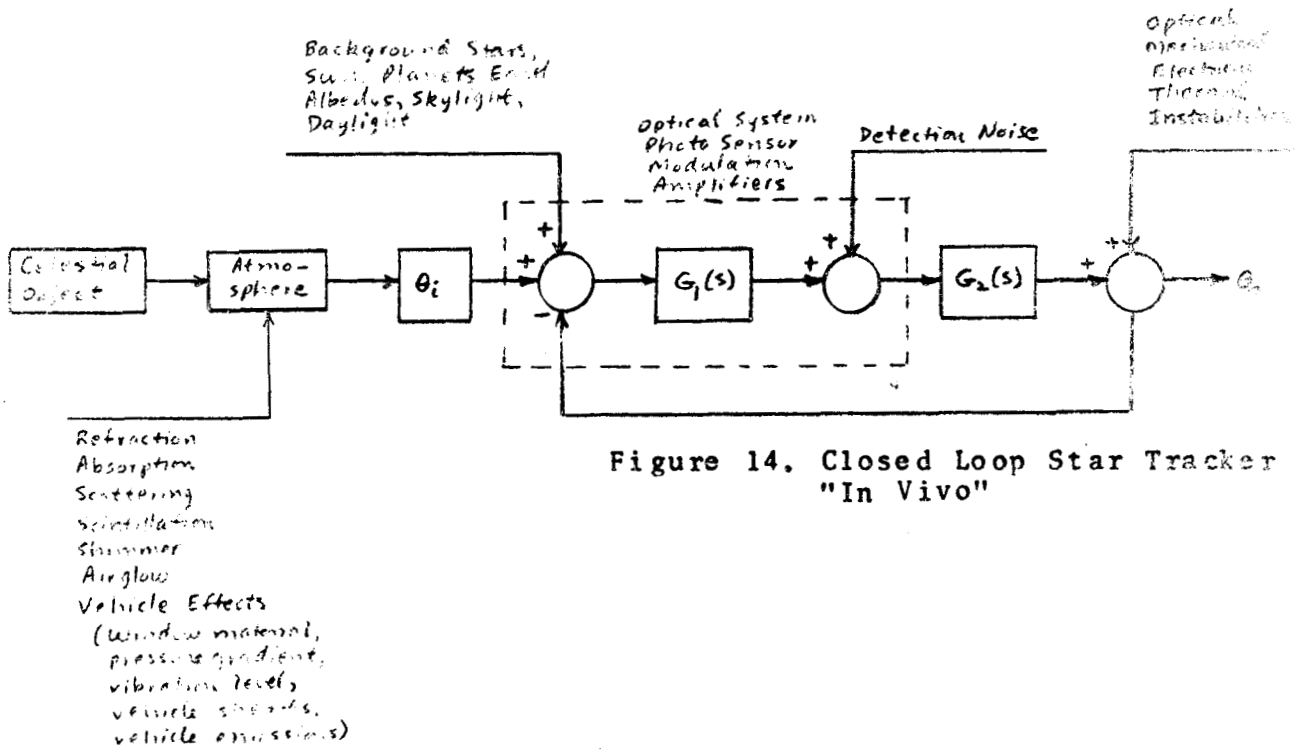

Figure 14. Closed Loop Star Tracker "In Vivo"

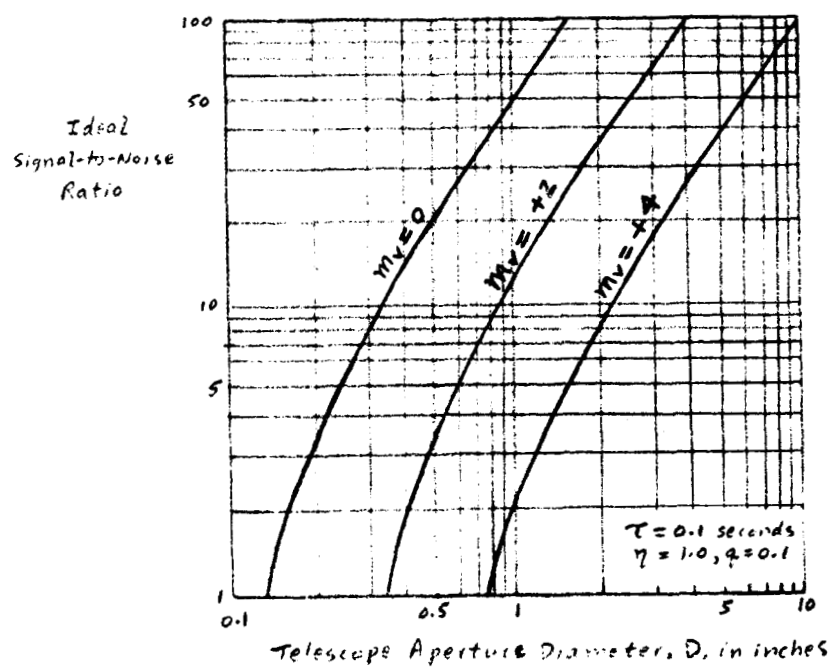

Figure 15. High Performance Photomultiplier System S/N with Night Sky Background (Reproduced from Ref.(17), Fig.(10).)

Figures 16 and 17 respectively, cf. Ref. (18). The error angle voltage Sv/Nv-ratio versus the photon arrival rate is plotted in Figure 18 for acquisition and null.

The guidance accuracy of the system described by Figs. 16-18 is determined as follows. The power from a star of the seventh magnitude is 1.04×10^{-11} erg/sec./cm^2/Å (cf. Eq. (1) above). The effective light-gathering area of the telescope system is 2.45×10^3 cm^2, and the efficiency of the sensor system is 7.1×10^{-3}.

$$P_R = 1.04 \times 10^{-11} \text{ erg/sec./cm}^2\text{/Å at } 4370 \text{ Å}$$
$$D_R = 2.45 \times 10^3 \text{ cm.}^2 \quad ; \quad \eta = 7.1 \times 10^{-3} \tag{5}$$

The power at the detector, P_D, is

$$P_D = \eta P_R D_R = 1.8 \times 10^{-10} \text{ erg/sec./Å} \tag{6}$$

Since the sensitive range of the detector is from 2900 to 5400 Å, the detector bandwidth B_D = 2500 Å. The energy of a photon at 4000 Å is

$$E = \frac{hc}{\lambda} = 5 \times 10^{-12} \text{ erg/ Photon} \tag{7}$$

where

h = Planck's constant, 6.623×10^{-27} erg-sec.

c = velocity of light, 3×10^8 m/sec.

λ = wavelength, 4×10^{-7} m.

The number of signal photons per second received at the detector is

$$N_S = \frac{P_D B_D}{E} = 0.9 \times 10^5 \text{ photon/sec.} \tag{8}$$

From Figure 18, the null voltage signal-to-noise ratio for this arrival rate is about 50. If this is normalized so that S_V=1.0 is the saturation value shown in the transfer characteristic of Figure 15, the noise angle corresponding to this error voltage is 0.012 arc second, cf. Ref. (18), p. 95. This rms error sensor noise voltage is associated principally with the photo-multiplier system, namely: random emission of photo electrons resulting from random arrival of photons on the photocathode thermal emission of electrons from the photo cathode, and resistive Johnson noise in the output load circuit of the photomultiplier. For the previous analysis,

Figure 16. Transfer Characteristic of the Z-Control Axis (Reproduced from Ref.(18,)Fig.(5))

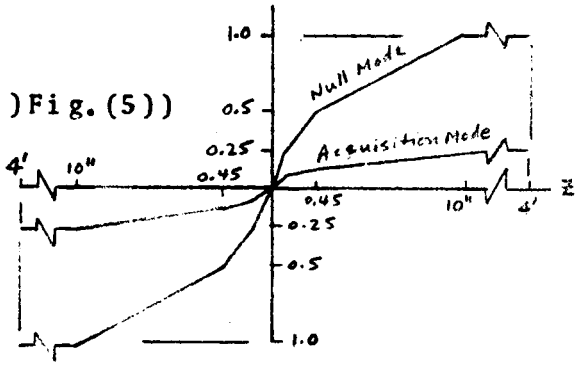

Figure 17. Transfer Characteristic of the Y-Control Axis (Reproduced from Ref.(18),Fig.(6))

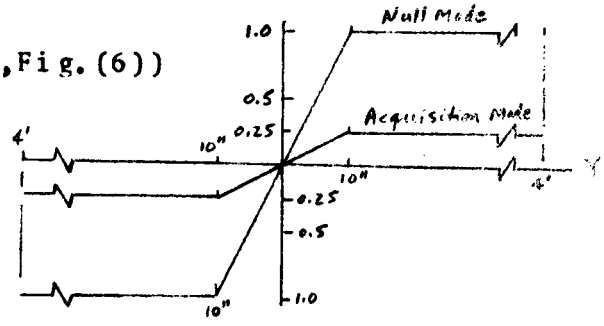

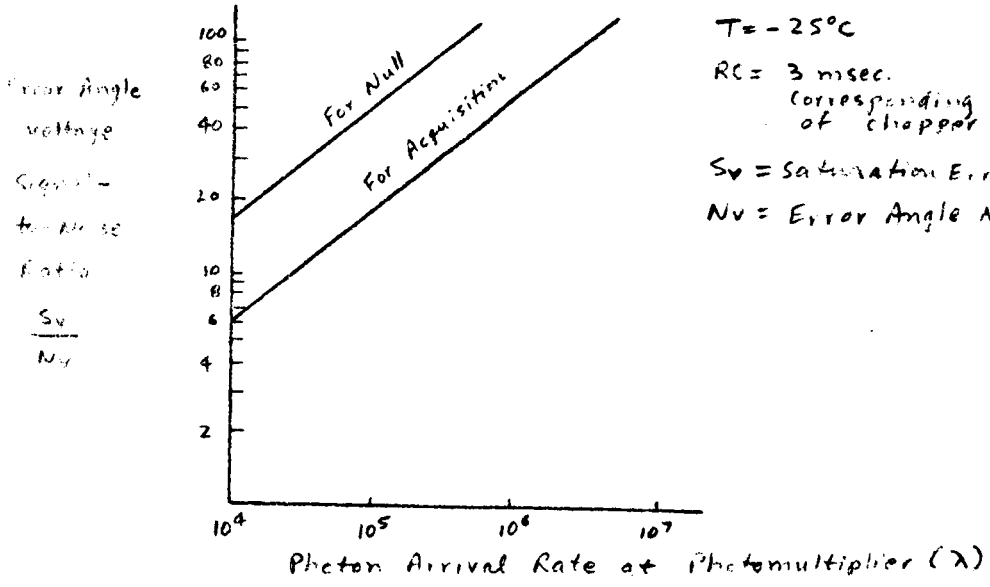

Figure 18. Sensor S/N Ratio vs. Photon Arrival Rate (Reproduced from Ref.(18), Fig.(9).)

the temperature is assumed to be -25°C, and the load circuit time constant is 3 msec. corresponding to 10 rps of chopper mirror.

For comparison with the beacon operation described in sections II A-C above, note that the beacon track signal of 2.5×10^{-8} watt "In Vivo" (2.5×10^{-7} In Vacuo) is many orders of magnitude above the seventh magnitude star analyzed above. Hence, the S/N ratio could be several orders of magnitude larger, and most probably, error noise signals corresponding to 0.001 arc second could be achieved. Then, the opto-mechanical system error stability and sensitivity would represent the limiting factors, cf. Figure 14, "In Vivo" star tracking.

C. ATMCSPHERIC BEAM SPREADING ANALYSIS*

In the first Bi-Monthly Report, Ref. (1), Section III, a considerable amount of material was presented covering "In Vivo" conditions of laser beam propagation through the earth's atmosphere. In particular, angle-of-arrival fluctuations, I(IIIC), atmospheric turbulent limitations on gain and directivity, I(IIID), intensity fluctuations, I(IIIE), and atmospheric turbulence limitations on optical heterodyne reception, I(IIIF) were analyzed. From the beam pointing system point of view, the angle-of-arrival fluctuations and the optical heterodyne limitations are the most serious objections to a "lumped" type of Earth Station receiving system, cf. I(IIF).

For example, from I(Table X, Figure 16), a 13.1cm diameter receiving aperture would exhibit a 1.75 arc second rms angular jitter and about 5 db of signal power loss for zero degree zenith angle reception, whereas a 1.31 meter dish has a 0.76 arc second jitter and about 23 db of signal power loss. The jitter for a 13.1 meter dish is 0.51 arc second and the loss would be 20 db greater, or about 43 db. The trade-offs for a "lumped" system are extremely limited compared to the possibilities for the "distributed" system.

In addition to these deviations from "In Vacuo" conditions, there is also the question of actual beam divergence or beam spreading due to atmospheric turbulence, briefly mentioned in I(IIIA). This section and the next describe the preliminary analytical efforts concerned with the space vehicle-to-Earth transmission. Propagation in the opposite direction is being separately analyzed and will be discussed in later technical reports, cf. I(Table VII).

1. Theory**

It is well known that, in the frequency domain, the relation between input and output is expressed by the relation

$$I(W,S) = \gamma(W, S)\, O(W, S) \qquad (1)$$

where I(W,S) and O(W,S) are respectively the two-dimensional Fourier transform of the image (output) and object (input) intensity distribution. $\gamma(W,S)$ is the two-dimensional transfer function of the medium, equal to the Fourier transform of the spread function which represents the intensity distribution of a point source after it has been affected by the medium.

**Based on notes prepared by S. Monaco

* Based on notes prepared by R. Arguello, S. Monaco, and A. Wallace.

The inverse Fourier transform of equation (1), will give us the two-dimensional intensity distribution of the image, that is

$$I(x,y) = \int_{-\infty}^{\infty} \gamma(\omega,s)\, O(\omega,s) \exp\left[i(\omega x + sy)\right] d\omega\, ds \qquad (2)$$

From I(x.y) the beam spreading in the x and y directions can be found.

By a rotation of coordinates the amount of the spreading in any direction could be determined.

From equation (2) it appears that to find I(x,y), the transfer function of the medium and the Fourier Transform of the function representing the intensity distribution of the object O(x,y) are needed.

Assuming the use of uni-mode c-w lasers, the intensity distribution, right out of the cavity, can be considered to be Gaussian.

The problem is not so easy if more than one mode of oscillation is present. In fact, in that case, the intensity distribution is not Gaussian, see Figure 19, and therefore is difficult to represent mathematically.

In this analysis, a uni-mode c-w laser will be considered as previously stated.

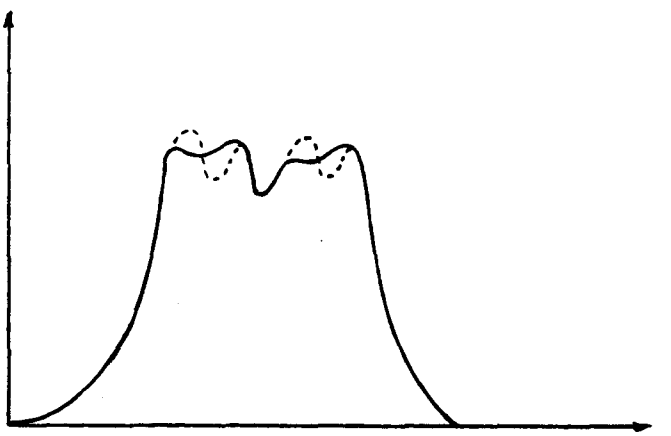

Figure 19. Intensity Distribution of a Multi-Mode c-w Laser.

Therefore the real problem is to find the transfer function of the medium, the atmosphere.

2. Atmosphere

The atmosphere is a turbulent absorbing medium, Ref. (21). Rigorously, a turbulent-random phenomenon must be handled statistically. It is reasonable to assume that outside our atmosphere there exists no significant turbulence, Figure 20, the width of the turbulent region can be assumed to be not larger. than 40 Km. It has been proved that the strength of the turbulence decreases as the elevation increases with a law expressed by the relation, Ref. (21):

$$A = 1.2 \times 10^{-12} \exp\left(-h/1600\right) \qquad (3)$$

where h is the altitude in meters. For 40 Km the strength of the turbulence is: A=1.67 x 10-23.

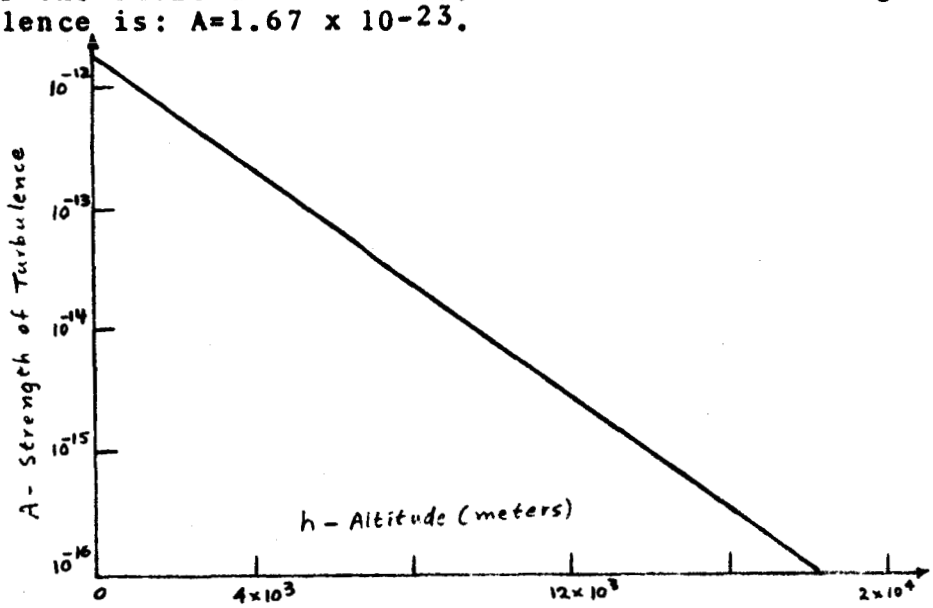

Figure 20. Strength of Turbulence based on Experimental Data (reported by Grain, Silverman, Tatarsky, Deam and Fannin, Ref. (21).)

Considering that the time for the light to cross a path of 40 Km is many order of magnitude less than the time needed for the turbulence characteristics to change, the atmospheric conditions frozen at a given instant can be visualized.

On the instantaneous basis, the atmosphere can be considered as made up of homogeneous- inhomogeneous, absorbing, non-fluctuating media.

In other words, it can be considered made up of a large number of homogeneous layers inside of which the index of refraction is constant, and a large number of inhomogeneities. The inhomogeneities, also called "turbulons", have been defined as "moving masses of air of varying physical and optical density" Ref. (22). In other words a turbulon is a volume of gas or fluid having an index of refraction differing significantly from that of the surrounding gas or fluid.

In Figures 21 and 22 two hypothetical turbulons are shown, resulting from rising warm air (Figure 21) and descending cool air (Figure 22), Ref. (22).

It is also apparent that in the "static" approach to the problem, construction of a model which realistically represents the atmosphere becomes a difficult task.

3. Models of the Atmosphere

The beam spreading will depend on the model of the atmosphere used. In order to understand the relation between beam spreading and atmosphere, four models are going to be considered:

a) Homogeneous - the atmosphere is assumed to be a homogeneous medium with one index of refraction represented by some middle value. It has been found that the index of refraction of the air decreases as the elevation increases, see Figure 23. The difference between the maximum and minimum values registered decreases with the elevation. To represent the homogeneous medium, we are going to consider a value along the middle line.

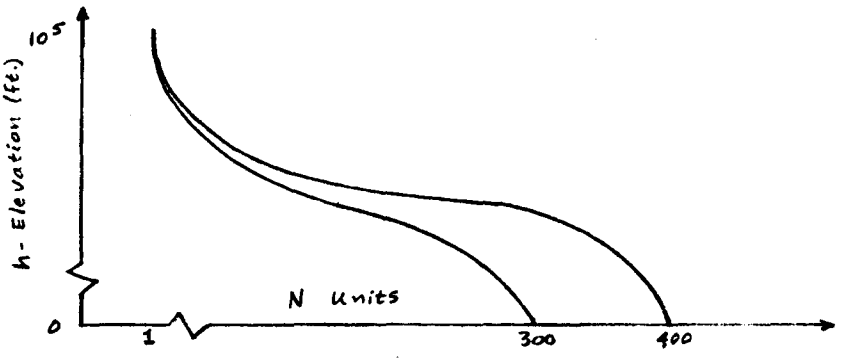

Figure 23. N units vs Elevation for Homogeneous Model

b) Homogeneous Layers - the atmosphere is assumed to be made of a large number of layers inside of which the index is constant. The width of the layers will be considered to be 100 feet

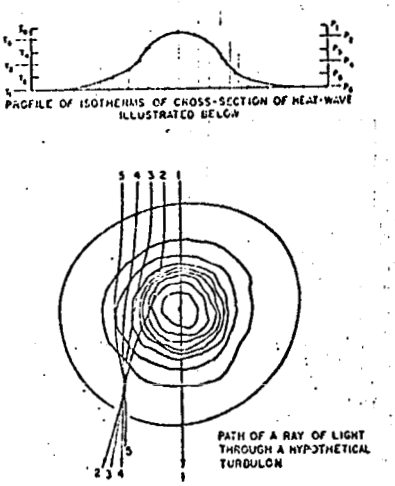

Figure 21. Turbulon Resulting from Warm Rising Air

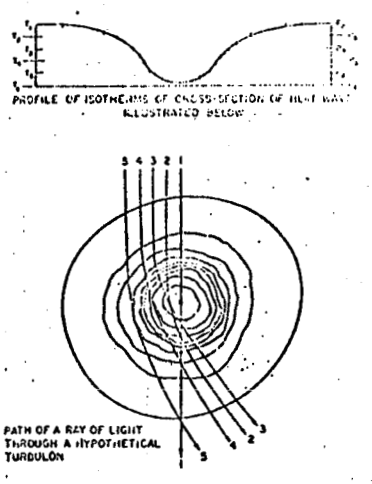

Figure 22. Turbulon Resulting from Cool Descending Air

(Reproduced from Ref.22)

for elevation 0-1000 feet, and larger for higher elevation.

c) Homogeneous Layers with One or More Inhomogeneities. The atmosphere is made up of homogeneous layers plus one or more inhomogeneities of the type indicated in Figure 21 and 22. The shape and the size of the inhomogeneity will play an important role in the beam spreading.

d) Turbulent Model. The index of refraction fluctuation will be considered in the analysis.

In the next period, the amount of the beam spreading for the four models will be computed.

D. STATIC HOMOGENEOUS BEAM PROPAGATION

In the previous section, it was stated that the spreading of a source of finite dimension can be found by plotting the intensity at the image plane. It was also stated that the intensity at the image plane is found from the inverse Fourier transform of the product of the transfer function of the mechanism and the Fourier transform of the intensity distribution of the input (source). This approach will be used only when considering the medium as turbulent. For simpler models of the atmosphere, namely, those considered in this section, the geometrical approach will be used.

As a first approximation, it will be assumed that the only decaying medium existing between deep space and earth is the Earth's atmosphere.

The Earth's atmosphere forms a layer around the Earth of a thickness which can be assumed, for any practical purpose, to be approximately 10 miles.

Based on experimental data reported by Crain and others, it appears, in fact, that the strength of the turbulence at 10 miles (16000 meters) is of the order of 10^{-16}, ref. (21).

Given the previous assumptions, two models of the atmosphere are considered below.

1. One Homogeneous Layer Model

The atmosphere is represented by one homogeneous, static medium of thickness 10 miles and an index of refraction, expressed in N units*, equal to 200. This value represents the middle value between unity (which indicates absence of atmosphere) and 400 N units (which represents the maximum value, registered at the ground).

In the complete absence of atmosphere, a beam coming from Mars, 1.4×10^8 miles away, will cover, on the Earth, an area which is a function of the beam divergency.

In Figure 24 three different beam angles are listed. Angle γ is in arc seconds, and the corresponding linear dimension covered at the Earth's surface, $\widehat{AB}$, is in miles, and its angular value, α is in degrees, assuming 1° equal to 60 miles.

---

* The relation between index of refraction, n , and N units, is expressed by the relation $N = (n-1)\ 10^6$.

γ (arc sec.)	$\overline{AB}$ (miles)	α (degrees)
1	$6.72 \cdot 10^2$	11.2
0.1	$6.72 \cdot 10^1$	1.12
0.01	$6.72 \cdot 10^0$	0.112

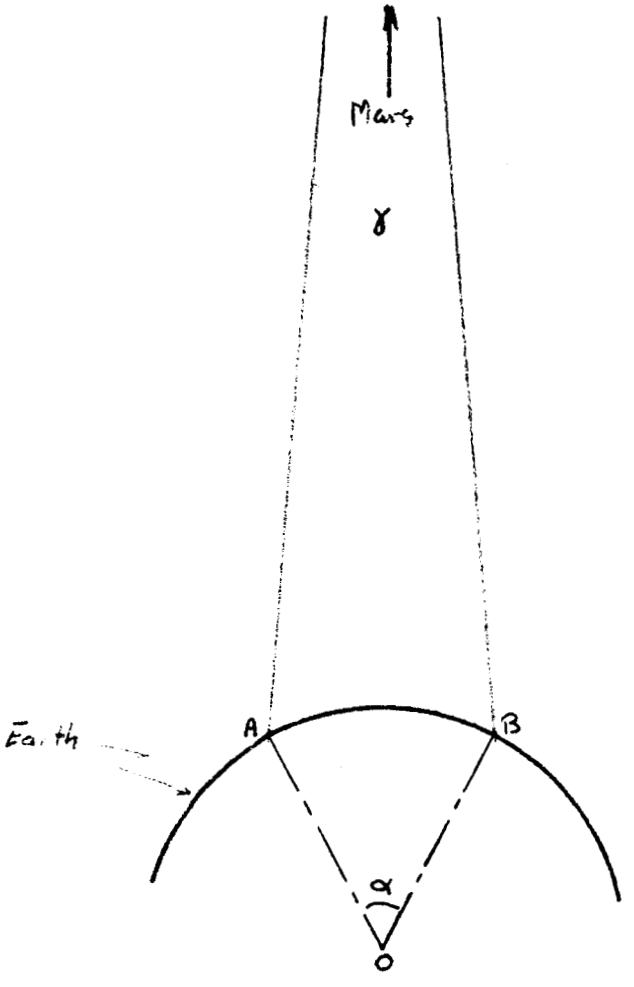

Figure 24. Homogeneous Model Geometry

If the atmosphere, as a homogeneous layer, is present at the boundary, space-atmosphere, the beam will be deviated according to the law of refraction.

The beam, going to a denser medium, becomes slightly convergent, Figure25.

From the law of refraction, we obtain the refracted angle

$$\varphi_1 = \sin^{-1}\left[\frac{n_0}{n_1}\sin\varphi_0\right] \qquad (1)$$

As a first approximation, we can assume

$$\varphi_0 = \gamma/2 + \alpha/2 \qquad (2)$$

Subtracting φ_1 from φ_0 we obtain the convergency angle, ΔE.

In Table III, we have listed ΔE in arc seconds and the corresponding linear values at the Earth surface $\widehat{AD}$ in feet for three different beam angles.

TABLE II
Homogeneous Model Beam Convergence

φ (arc Sec)	ΔE (arc Sec)	$\widehat{AD}$ (ft)
1	4.0450	1.0249
0.1	0.4036	1.02×10^{-1}
0.01	0.0397	9.53×10^{-3}

From the results it appears that in the space-to-earth propagation the Earth's atmosphere, considered homogeneous, slightly reduces the spreading of the beam. In the case considered, for example, the linear spreading of a one arc second beam is reduced only 2.05 Ft in 672 miles.

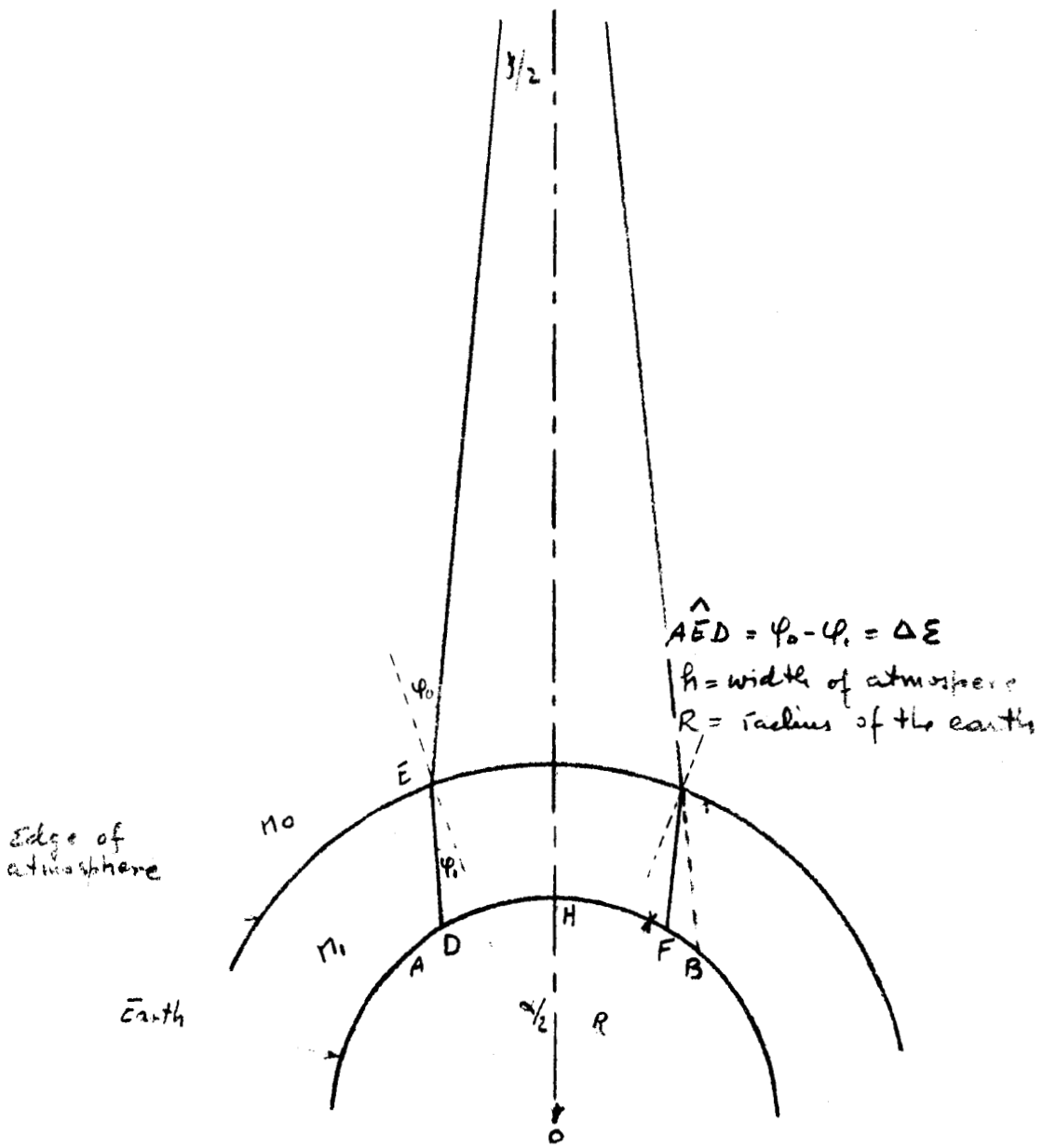

Figure 25. Homogeneous Model Refraction

2. Three Homogeneous Layers Model

The atmosphere is made up of three homogeneous layers, each one having a constant index, see Figure 26.

The three layers are characterized by the following indices of refraction, in N units; $N_1 = 50$, $N_2 = 200$, $N_3 = 350$, and the corresponding thicknesses in miles $d_1 = 6.0$, $d_2 = 3.0$, $d_3 = 1.0$. As in the previous model, $\phi = \gamma/2 + \alpha/2$ is assumed. A further assumption made, in this case, is that the tangents at the points of incidence E, E_1, E_2, are parallel, which implies that the angle of refraction of the previous layer is equal to the angle of incidence of the next layer.

Applying the law of refraction to each layer, the convergency produced by each layer has been found as well as the resultant linear spreading.

The results are listed in Table III.

TABLE III

Three Homogeneous Layer Beam Convergence

γ (arc sec)	ΔE_1 (arc sec)	ΔE_2 (arc sec)	ΔE_3 (arc sec)	$\widehat{AD}$(Ft)
1	1.0114	3.0342	3.0331	0.4619
0.1	0.1015	0.3023	0.3022	0.046
0.01	0.0096	0.0303	0.0304	0.005

From Table III, it appears that in the case in which the atmosphere is made up of three homogeneous static layers, the convergency produced for a one arc second beam, is one foot in the 672 miles of arc length. The reduction in spreading in the case of three homogeneous layers is approximately one-half of that obtained in the case of one homogeneous layer, but in both cases, these are negligible.

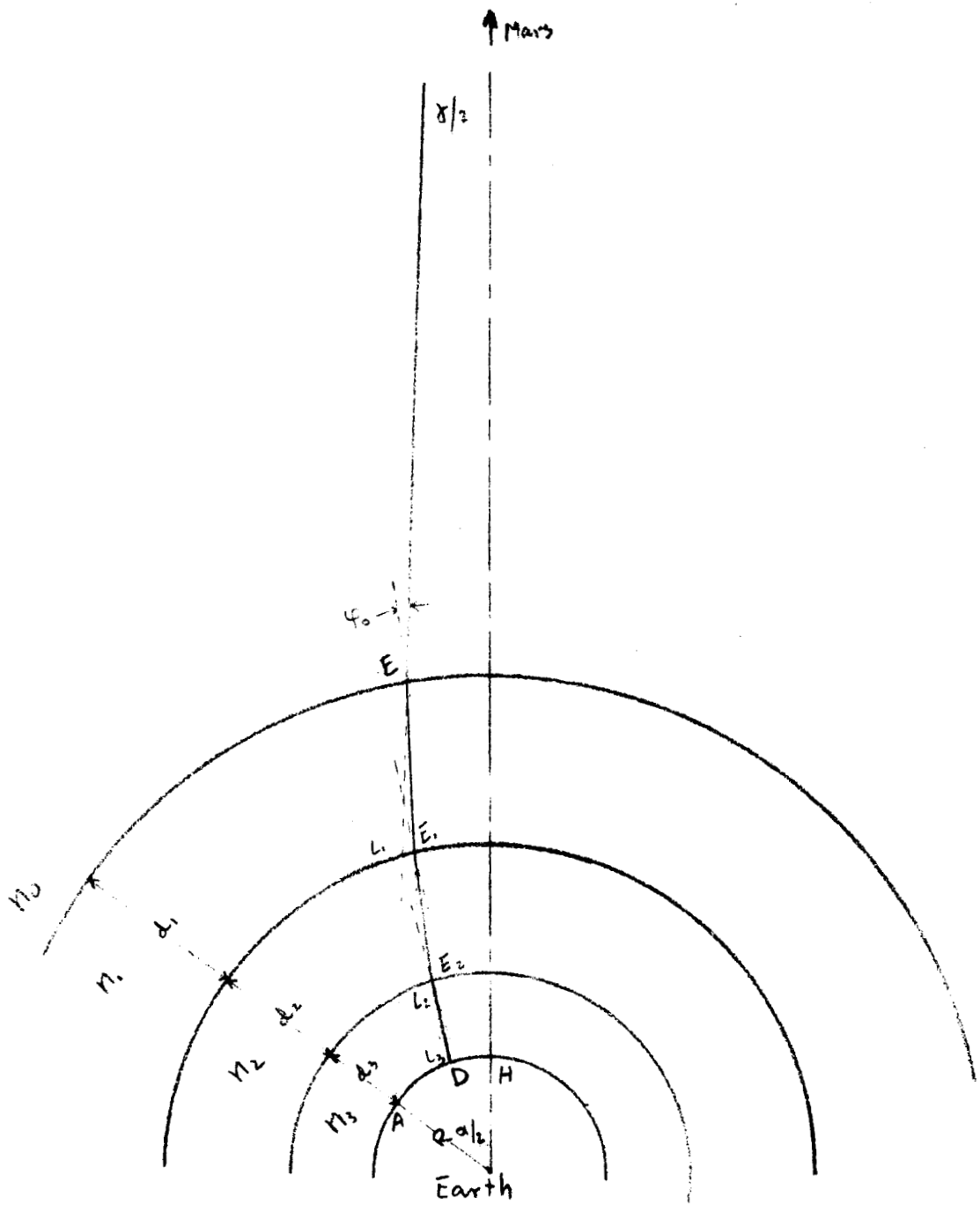

Figure 26. Three Homogeneous Layer Refraction

It can be concluded that the spreading of a monochromatic light beam propagating from space-to-Earth will not be affected by a static, homogeneous atmosphere.

E. REFERENCE AXES SYSTEMS

The results of the previous sections show that the principal atmospheric effects will derive from turbulent conditions, cf. 1 (III A-F). Accordingly, the Reference Axes system performance will be affected by the statistics of beam spreading, angle of arrival fluctuations, and scintillation, since the closed loop tracking from space-to-Earth and vice versa defines part of these axes, cf. Section II above. The investigation of suitable system configurations both for the space vehicle and the Earth Station is now under way to include these atmospheric effects, subject to the other system constraints of angular accuracy and extraneous background radiation.

Other possible Reference Axes systems can be based on other geometrical and analytical techniques, such as the use of a nuclear gyro instead of a Canopus tracker or precision Sun Sensor). In addition, rate gyros can also be considered either in a gimballed (geometrical) or strapped-down (analytical) configuration. Other possible systems can be based on the matching in a computer of velocity measurements derived either from the DSIF network or laser beam pointing Earth Station transmission.

Inasmuch as it has been shown that the accuracy requirements on the celestial sensor Reference Axis or its equivalent are not too severe, cf. Section IID above, these other possibilities offer promise for simplifying the space vehicle equipment configurations. On the other hand, if future space probes carry vehicle attitude stabilization systems such as Sun Sensors and Canopus trackers of sufficient accuracy, then the Reference Axis subsystem of the laser beam pointing control can be implemented with these on-board systems.

IV. BEAM MEASURING AND POSITIONING*

The block diagrams of Section II A, Figures 1 and 2, show the closed loops prevailing in the laser beam pointing system. The choice of a hybrid configuration has been fully justified by the arguments given in 1 (II E, F), and these are further confirmed by the demonstration of the lower order of accuracy required in the reference Axis subsystem.

Of considerable importance for a reliable system design is the existence of feedback loops surrounding a critical path or component. In the previous discussions of beam measuring and positioning, 1 (IV, p. 71), the desirability of enclosing the lead prediction fine beam deflection subsystem within a feedback loop was pointed out in order to relieve the requirements for high accuracy, extreme linearity, and the utmost stability. This was followed by discussions of various principles of optical beam deviation, 1 (IV A), and examples of beam steering techniques, 1 (IV B).

The hybrid system block diagrams of Figures 1 and 2 demonstrate that the complete tracking loop encloses the lead prediction subsystems both in the space vehicle and the Earth Station. If the space vehicle's trajectory is such that the angular rates of change of the respective lines of sight are sufficiently low, then deficiencies in the lead angle beam pointing can be corrected by the feedback properties of the closed loop tracking system.

A mathematical analysis of the trajectories for the Mars Fly-By mission has been carried out (Appendix A), and the mathematical details of the lead prediction problem have been determined (Appendices B-D). Numerical calculations corresponding to these equations are presented in Section IV A below which show that angular rates are of the order of 10^{-5} arc second/second or less. A preliminary analysis of the feedback properties of the closed loop tracking system, Section IV B, shows that these angular rates are well below the limitations on the system velocity constant imposed by the transport lags in the loop. Hence, the door is open to implementation of a lead prediction feedback circuit.

The performance of the closed loop system path from Earth-to-space can be further improved by taking advantage of the pulsed character of the Earth Station laser beacon, cf. Section II B, II C above. Since the tracking loop will assume the form of a sampled-data servomechanism, time gating can be used to reduce system internal and external noise during the interpulse intervals. These techniques are described in Section IV C.

Section VI D summarizes the overall characteristics of the laser beam pointing system and briefly describes an Earth Station

---

* Based on notes prepared by A. Wallace, G. Strauss, S. Winsberg.

distributed type of receiving system which is a ten by ten array of coherent receivers. The same array is used to provide error signals to the space vehicle for closed loop correction of its laser beam pointing subsystem. The boresight maintenance subsystem requirements are also eased as described in Section IVE.

A. LEAD ANGLES AND ANGULAR RATES*

The angle between the required line of sight of a space vehicle to Earth (or Earth to vehicle) transmitter and the observed line of sight has been calculated for various points on a Mars fly-by mission using data for a typical transfer ellipse. The rate of change of the lead angle has also been calculated. These results are given in this section.

Expressions for the lead angle between the required line of sight of the transmitter and the observed line of sight have been developed in Appendices C and D respectively. These expressions are functions of the relative velocity of the space vehicle and the angle between the relative velocity of the vehicle and the observed line of sight. The lead angle may thus be calculated from a doppler measurement of the radial velocity, a range measurement, and available trajectory data. For the present purposes, the lead angles were calculated using a typical transfer ellipse trajectory taken from Ref. (23). From the knowledge of the eccentricity of the transfer ellipse, the initial and final positions of the vehicle, and the semi-major axis of the transfer ellipse, obtained from Ref. (23), the necessary trajectory data was calculated from the equations developed in Appendix A.

1. Trajectory Data

The trajectory data was obtained from a transfer ellipse calculated by Battin et. al, Ref. (23), for December 13, 1964. For these purposes, it was assumed that the orbits of Earth and Mars are coplanar (when in fact they are inclined at 1°), and that their eccentricities are zero (when in fact $E_{Earth} = 0.16$ and $E_{Mars} = 0.093$).
These approximations do not appreciably affect the lead angle. (Diagrams of orbits calculated with and without these approxmations are presented in Ref. 23. The trajectory data are shown in Figure 27.

---

* Based on notes prepared by S. Winsberg.

$T_{Earth - Mars} = 0.525$ years

e (Transfer Ellipse) = 0.25

a (Transfer Ellipse) = 1.31 AU

$R_E = 1$ AU

$R_M = 1.52$ A.U.

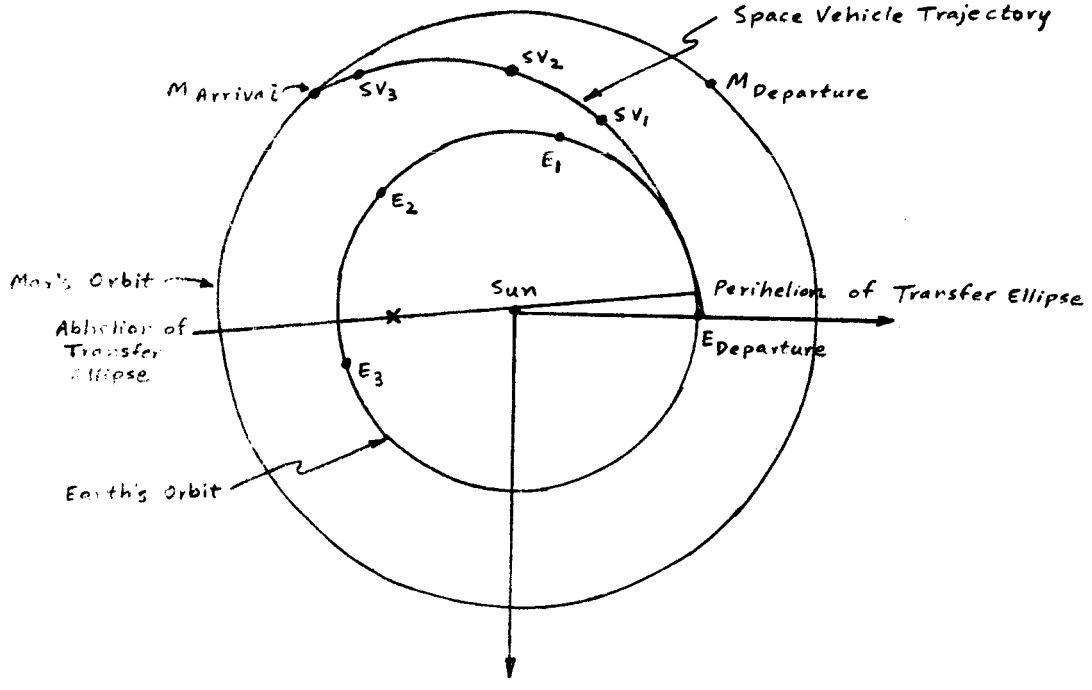

Position	$\lvert\vec{R}_{rel}\rvert$ A.U.	$\lvert\vec{R}_{rel}\rvert$ $\times 10^6$ miles	$\lvert\vec{V}_{rel}\rvert$ mi./sec.	α arc sec.	$\lvert\dot{\alpha}\rvert$ arc sec./sec.
1	0.1535	12.8	6.43	10.4	0.745×10^{-5}
2	0.95	79.3	9.95	21.7	0.03×10^{-5}
3	1.395	117.6	20.2	40.3	0.436×10^{-5}

Figure 27. Earth to Mars Fly-By Mission

2. Lead Angles

From Appendix C, the lead angle, α, is given to order $\frac{|V_{rel}|}{c}$ by,

$$\sin\alpha = \frac{2|\vec{V}_{rel}|}{c} \sin\beta \qquad (1)$$

where β is the angle between the relative velocity and the observed line of sight.

$\vec{V}_{rel}$ is the relative velocity of the Earth Station to the space vehicle (or the space vehicle to the Earth Station)

c is the velocity of light.

Lead angles were calculated for the three positions during the fly-by mission shown in Figure 27. The lead angles required at these positions are indicated in the data as well as the range and the relative velocity of the space vehicle. The relative velocity of the space vehicle has been assumed constant over periods of time on the order of the transit time. The transit time is given by $\Delta t = \frac{|\vec{R}_{rel}|}{c}$, where $|\vec{R}_{rel}|$ is the observed range. Variations in the relative velocity (in magnitude or direction) during the transit time are small and would constitute a higher order correction to the lead angle.

3. Lead Angle Rates

The rate of change of the lead angle is given in Appendix D. When the relative velocity is assumed constant over periods of time on the order of $\frac{|R_{rel}|}{c}$, $\dot{\alpha}$ is given by,

$$\dot{\alpha} = \frac{2}{c|\vec{R}_{rel}| \tan\beta'} \left(|\vec{V}_{rel}|^2 - |\vec{V}_{rel}| \frac{d|\vec{R}_{rel}|}{dt} \cos\beta'\right) \quad (2$$

Values of $\dot{\alpha}$ for the three points during a Mars fly-by mission are indicated on Figure 27. Since these angular rates are so small, it is conceivable that the closed loop tracking can monitor the lead prediction by feedback, as previously described.

B. CLOSED LOOP FEEDBACK ANALYSIS*

A simplified servo loop is postulated to describe the operation of the closed loop controlling the space-vehicle transmitter beam direction, measuring deviations from beam center at the Earth Station receiver, and transmitting error signals back. The time lag introduced by the back-and-forth transmission strongly determines the dynamic performance expected from the servo.

In view of the long transmission time required for deep-space operation ,1 (Table V), coupled with large relative velocity of the space vehicle to the Earth Station and the narrow transmitting beam, it becomes necessary to introduce transmitter lead with respect to the laser beam received from Earth. This is discussed in Section IV A above and App. A-D, describing the Bradley and transit time corrections. The local receiver tracking loop aboard the space vehicle thus tracks the Earth Station's apparent, rather than actual position. The lead angle, measured between receiver and transmitter axis must be computed on the basis of the component of Earth Station-space vehicle's relative velocity normal to their line of sight. This computation might either be carried out aboard the space vehicle, or at the Earth Station, and communicated to the space vehicle, using the analysis previously described in Section IVA.

One possible mode of operation, which might permit this calculation to be performed with modest accuracy, and which also would reduce the effects of non-linearities in the transmitter beam deflection system, as well as of transients, features a feedback loop. At the Earth Station, techniques can be devised for detecting the two components of the transmitter beam-pointing error, and the error information transmitted back to the space vehicle. The detailed mechanism for this error measurement will be described in a later report. A simple Class I servo aboard the space craft would then translate the error information to correct the beam deflection. Figure 28 indicates the servo, including the transportation lag from Earth Station to space vehicle (in the forward path) and a like delay from space vehicle to Earth Station (in the feedback path).

2. Transfer Function Including Transportation Lag

The configuration shown in Figure 28 has a transfer function given by

$$G(s) = \frac{\theta_o(s)}{\theta_i(s)} = \frac{K\, e^{-sT}/sT'}{1 + K\, e^{-2sT}/sT'}$$

where T is the one-way transportation lag (transmission delay, R/c) from Earth Station to the space vehicle, T' is the integrator time constant, and K is a non-dimensional constant taking account

* Based on notes prepared by G. Strauss and A. Wallace

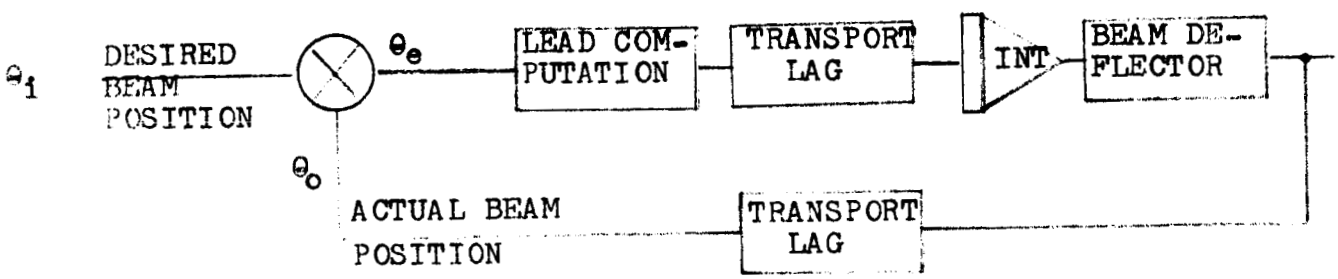

Figure 28. Simplified Servo Model of Closed Loop Tracking

of other gain factors. The steady-state output error of this servo in response to a step input is zero. For a linearly varying input, $\theta_i(t) = \theta t/T''$, the steady-state output error is $\theta T'/KT''$.

Effects of the transportation lag may be simply assessed by use of logarithmic gain and phase plots, Ref. (24). The exponential in 2T associated with the loop gain of the device has the effect of introducing phase shift which is linearly proportional to frequency; that is, at $f = 1/2T$, 360 degrees of phase shift not related to gain reduction is added to the normal phase shift of the system. Figure 29 presents a phase-frequency plot for several values of range. It can be seen that the phase shift introduced by the transportation lag places severe restrictions upon the permissible velocity constant K/T'. At a space vehicle range, on the order of 0.2 AU, total loop phase shift of 145 degrees (for a 35 degree phase margin) corresponds to an angular frequency of only 5 milliradians per second, corresponding to a velocity constant of 1/200. Modification of the servo by inclusion of a lead-lag network would permit increase of low-frequency gain and some improvement of performance.

At R = 0.5 A.U., $K/T' = 0.002$, and for 1 A.U., $K/T' = 0.001$. For an angular rate of 10^{-5} arc sec./sec., the steady state error would be less than 10^{-2} arc second for integrator time constants no larger than one second, and less than 10^{-3} second for a 0.1 second time constant. If required, the system gain can be adaptively adjusted as a function of range to minimize the effects of changing transportation lag.

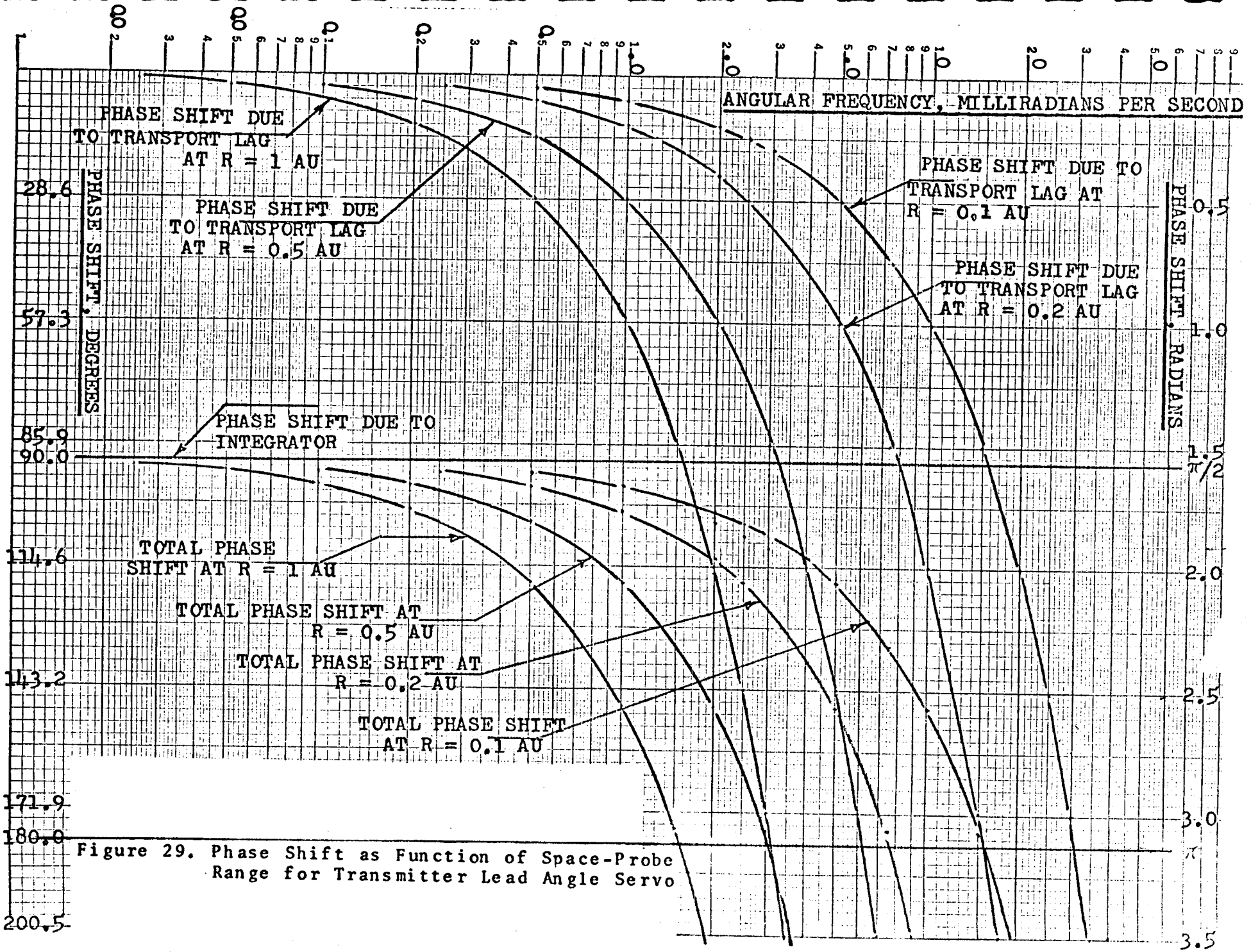

Figure 29. Phase Shift as Function of Space-Probe Range for Transmitter Lead Angle Servo

C. PULSED SIGNAL GATING NOISE REDUCTION*

The use of a pulsed ruby laser as the Earth Station transmitter as described in Sections II B, C above provides high peak power at a very low duty cycle. A gating process can be used to render the space vehicle tracking system immune to noise during the long interpulsed periods. Assuming that the tracking loops will take the form of sampled-data servomechanisms, the error-sampling zero-order hold circuit performs the gating function. A method for generating the required enabling pulses is discussed below.

The pulsed laser, capable of generating peak power on the order of one megawatt, is required since the space vehicle receiver is assumed to be noncoherent. The power available from gas-type lasers (which can furnish modulated cw emission) is too low to ensure reliable acquisition and tracking within the available search time and against the Earth's bright background, Section II B. The high power from the Q-spoiled ruby laser is available only in short pulses, on the order of 25 to 50 nanoseconds, at repetition rates (in the present state-of-the art) up to 50 pps. The resulting duty cycle is about 2.5×10^{-6}. The pulsed nature of the error signal requires error-sampled tracking loops, whose sampling switch isolates the error-processing circuits and output plant from all predetection and post-detection noise, at all times except during the sampling interval. The hold circuit following the sampling switch will ideally retain the sampled potential until the next switch closure (or some time function of the sampled potential, depending upon the order of hold circuit used). Figure 30 shows the sampled data servomechanism interconnections.

The pulsed error signals are subject to some deterioration in the photo-electric detection and amplification preceding the sampling switch. For this reason, it is desirable that the sample be taken during the middle of the pulse. The repetition rate is, of course, that of the beacon, and an exact time relation between sampling pulse and error pulse must be established to permit pulse top sampling.

A pulse train of the proper frequency (the same as the beacon transmitter pulsing rate) can be locally generated at the space vehicle. This may be accomplished either by a crystal-oscillator frequency divider (where slow phase drift resulting from frequency drift is corrected by the synchronization loop), or by a free-running oscillator, synchronized by pulses transmitted over the microwave communications system. In the latter case, no requirement for fast pulse response exists, since the synchronization pulses need not be short.

*Based on notes prepared by G. Strauss

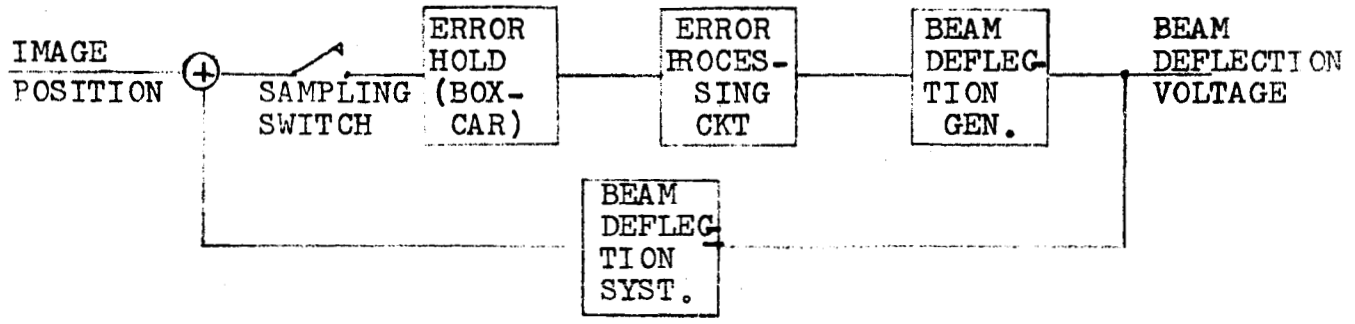

Figure 30. Sampled Data Servo for Electronically Deflected Light Detector

Figure 31. Synchronization Loop

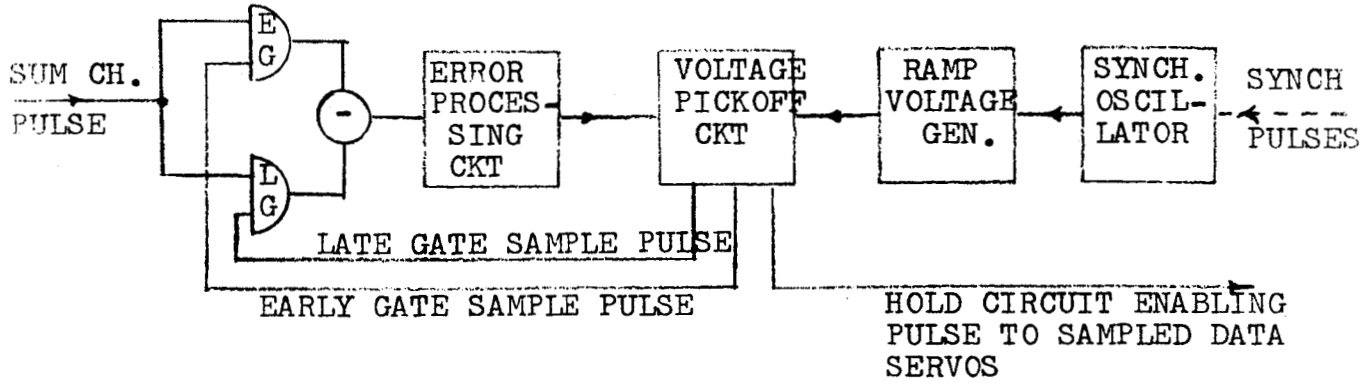

The synchronization loop shown in Figure 31 utilizes the sum channel output from the photo-detector, which is sensibly independent of error amplitude. Two contiguous sampling waveforms (early and late gates) are used to sample the sum channel pulse, and the difference between the samples constitutes the error signal of the synchronization loop. This error signal is used, after stretching and single or double integration, to bias a voltage pickoff, whose signal input samples a ramp-voltage waveform synchronized by the local pulse generator. The pickoff generates the early and late gate sampling pulses which will, in the closed-loop operation, split the sum channel pulse in half. The sampling pulse required for the Hold circuit of Figure 30 (actually, the switch closure) can be derived from the same circuit.

D. MEASURING AND POSITIONING TECHNIQUES*

It has been demonstrated in the previous sections of this report and Ref. (1) that systems analysis, based on providing closed loops wherever possible, can reduce considerably the requirements for extreme precision or accuracy in critical subsystems and components. On the other hand, similar considerations argue for the use of more sophisticated techniques to override the random effects of some system variables such as the atmosphere, cf. 1 (III).

Accordingly, for practical reasons based on the state-of-the-art in cw lasers, it is deemed advisable to introduce high power pulsed laser transmitters as the source for the Earth Station beacon, implying the use of noncoherent receiver-trackers for the space vehicle. This design bypasses the low power limitations of cw laser transmitters and the difficulties associated with the provision of coherent receivers in the space vehicle. Simultaneously, more sophisticated time gating techniques as described above can be used to eliminate interference from external radiation sources such as the sunlit Earth and other celestial objects.

For the space vehicle, a cw laser transmitter is required to implement high data rate transmissions, cf. 1 (II A, B). On the Earth, it is mandatory to use narrow bandwidth coherent receivers (5-10 mcs.) to eliminate extraneous radiation interference. Since the Earth Station is not constrained by size and weight considerations like the space vehicle, the difficulties associated with local oscillator stability, etc. can be overcome. However, as previously remarked, the "In Vivo" atmospheric propagation requirement imposes additional limitations so that "lumped" system designs do not appear to be suitable.

* Based on notes prepared by A. Wallace

Accordingly, a "distributed" receiving system configuration is now being investigated, which will take advantage of both spatial and temporal averaging to achieve the accuracy required for beam widths ranging from 0.01-1.0 arc second. The first design being considered consists of a ten by ten square array of five inch aperture coherent receivers, using ten local oscillators in serial feed per column. This array obviates the coherence degradation due to atmospheric turbulence described in 1 (III F)since each aperture is limited to 12.7 cm. Since the outputs will be noncoherently summed, the effective aperture of the array is equivalent to a fifty inch coherent parabolic telescope. The gain in accuracy due to spatial averaging would be ten-fold, corresponding to a reduction in rms value of angle of arrival fluctuation from 1.75 arc seconds to 0.175 arc second. Time averaging of 1000 pulses in a 0.1 second interval could yield a further ten-fold reduction to 0.0175 arc second.

Correlation techniques using the aircraft atmospheric monitor mentioned in Section IIA above should result in a further decrease of angle of arrival fluctuation values if such is found to be required.

In addition to the spatial and temporal averaging, the array can be partitioned to provide a three sensor interferometer both vertically and horizontally (that is, two orthogonal axes in the plane perpendicular to the line of sight to the space vehicle) to provide error signals to the space vehicle for its closed loop correction of the transmitter beam pointing directions, cf. Section IV C above. In the Earth Station, extremely accurate fine beam deflection and angle readout systems can be provided, but it is obviously desirable to reduce the need for such accuracy in the space vehicle. Hence, the question of providing closed loop correction of Earth Station beacon transmission is a matter for trade-off analysis to be conducted later in the program.

The foregoing question is also associated with the beam forming system to be used in the space vehicle. Although diffraction-limited optics of about fifty inches can be considered in the space vehicle for a 0.1 arc second beamwidth, the transition to a 0.01 arc second beamwidth requires a ten-fold increase in diameter. It appears that this requirement will call for the use of adaptive array techniques, locked to the Earth Station's beacon signal, cf.1 (IIE, F), These techniques are now under study.

With regard to the transmission from Earth to space, turbulence effects on direction of transmission can be severe for very narrow beam systems. A wider beam (3-10 seconds) will illuminate the space vehicle even in the presence of small fluctuations (1-2 seconds). However, a more narrow beam (one second) yields a tighter tracking loop, but at the expense of greater need for accurate prediction of direction of transmission "In Vivo".

Since a number of possibilities exist for implementation of the space vehicle and Earth Station systems (detectors, beam deflectors, gimballing configurations, etc.), various system arrangements are also now under investigation.

E. BORESIGHT MAINTENANCE*

Various boresight maintenance configurations have been previously described 1 (V A, B). It was previously noted in 1 (V B) that enclosing the fine beam steering control in the closed loop would dilute the requirements on extreme accuracy for this mode of operation. It is now seen that the closed loop configuration described in this report does include the boresight conditions within its monitoring functions.

For this reason, work on the boresight maintenance problem has paused at the stage set by the block diagram in Figure 2, which delineates its position in both the space vehicle and the Earth Station systems. In fact, if the space vehicle does not provide closed loop error correction for the Earth station, boresight maintenance becomes more critical for the latter. On the other hand, since constraints on size, weight, and complexity are not severe for Earth, provision is more easily made on Earth as described in 1 (V B). Further, the pulsed beacon mode allows for the use of look-through techniques on the Earth transmitter to verify the boresight.

On the space vehicle, the primary boresight reference is that of the receiver-tracker aperture locked on to the LOS to Earth. Slow boresight variations of the cw laser transmitter can be accommodated by a look-through technique resetting the fine beam system to null in order to inject the cw laser signal into the main tracking loop for setting up corrective biases in the fine beam deflection. The look-through period can be as short as 100 nanoseconds, keyed to the pulse gating circuitry previously described, Section IV C. Work on boresight maintenance following this approach will be resumed later in the program.

V. CONCLUSIONS

1. Generalized block diagrams have been prepared for the hybrid laser beam pointing system covering both the space vehicle and Earth Station systems.

2. A detailed acquisition and track procedure has been evolved, using DSIF inputs for preliminary coarse data, which is based on a pulsed laser source as the Earth Station beacon.

3. Signal-to-noise calculations for the space vehicle tracker with a pulsed signal input indicate that very high tracking accuracy should be obtainable for a high power laser source. Supplementing the normal tracking techniques with time gating will considerably reduce interference due to extraneous noise sources.

4. The Reference Axes needed in the space vehicle are provided by the tracker LOS to Earth and an additional directional reference such as a canopus tracker or a sun sensor or a nuclear gyro, etc. Error analysis indicates only moderate accuracy is needed for the additional reference. Contemporary celestial sensors are adequate for this purpose.

5. Preliminary analysis of beam spreading for static homogeneous and multilayer models shows that these effects are negligible. Atmospheric turbulence represents the major source of disturbance.

6. Trajectory analysis for a Mars Fly-By mission has been carried out, and numerical values have been obtained for selected points of lead angle corrections, angular rates, and other trajectory parameters.

7. Analysis of the closed loop performance of the system shows that the transmission lag does not introduce major problems in system performance. In addition, the closed loop encloses the fine beam deflection system, thereby diluting some of the accuracy needed in this system.

8. A distributed receiving system for the Earth Station is postulated whose design bypasses the coherence degradation to be expected for lumped coherent systems. In addition, this configuration provides error signals to the space vehicle to enclose the latter's beam pointing system.

9. Selection of a pulsed laser transmitter for the Earth Station allows the use of a noncoherent space vehicle receiver-tracker, obviating the problems associated with a space-borne coherent receiver and the limitations of low power cw transmission. The space vehicle transmitter, being cw of necessity for data transmission purposes, is low power and requires the use of coherent receivers for the Earth Station where they are feasible. The distributed receiving system overcomes the atmospheric limitations on coherent reception.

10. Boresight maintenance in the space vehicle is encompassed within the closed loop tracking system. Look-through techniques may be used for the correction of slow boresight drift.

VI. PROJECT ACTIVITIES FOR NEXT PERIOD

1. Project activities for the next period will follow the task sequence described in Section I, esp. Sect. I B, Figure 2. Because of delays and personnel changes, some tasks originally scheduled for the first period have been postponed to the second and third periods. Phase II activities will be initiated.

2. In addition, emphasis will be placed on further atmospheric propagation analysis, in both directions of propagation, i.e., space-to-Earth, Earth-to-space. Specific system configurations for the space vehicle and Earth Stations will be evolved for the Phase II error and trade-off analyses.

VII. CONFERENCES

Various project personnel attended the Optical Society of America meeting in New York on October 9, 1964 to hear selected papers on topics related to the beam pointing system.

VIII. MANPOWER UTILIZATION

A. October-November, 1964.
Project Director: A. Wallace - 288 hours
Project Engineer: G. Strauss - 312 hours

B. December-January, 1965.
Project Director: A. Wallace (1) - 312 hours
Project Engineer: G. Strauss (1) - 304 hours (2)

Notes: (1) Full-time program participants.
(2) Assigned to program on October 5, 1964.

IX. BIBLIOGRAPHY

(1) A. Wallace, "Study of Laser Pointing Problems," First Bi-Monthly Technical Report, No. KIC-RD-000162-1, NASA Contract No. NASW-929, Kollsman Instrument Corporation, Elmhurst, New York, 15 October 1964.

(2) A. Wallace, "Epistemological Foundations of Machine Intelligence," November 11, 1963, Contract No. AF33(657)-9482, AF Report No. ASD-TDR-63-878.

(3) "Mariner Mission to Venus," by the Staff, Jet Propulsion Laboratory, McGraw-Hill Book Company, New York, 1963.

(4) R.P. Mathison, "Tracking Techniques for Interplanetary Spacecraft," Technical Report No. 32-284, Jet Propulsion Laboratory, August 1, 1962.

(5) E.B. Moss, "Some Aspects of the Pointing Problem for Optical Communication in Space," AIAA First Annual Meeting and Technical Display, Washington, D.C., 29 June-2 July 1964.

(6) K.L. Brinkman, W.K. Pratt, E.J. Vourgourakis, "Design Analysis for a Deep Space Laser Communications System," pp. 35-46, Microwaves, Vol. 3, No. 4, April, 1964.

(7) J.A. Fusca, "Laser Communications," pp. 58-77, Space/Aeronautics, Vol. 41, No. 5, May, 1964.

(8) Peter van de Kamp, "Problems of Long-Focus Photographic Astronomy," pp. 9-15, Applied Optics, Vol. 2, No. 1, January, 1963.

(9) R.M.L. Baker, Jr., M.W. Makemson, "An Introduction to Astrodynamics," Academic Press, New York, 1960.

(10) S. Moskowitz, P. Weinschel, "Instrumentation for Space Navigation," pp. 289-306, IEEE Transactions on Aerospace and Navigational Electronics, Vol. ANE-10, No. 3, September 1963.

(11) H.H. Koelle, Editor, "Handbook of Astronautical Engineering," First Edition, McGraw-Hill Book Company, New York, 1961.

(12) A.M. Naqvi, R.J. Levy, "Some Astronomical and Geophysical Considerations for Space Navigation," pp. 154-170, same issue as Ref. (10).

(13) F.P. Scott, "Limitations Imposed on Celestial Navigation due to Inaccuracies of Star Positions," pp. 20-25, Navigation, Vol. 11, No. 1, Spring, 1064.

(14) E.T. Whittaker, "A Treatise on the Analytical Dynamics of Particles and Rigid Bodies," Fourth Edition, Chap. 1, 2, 3, Dover Publications, New York, 1944.

(15) R.J. Doran, "The Celestial Tracker Issue," pp. 150-151, same issue as Ref. (10).

(16) American Institute of Physics Handbook, Sect. 6g-4, McGraw-Hill, New York, 1957.

(17) J.E. Abate, "Star Tracking and Scanning Systems - Their Performance and Parametric Design ," pp. 171-181, same issue as Ref. (10).

(18) N.A. Gunderson, "Fine Guidance Sensor for High-Precision Control of the OAO," pp. 91-95, Journal of Spacecraft and Rockets, Vol. 1, No. 1, January-February, 1964.

(19) F.V. McCanless, "A Systems Approach to Star Trackers," pp. 182-193, same issue as Ref. (10).

(20) R.E. Papsco, "The Stabilization and Control System for the Orbiting Astronomical Observatory," pp. 3-14, Navigation, Vol. 11, No. 1, Spring, 1964.

(21) Tatarski, V.I., "Wave Propagation in a Turbulent Medium" (McGraw-Hill Book Company, Inc., New York 1961).

(22) R.B. Walton - Summary of Investigations of Heatwave Effects on Photographic Images - NAVWEPS Report 7773 October 1962.

(23) R. Battin et al "A Recoverable Interplanetary Space Probe," Report R-235, MIT Instrumentation Laboratory, July 1959.

(24) "Automatic Feedback Control System Synthesis," John G. Truxal, McGraw-Hill, 1955.

APPENDIX A

TRAJECTORIES FOR MARS FLY-BY MISSION *

I. INTRODUCTION

Suitable trajectories for Mars fly-by missions have been determined (Refs. A-1, A-2). Given a trajectory, the position and velocity of the spacecraft relative to the earth can be determined at any time after launch. In the event that such data is not available the expressions derived herein may be used to yield detailed data for a particular mission.

II. TRAJECTORY PARAMETERS

The trajectories described in Refs. A-1, A-2 were determined using the valid assumption that the spacecraft is influenced by only one body at any time. The vehicle travels about the sun on an ellipse. One point of the ellipse is common to the Earth's orbit (that is, the launch point); and one point on the ellipse is common to the planet's (Mars) orbit (that is, the arrival point). The influence of Mars is considered to be an impulse function occurring at the time of arrival. This appendix is concerned with the transfer ellipse. The semi-major axis, a, and the eccentricity E of the transfer ellipse are known. The launch time, T_L, and the arrival time, T_A, are known. For any given time, the positions of the planets can be obtained from the ephemerides, referenced to a given coordinate system and epoch. For the present purposes, the coordinate system and epoch used in Ref. A-1 were chosen. These are the heliocentric ephemerides of the planets referenced to the mean equator and equinox of 1950.0. From these ephemerides the position of the Earth $\vec{R}_E'(T)$ can be found at time T and the position of Mars $\vec{R}_M'(T)$ at time T. In Ref. A-1, these coordinates are transformed to a heliocentric ecliptic mean-of-launch-date system, for practical and computational purposes. First, a rotation is made to heliocentric equatorial coordinates mean of 1950.0 to heliocentric equatorial mean of launch date. This is accomplished by means of Matrix A, whose elements are given below.

* Based on notes prepared by S. Winsberg

$$
\begin{aligned}
a_{11} &= 1 - 0.00029697T^2 - 0.00000013T^3 \\
a_{12} &= -a_{21} = -0.02234988T - 0.00000676T^2 + 0.00000221T^3 \\
a_{13} &= -a_{31} = -0.00971711T + 0.00000207T^2 + 0.00000096T^3 \\
a_{22} &= 1 - 0.00024976T^2 - 0.00000015T^3 \\
a_{23} &= -a_{32} - 0.00010859T^2 - 0.00000003T^3 \\
a_{33} &= 1 - 0.00004721T^2 + 0.00000002T^3
\end{aligned}
\qquad \text{(A-1)}
$$

where T is the number of Julian Centuries of 36,525 days past the epoch 1950.0

The second notation transforms the coordinates from heliocentric equatorial mean of launch date coordinates to heliocentric ecliptic mean of launch date. This is accomplished by means of matrix $E_1(-e)$:

$$
E_1(e) = \begin{Bmatrix} 1 & 0 & 0 \\ 0 & \cos e & -\sin e \\ 0 & \sin e & \cos e \end{Bmatrix} \qquad \text{(A-2)}
$$

where e is the mean obliquity of the ecliptic on the launch date and sin e and cos e are approximated by:

$$
\begin{Bmatrix} \text{sine} = \sin e_o + P(T)\cos e_o - 1/2\ P^2(T)\sin e_o \\ \text{cose} = \cos e_o - P(T)\sin e_o - 1/2\ P^2(T)\cos e_o \end{Bmatrix} \qquad \text{(A-2a)}
$$

where:

$$P(T) = -0.000227111T - 0.0000000286T^2 + 0.00000000878T^3$$

e_o is the mean obliquity of the ecliptic for 1950.0

Now, in general, the components of the position vectors $\vec{R}_E$ and $\vec{R}_M$ are found in mean-equinox ecliptic-of-launch-date coordinates by:

$$
\begin{Bmatrix} \vec{R}_M \\ \vec{R}_E \end{Bmatrix} = E_1(-e)A \begin{Bmatrix} \vec{R}_M' \\ \vec{R}_E' \end{Bmatrix} \qquad \text{(A-3)}
$$

The heliocentric angle traversed by the vehicle from launch to arrival, ψ, is computed from

$$\cos\psi = \frac{\vec{R}_E(T_L) \cdot \vec{R}_M(T_A)}{\left|\vec{R}_E(T_L)\right| \left|\vec{R}_M(T_A)\right|} \qquad \text{(A-4)}$$

$$\sin\psi = \text{sgn}\left[\left(\vec{R}_E(T_L) \times \vec{R}_M(T_A)\right) \cdot \hat{K}\right] \left[1-\cos^2\psi\right]^{1/2}$$

where $\hat{K}$ is the unit vector normal to the ecliptic plane in the direction of the ecliptic north pole.

The unit vector $\hat{W}$ normal to the vehicles orbit plane is given by:

$$\hat{W} = \frac{\vec{R}_E(T_L) \times \vec{R}_M(T_A)}{\left|\vec{R}_E(T_L)\right| \left|\vec{R}_M(T_L)\right| \sin\psi} \qquad \text{(A-5)}$$

and the inclination of the orbit to the ecliptic plane i, may be found from

$$\cos i = \hat{W} \cdot \hat{K} \qquad \text{(A-6)}$$

Figures A-1 and A-2 show heliocentric ecliptic coordinates and the plane of the transfer ellipse.

Consider figures A-3 and A-4, which represent the transfer ellipse for $\psi < \pi$ and $\psi > \pi$.

Now, from the equation for an ellipse,

$$\left|\vec{R}_{veh}\right| = \frac{a\,(1-\epsilon^2)}{(1 + \epsilon\cos\theta)} \qquad \text{(A-7)}$$

where θ varies from θ_L to $(\theta_L + \psi)$ (A-8)

and $$\left|R_E(T_L)\right| = \frac{a\,(1-\epsilon^2)}{(1+\epsilon\cos\theta_L)} \qquad \text{(A-9)}$$

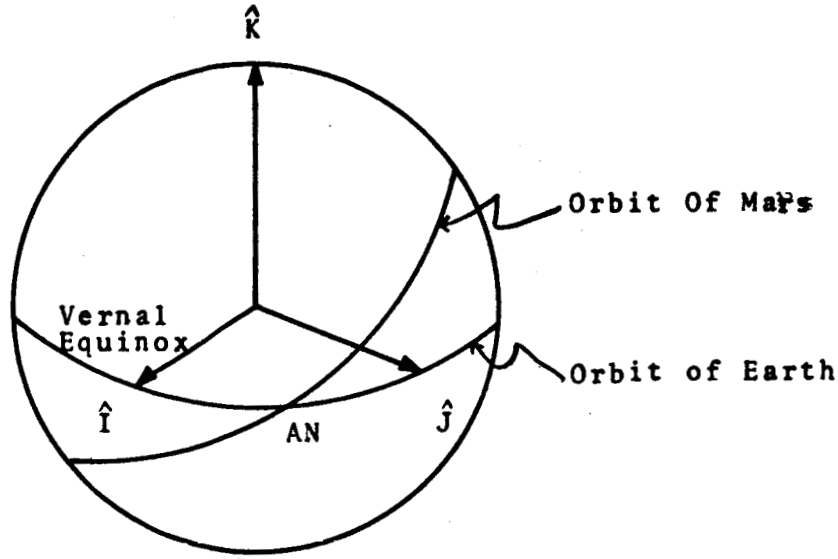

Figure A-1. Heliocentric Ecliptic Coordinates

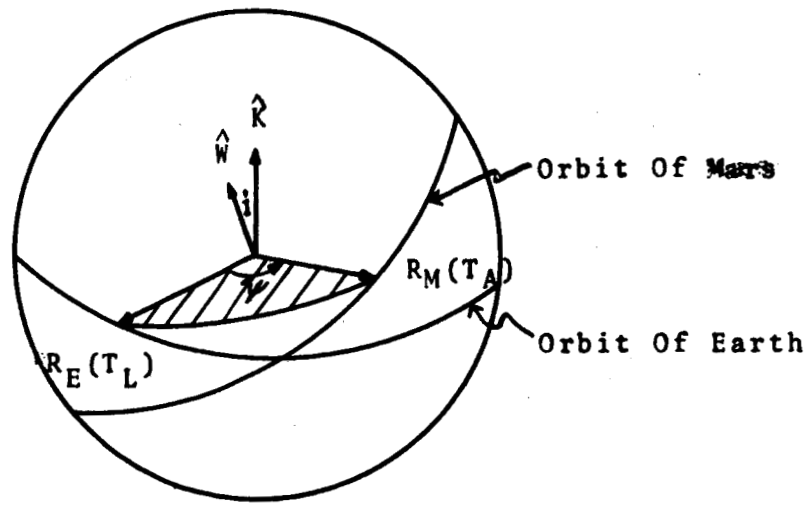

Figure A-2. Plane Of Transfer Ellipse

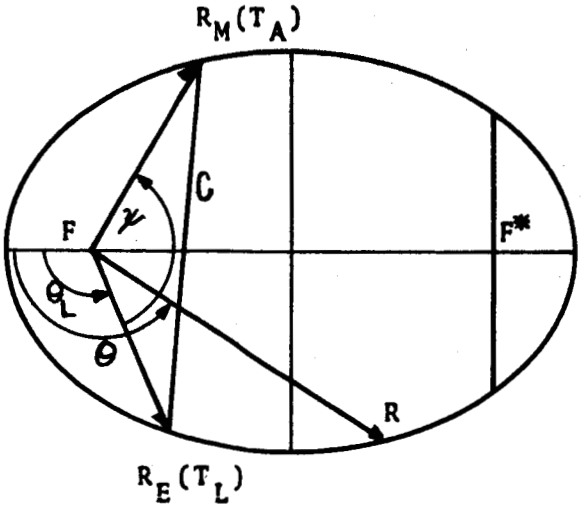

Figure A-3. Transfer Ellipse $\psi < \pi$

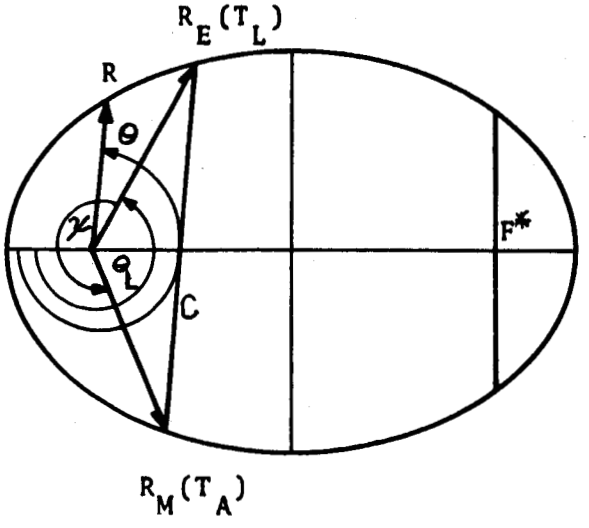

Figure A-4. Transfer Ellipse $\pi < \psi < 2\pi$

III. VEHICLE POSITION VECTOR IN HELIOCENTRIC ECLIPTIC MEAN OF LAUNCH DATE COORDINATES:

Consider a right-handed coordinate system $(\hat{X}'', \hat{Y}'', \hat{W})$ with $\hat{X}''$ in the direction $\Theta = 0$. Then, from Figures A-3 and A-4,

$$\vec{R}_{veh} = R\cos\Theta\,\hat{X}'' + R\sin\Theta\,\hat{Y}'' \qquad \text{(A-10)}$$

and, from equation (A-7)

$$\vec{R}_{veh} = \frac{a(1-\epsilon^2)}{(1+\epsilon\cos\Theta)}\,[\cos\Theta\,\hat{X}'' + \sin\Theta\,\hat{Y}''] \qquad \text{(A-11)}$$

Now consider the right-handed coordinate system

$$\frac{\vec{R}_E(T_L)}{\left|\vec{R}_E(T_L)\right|}\ \hat{Y}',\ \hat{W}.$$

Then,

$$\vec{R}_{veh} = \frac{a(1-\epsilon^2)}{(1+\epsilon\cos\Theta)}\left[\cos(\Theta-\Theta_L)\frac{\left|\vec{R}_E(T_L)\right|}{\left|\vec{R}_E(T_L)\right|}\hat{+} \sin(\Theta-\Theta_L)\hat{Y}\right] \qquad \text{(A-12)}$$

Now consider the ecliptic mean-of-launch date right-handed coordinate system $(\hat{I}, \hat{J}, \hat{K})$. The unit vector $\hat{I}$ is in the direction of the vernal equinox; $\hat{K}$ is perpendicular to the ecliptic plane. The angle i is the angle between $\hat{K}$ and $\hat{W}$; and let the angle ρ be the angle between $\frac{\vec{R}_E(T_L)}{\left|\vec{R}_E(T_L)\right|}$ and $\hat{I}$, the direction of the vernal equinox. Thus,

$$\cos i = \hat{W}\cdot\hat{K}$$

$$\sin i = \operatorname{sgn}\left[(\hat{K}\times\hat{W})\cdot\frac{\vec{R}_E(T_L)}{\left|\vec{R}_E(T_L)\right|}\right](1-\cos^2 i)^{1/2} \qquad \text{(A-13)}$$

and

$$\cos\rho = \frac{\vec{R}_E(T_L)}{\left|\vec{R}_E(T_L)\right|}\cdot\hat{I}$$

$$\sin\rho = \operatorname{sgn}\left[\left(\frac{\vec{R}_E(T_L)}{\left|\vec{R}_E(T_L)\right|}\times\hat{I}\right)\cdot\hat{K}\right](1-\cos^2\rho)^{1/2} \qquad \text{(A-14)}$$

Therefore, in order to transfer to heliocentric ecliptic coordinates, first rotate about the $\vec{R}_E(T_L)$ axis i degrees by $\frac{\vec{R}_E(T_L)}{|\vec{R}_E(T_L)|}$ means of the matrix $E_1(-i)$, and then rotate ρ degrees about the $\hat{R}$ axis by means of the matrix $E_3(\rho)$. Quantities $E_1(i)$ and $E_3(\rho)$ are given below.

$$E_1(i) = \begin{bmatrix} 1 & 0 & 0 \\ 0 & \cos i & -\sin i \\ 0 & \sin i & \cos i \end{bmatrix} \qquad \text{(A-15)}$$

$$E_3(\rho) = \begin{bmatrix} \cos\rho & -\sin\rho & 0 \\ \sin\rho & \cos\rho & 0 \\ 0 & 0 & 1 \end{bmatrix} \qquad \text{(A-16)}$$

Thus,

$$\vec{R}_{veh}\ (\hat{I}\ \hat{J}\ \hat{K}) = E_3(\rho)\ E_1(-i)\vec{R}_{veh}\left[\frac{\vec{R}_E(T_L)}{|\vec{R}_E(T_L)|}\ ,\ \hat{Y}, \hat{W}\right] \qquad \text{(A-17)}$$

Equation (A-17) is an expression for the vehicle position in heliocentric ecliptic mean-of-launch-date coordinates. It is given as a function of θ. However, θ may be expressed as a function of t, the time after launch, as follows: (A derivation of this expression may be found in Refs. A-2 and A-3).

When $0 \le \theta_L \le \pi$ and $0 \le \theta_L + \gamma \le \pi$
or when $\pi \le \theta_L \le 2\pi$ and $\pi \le \theta_L + \gamma \le 2\pi$

$$\text{then } t = \sqrt{a^3/GM_S}\ [(\alpha - \sin\alpha) - (\beta - \sin\beta)] \qquad \text{(A-18)}$$

where G = universal gravitational constant
M_S = mass of the sun

(A-18) Cond.

$$\sin \alpha/2 = \sqrt{\frac{|R_{veh}\ (T)| + |R_E(T_L)| - |C|}{4a}}$$

$$\sin \beta/2 = \sqrt{\frac{|R_{veh}\ (T)| + |R_E(T_L)| + |C|}{4a}}$$

$$\vec{C} = \vec{R}_{veh}\ (T) - \vec{R}_E(T_L)$$

In all other cases

$$t = \sqrt{a^3/GMs}\ [\ 2\pi - (\alpha - \sin\alpha) - (\beta - \sin\beta)\ ] \qquad (A\text{-}19)$$

Since the position of the vehicle has been expressed in heliocentric-ecliptic-mean-of-launch date coordinates as a function of Θ and Θ_L, and t has been expressed as a function of these variables, an expression has been obtained for the vehicle position as a function of the time t after launch.

IV. RELATIVE POSITION OF VEHICLE TO EARTH

Using equations (A-17) and(A-18), $\vec{R}_{veh}$ can be computed as a function of t, the time after launch in heliocentric ecliptic mean-of-launch-date coordinates; and using equation (A-3), $\vec{R}_e$ can be computed as a function of t in the same coordinates. Then, the relative position of the vehicle to Earth can be computed in heliocentric ecliptic mean-of-launch date coordinates.

$$\vec{R}_{veh\text{-}E}(t)_{\hat{I}\hat{J}\hat{K}} = \vec{R}_{veh\ \hat{I}\hat{J}\hat{K}}(t) - \vec{R}_{E\ \hat{I}\hat{J}\hat{K}}(t) \qquad (A\text{-}20)$$

where

$$t = T - T_L$$

To obtain the position of the vehicle relative to a particular lattitude and longitude on Earth, the relative position of the vehicle is first transformed from heliocentric ecliptic to heliocentric equatorial, by means of the matrix $E_1(e)$, where $E_1(e)$ is defined as in equation (A-2). Note that:

$$E_1(e) = E_1^{-1}(-e) \ ; \text{ and } E_1^{-1}(e) = E_1(-e) \qquad (A\text{-}21)$$

that is,

$$\vec{R}_{veh\text{-}E\ \hat{i}\hat{j}\hat{k}}(t) = \vec{E}^{1}(e)\ \vec{R}_{veh\text{-}E\ \hat{I}\hat{J}\hat{K}}(t) \qquad (A\text{-}22)$$

where $\hat{i}\hat{j}\hat{k}$ indicates heliocentric equatorial coordinates.

Now the relative position of the vehicle in heliocentric equatorial coordinates is just the position of the vehicle in geocentric equatorial coordinates. Thus,

$$\vec{R}_{veh}(t)_{\hat{I}\hat{L}\hat{P}} = \vec{R}_{veh\text{-}E}(t)_{\hat{i}\hat{j}\hat{k}} = E(e)\,\vec{R}_{veh\text{-}E}(t)_{\hat{I}\hat{J}\hat{K}} \qquad \text{(A-23)}$$

where the subscript $\hat{I}\hat{L}\hat{P}$ indicates geocentric equatorial coordinates.

At a given point on the Earth defined by angles α and σ (see Figure A-5),

$$\vec{R}_{veh}(t, \alpha\ \sigma)_{VEN} = [E_2(-\sigma)\,E_3(\alpha)\,\vec{R}_{veh}(t)_{\hat{I}\hat{L}\hat{P}} - r\hat{V}] \qquad \text{(A-24)}$$

where r = radius of the Earth quantity E_3 has been defined in equation (A-16), and E_2 is defined below.

$$E_2(\sigma) = \begin{bmatrix} \cos\sigma & 0 & \sin\sigma \\ 0 & 1 & 0 \\ -\sin\sigma & 0 & \cos\sigma \end{bmatrix} \qquad \text{(A-25)}$$

The position of the Earth in the coordinate system on the vehicle $(\hat{S}_1\ \hat{S}_2\ \hat{S}_3)$ is given by

$$\vec{R}_E(t)_{(\hat{S}_1\hat{S}_2\hat{S}_3)} = E_1(\eta_3)\,E_2(-\eta_2)\,E_3(\eta_1)\,(\vec{R}_{E\text{-}veh}(t)_{\hat{I}\hat{J}\hat{K}}) \qquad \text{(A-26)}$$

where

$$\vec{R}_{E\text{-}veh}(t) = -\vec{R}_{veh\text{-}E}(t) = \vec{R}_E(t) - \vec{R}_{veh}(t)$$

and η_1, η_2, η_3, are defined in Figure A-6.

V. RELATIVE VELOCITY OF VEHICLE AND EARTH

The velocity of the vehicle in the heliocentric ecliptic mean-of-launch-date system is given by

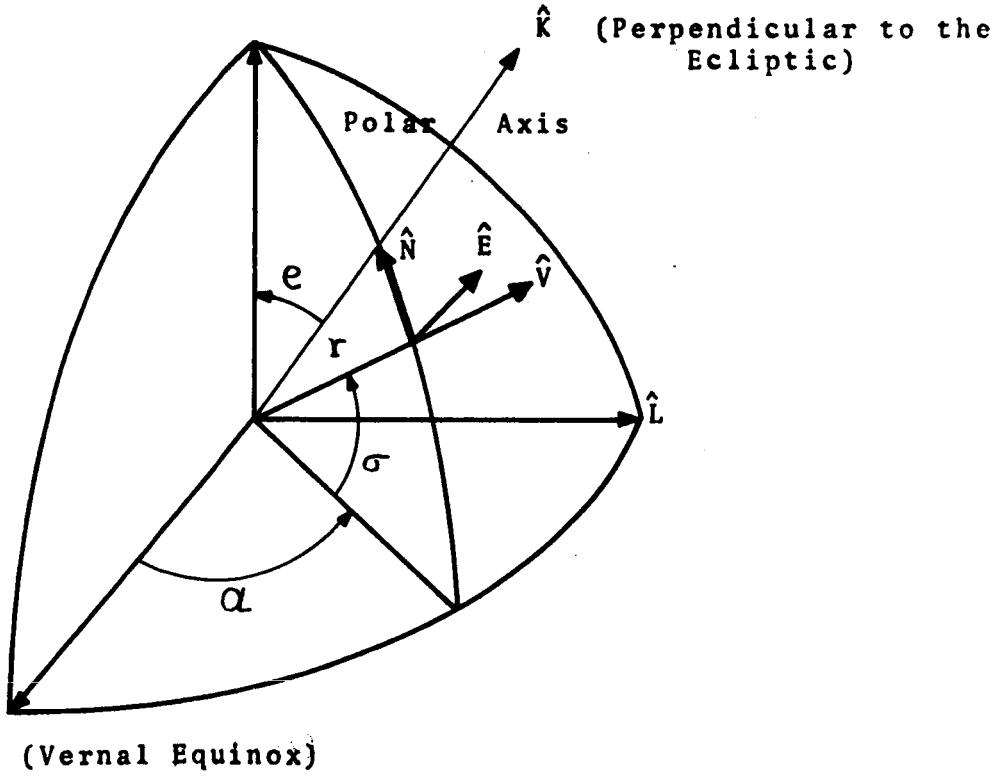

Figure A-5. Ecliptic ($\hat{I}\hat{J}\hat{K}$) Geocentric Equatorial ($\hat{I}\hat{L}\hat{P}$) and ($\hat{V}\hat{E}\hat{N}$) Coordinates

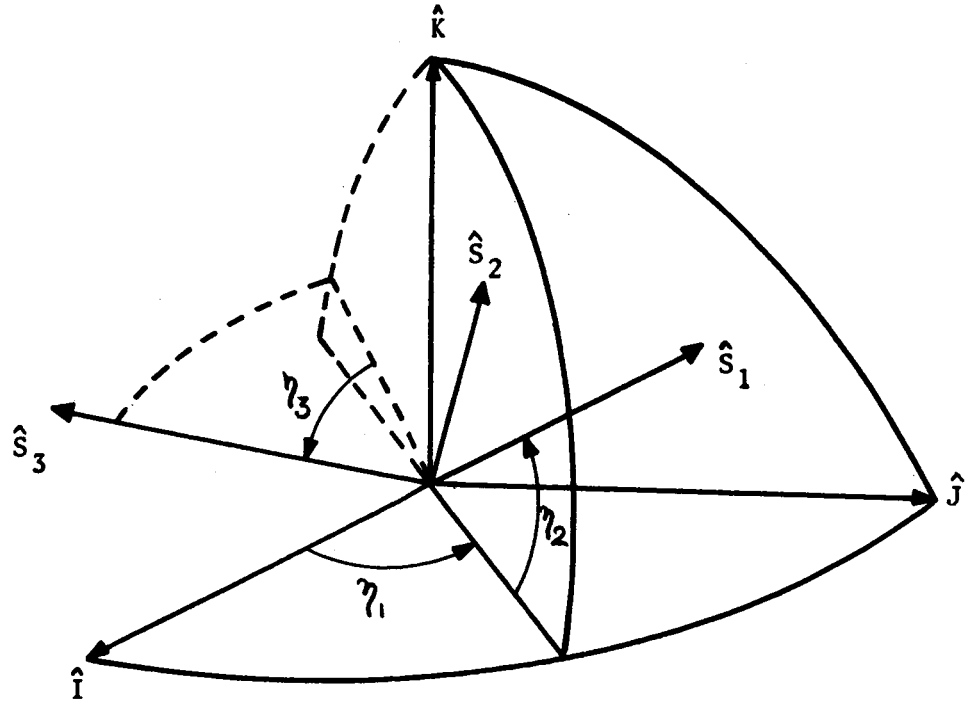

Figure A-6. Ecliptic $\hat{I}\hat{J}\hat{K}$ and Vehicle $\hat{S}_1\hat{S}_2\hat{S}_3$ Coordinates

$$\vec{V}_{veh}{}_{\hat{I}\hat{J}\hat{K}}(t) = \frac{\left|\vec{V}_{veh}(t)\right|}{\left|\vec{R}_{veh}(t)\right|}\left[\left(\hat{W} \times \vec{R}_{veh}(t)\right)\cos\Gamma_{veh} + \vec{R}_{veh}(t)\sin\Gamma_{veh}\right] \quad (A\text{-}27)$$

Where $\vec{R}_{veh}$ and $\hat{W}$ are expressed in heliocentric coordinates

$$\left|\vec{V}_{veh}(t)\right| = \sqrt{GM_S\left(\frac{2}{\left|\vec{R}_{veh}(t)\right|} - 1/a\right)}$$

$$\sin\Gamma_{veh} = \left[\sqrt{\frac{\left|\vec{R}_{veh}(t)\right|}{(1-\epsilon^2)\,(2a-\left|\vec{R}_{veh}\right|)}}\right]\epsilon \sin\theta$$

$$0 \leq \Gamma_{veh} \leq \pi/2 \quad \text{if} \quad 0 \leq \theta \leq \pi$$

$$-\pi/2 \leq \Gamma_{veh} \leq 0 \quad \text{if} \quad \pi \leq \theta \leq 2\pi$$

The velocity of the Earth in heliocentric ecliptic mean-of-launch-date coordinates is given by:

$$\vec{V}_{E}{}_{(\hat{I}\hat{J}\hat{K})}(t) = \frac{\left|V_E(t)\right|}{\left|R_E(t)\right|}\left[(\hat{K} \times \vec{R}_E(t))\cos\Gamma_E + \vec{R}_E(t)\sin\Gamma_E\right] \quad (A\text{-}28)$$

where $\vec{R}_E(t)$ is expressed in heliocentric coordinates

$$\left|V_E(t)\right| = \sqrt{GM_S\left(\frac{2}{\left|\vec{R}_E(t)\right|} - \frac{1}{a_E}\right)}$$

$$\sin\Gamma_E = \left[\sqrt{\frac{\left|\vec{R}_E\right|}{(1-\epsilon_E{}^2)\,(2a_E-\left|\vec{R}_E(t)\right|)}}\right]\epsilon_E \sin\theta_E$$

$$\sin\theta_E = \frac{\vec{R}_E}{\left|\vec{R}_E\right|} \cdot \hat{Q}$$

$$\cos\theta_E = \frac{\vec{R}_E}{\left|\vec{R}_E\right|} \cdot \hat{U}$$

$$\hat{Q} = \hat{K} \times \hat{U}$$

$\hat{U}$ is the unit vector towards the Earth perihilion

a_E = the semi-major axis of the Earth's orbit

e_E = the eccentricity of the Earth's orbit

Therefore, the relative velocity of the vehicle to the Earth in heliocentric ecliptic mean-of-launch-date coordinates is given by:

$$\vec{V}_{\substack{veh-E \\ \hat{I}\hat{J}\hat{K}}}(t) = \vec{V}_{\substack{veh \\ \hat{I}\hat{J}\hat{K}}}(t) - \vec{V}_{\substack{E \\ \hat{I}\hat{J}\hat{K}}}(t) \qquad \text{(A-29)}$$

The relative velocity of the vehicle in other coordinate systems is indicated in Table A-I.

Table A-I summarizes the results of this appendix. All the symbols used in the table are presented in the body of this appendix.

TABLE A-1. TRAJECTORY DATA

VECTOR	COORDINATE SYSTEM	SYMBOL	EXPRESSION
Position of Earth	Heliocentric Equatorial mean of 1950.0	$R_E^1(t)$	Found from ephemerides
Position of Earth	Heliocentric ecliptic mean-of-launch date	$\vec{R}_{E_{\hat{I}\hat{J}\hat{K}}}(t)$	$\vec{R}_{E_{\hat{I}\hat{J}\hat{K}}} = E_1(-e)A(T_L)\,R_E^1$
Position of Vehicle	Heliocentric ecliptic mean-of-launch date	$\vec{R}_{veh_{\hat{I}\hat{J}\hat{K}}}(t)$	$R_{veh_{\hat{I}\hat{J}\hat{K}}}(t) = E_3(\rho)\,E_1(-i)\begin{bmatrix}\frac{a(1-\epsilon^2)}{(1+\epsilon\cos\theta)}\end{bmatrix}\begin{bmatrix}\cos(\theta-\theta_L)\\ \sin(\theta-\theta_L)\end{bmatrix}$
Relative position of Vehicle to Earth	Heliocentric ecliptic mean-of-launch date	$\vec{R}_{veh-E_{IJK}}(t)$	$\vec{R}_{veh-E_{IJK}}(t) = \vec{R}_{veh_{IJK}}(t) - R_{E_{IJK}}(t)$
Position of Vehicle	Geocentric equatorial mean-of-launch date	$\vec{R}_{veh_{\hat{I}\hat{L}\hat{P}}}(t)$	$R_{veh_{ILP}}(t) = E_1(e)\,R_{veh_{IJK}}(t)$
Position of Vehicle	Local coordinate system on Earth	$\vec{R}_{veh_{\hat{V}\hat{E}\hat{N}}}(t)$	$\vec{R}_{veh_{VEN}}(t) = [E_2(-\sigma)E_3(\alpha)R_{veh_{ILP}} - r\,\hat{V}]$
Position of Earth	Vehicle coordinates	$\vec{R}_{E_{\hat{S}_1\hat{S}_2\hat{S}_3}}(t)$	$\vec{R}_{E_{\hat{S}_1\hat{S}_2\hat{S}_3}}(t) = E_1(\eta_3)E_2(-\eta_2)E_3(\eta_1)\left[-\vec{R}_{veh-E_{\hat{I}\hat{J}\hat{K}}}(t)\right]$
Velocity of Vehicle	Heliocentric ecliptic mean-of-launch date	$\vec{V}_{veh_{IJK}}(t)$	$V_{veh_{IJK}}(t) = \lvert\vec{V}_{veh}\rvert\left[\frac{(\hat{N}\times\vec{R}_{veh}(t))_{IJK}}{\lvert\vec{R}_{veh}(t)\rvert}\cos\Gamma_{veh} + \vec{R}_{veh_{IJK}}(t)\sin\Gamma_{veh}\right]$
Velocity of Earth	Heliocentric ecliptic mean-of-launch date	$\vec{V}_{E_{IJK}}(t)$	$V_{E_{IJK}}(t) = \lvert V_E\rvert\left[\frac{(\hat{K}\times\vec{R}_E(t))_{IJK}}{\lvert\vec{R}_E(t)\rvert}\cos\Gamma_E + \vec{R}_{E_{IJK}}(t)\sin\Gamma_E\right]$
Relative Velocity of Vehicle to Earth	Heliocentric ecliptic mean-of-launch date	$V_{veh-E_{IJK}}(t)$	$V_{veh-E_{IJK}} = \vec{V}_{veh_{IJK}}(t) - \vec{V}_{E_{\hat{I}\hat{J}\hat{K}}}(t)$
Velocity of Vehicle	Geocentric equatorial mean-of-launch date	$\vec{V}_{veh_{\hat{I}\hat{L}\hat{P}}}(t)$	$\vec{V}_{veh_{\hat{I}\hat{L}\hat{P}}}(t) = E_1(e)\,\vec{V}_{veh-E_{\hat{I}\hat{J}\hat{K}}}(t)$
Velocity of Vehicle	Local coordinate system on Earth	$\vec{V}_{veh_{\hat{V}\hat{E}\hat{N}}}(t)$	$\vec{V}_{veh_{\hat{V}\hat{E}\hat{N}}} = E_2(-\sigma)E_3(\alpha)\vec{V}_{veh_{\hat{I}\hat{L}\hat{P}}}(t) - v\hat{E}$ v=Earth's rotation velocity
Velocity of the Earth	Vehicle coordinate	$\vec{V}_{E_{\hat{S}_1\hat{S}_2\hat{S}_3}}(t)$	$V_{E_{S_1S_2S_3}}(t) = E_1(\eta_3)E_2(-\eta_2)E_3(\eta_1)\left[-\vec{V}_{veh-E_{\hat{I}\hat{J}\hat{K}}}(t)\right]$

APPENDIX B

TRANSIT TIME CORRECTIONS*

I. INTRODUCTION

The line of sight of an Earth-to-vehicle or vehicle-to-Earth transmitter must take into account the time required for signal transmission. During this time the relative positions of vehicle and Earth have changed.

II. EARTH-TO-VEHICLE TRANSMITTER

The transmitted signal travels with velocity c. Denoting the transit time as Δt,

$$\underset{\hat{V}\hat{E}\hat{N}}{R_{veh}}(t+\Delta t) = c\Delta t\,\hat{X} = \underset{\hat{V}\hat{E}\hat{N}}{\vec{R}_{veh}}(t) + \underset{\hat{V}\hat{E}\hat{N}}{\vec{V}_{veh}}(t)\left[\Delta t\right] \qquad \text{(B-1)}$$

where

$\underset{\hat{V}\hat{E}\hat{N}}{\vec{R}_{veh}}(t)$ = vehicle position in earth coordinate system at time t after launch

$\underset{\hat{V}\hat{E}\hat{N}}{\vec{V}_{veh}}(t)$ = vehicle velocity in Earth coordinate system at time t after launch

$\hat{X}$ is a unit vector in the direction of the transmitter

It is assumed that the velocity of the vehicle is constant during the transit time. Since $\frac{Vveh}{c} \ll 1$, special relativistic effects have been neglected. One must now solve for Δt.

Consider Figure B-1. From the law of cosines and the law of sines

$$\cos\alpha = \frac{c^2(\Delta t)^2 + \left|\underset{\hat{V}\hat{E}\hat{N}}{\vec{R}_{veh}}(t)\right|^2 - \left|\underset{\hat{V}\hat{E}\hat{N}}{\vec{V}_{veh}}(t)\right|^2(\Delta t)^2}{2c(\Delta t)\left|\vec{R}_{veh}(t)\right|} \qquad \text{(B-2)}$$

* Based on notes prepared by G. Schuster and S. Winsberg

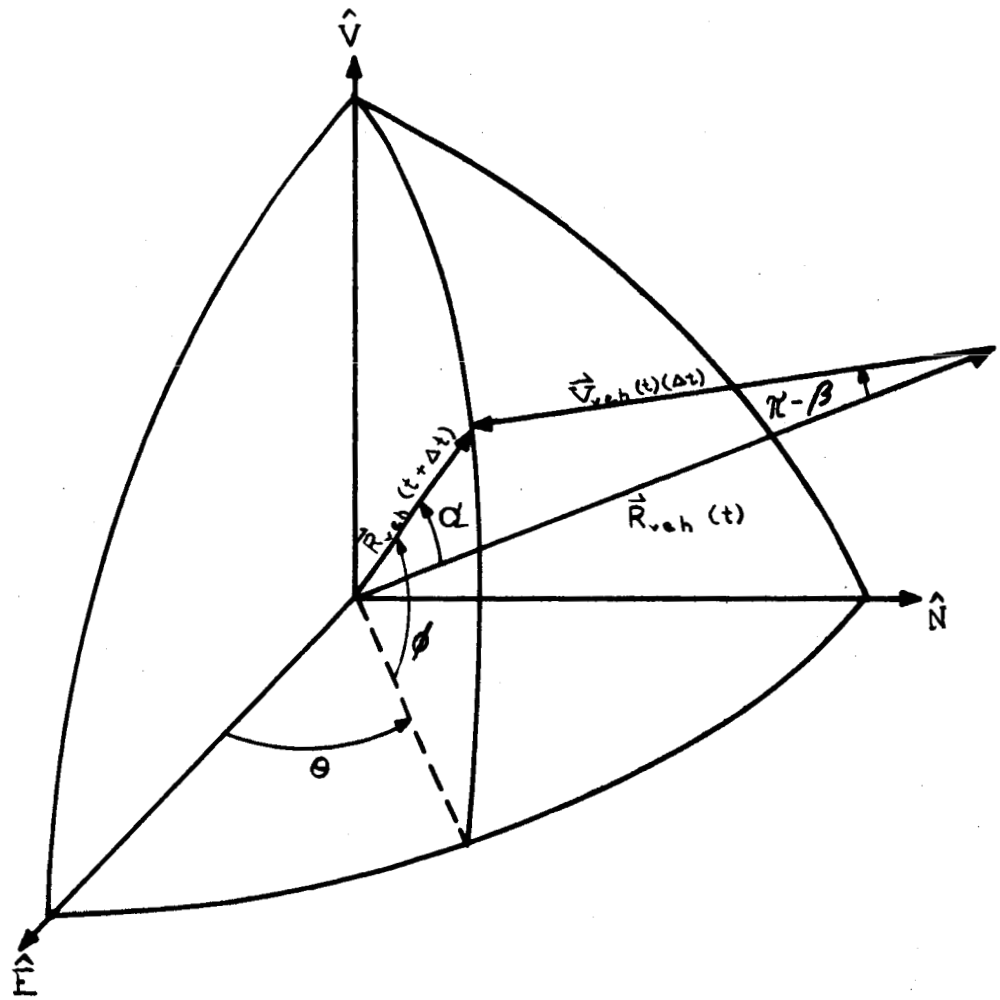

Figure B-1. Azimuth and Altitude Angles of Earth to Vehicle Transmitter

$$\cos\beta = \frac{\vec{R}_{veh}(t) \cdot \vec{V}_{veh}(t)}{\left|\vec{R}_{veh}(t)\right| \left|\vec{V}_{veh}(t)\right|} \qquad \text{(B-3)}$$

$$\sin\alpha = \frac{\left|V_{veh}(t)\right| \sin\beta}{c} \qquad \text{(B-4)}$$

Combining equations (B-2), (B-3), and (B-4)

$$\Delta t = \frac{2c\left|\vec{R}veh(t)\right| \cos\alpha \pm \sqrt{4c^2\left|\vec{R}_{veh}(t)\right|^2\cos^2\alpha - 4\left|\vec{R}_{veh}(t)\right|^2(c^2 - \left|V_{veh}(t)\right|^2)}_{veh}}{2(c^2 - v^2)} \qquad \text{(B-5)}$$

Re-arranging and manipulating equation (B-5)

$$\Delta t = \frac{c\left|\vec{R}_{veh}(t)\right| \cos\alpha \pm \left|\vec{V}_{veh}(t)\right| \left|\vec{R}_{veh}(t)\right| \cos\beta}{(c^2 - v^2)} \qquad \text{(B-6)}$$

or

$$\Delta t = \frac{\left|R_{veh}(t)\right| \left[\cos\alpha \pm \frac{\left|\vec{V}_{veh}(t)\right|}{c} \cos\beta\right]}{c\left[1 - \frac{|V_{veh}(t)|^2}{c^2}\right]} \qquad \text{(B-7)}$$

In order to determine the correct sign in equation (B-7), consider the following special cases.

Case I: $\alpha = 0$ $\beta = 0$: The vehicle is travelling away from the Earth in the line of sight. In this case the positive sign must be chosen

$$\Delta t = \frac{\left|\vec{R}_{veh}(t)\right| \left[1 + \frac{\left|V_{veh}(t)\right|}{c}\right]}{c\left[1 - \frac{|V_{veh}(t)|^2}{c^2}\right]}$$

Case II $\alpha = 0, \beta = \pi$: The vehicle is travelling towards the Earth in the direction of the line of sight. Again the positive sign must be chosen.

$$\Delta t = \frac{\left|\vec{R}_{veh}(t)\right| \left[1 - \frac{\left|\vec{V}_{veh}(t)\right|}{c}\right]}{c\left[1 - \frac{\left|V_{veh}(t)\right|^2}{c^2}\right]}$$

Therefore, in general

$$\Delta t = \frac{\left|\vec{R}_{veh}(t)\right| \left[\cos\alpha + \frac{\vec{V}_{veh}(t) \cos\beta}{c}\right]}{c\left[1 - \frac{\vec{V}_{veh}(t)^2}{c^2}\right]} \qquad \text{(B-8)}$$

Now consider equation (B-1). The transmitter must be oriented in the direction of the vector $\vec{R}_{veh_{\hat{V}\hat{E}\hat{N}}}(t + \Delta t)$, that is, in the direction of the unit vector $\hat{X}$. But

$$\hat{X} = \left[\frac{\vec{R}_{veh}(t)}{c(\Delta t)} + \frac{\vec{V}_{veh}(t)}{c}\right] \qquad \text{(B-9)}$$

where Δt is given by equation (B-8). Now $\hat{X}$ may be written as

$$\hat{X} = a\hat{N} + b\hat{E} + d\hat{V} \qquad \text{(B-10)}$$

From Figure B-1, the azimuth angle Θ, and altitude angle $\emptyset$ are then given by

$$\Theta = \tan^{-1}(a/b)$$
$$\emptyset = \tan^{-1}\left[\frac{d}{(a^2+b^2)^{1/2}}\right] \qquad \text{(B-11)}$$

III. VEHICLE-TO-EARTH TRANSMITTER

Consider Figure B-2. By analogy with the previous case

$$\vec{R}_{E_{\hat{S}_1\hat{S}_2\hat{S}_3}}(t+\Delta t) = c(\Delta t)\hat{Y} = \vec{R}_{E_{\hat{S}_1\hat{S}_2\hat{S}_3}}(t) + \vec{V}_{E_{\hat{S}_1\hat{S}_2\hat{S}_3}}(t)(\Delta t) \qquad \text{(B-12)}$$

where

$$\Delta t = \frac{\left|\vec{R}_{E_{\hat{S}_1\hat{S}_2\hat{S}_3}}(t)\right| \left[\cos\delta + \frac{\left|\vec{V}_{E_{\hat{S}_1\hat{S}_2\hat{S}_3}}(t)\right| \cos\gamma}{c}\right]}{c\left[1 - \frac{\left|V_{E_{\hat{S}_1\hat{S}_2\hat{S}_3}}(t)\right|^2}{c^2}\right]}$$

$\vec{R}_{E_{\hat{S}_1\hat{S}_2\hat{S}_3}}(t)$ = position of Earth in vehicle coordinate system

$\vec{V}_{E_{\hat{S}_1\hat{S}_2\hat{S}_3}}(t)$ = velocity of Earth in vehicle coordinate system

$\hat{Y}$ is a unit vector in the direction of the transmitter

c is the velocity of light

$$\sin\delta = \frac{\left|V_{E_{\hat{S}_1\hat{S}_2\hat{S}_3}}(t)\right|}{c} \sin\gamma \qquad \delta \leq \pi$$

$$\cos\gamma = \frac{\vec{R}_{E_{\hat{S}_1\hat{S}_2\hat{S}_3}}(t) \cdot \vec{V}_{E_{\hat{S}_1\hat{S}_2\hat{S}_3}}(t)}{\left|\vec{R}_{E_{\hat{S}_1\hat{S}_2\hat{S}_3}}(t)\right| \left|\vec{V}_{E_{\hat{S}_1\hat{S}_2\hat{S}_3}}(t)\right|} \qquad \gamma \leq \pi$$

Now consider equation (B-12) and Figure B-2. The transmitter must be oriented in the direction of the unit vector $\hat{Y}$.

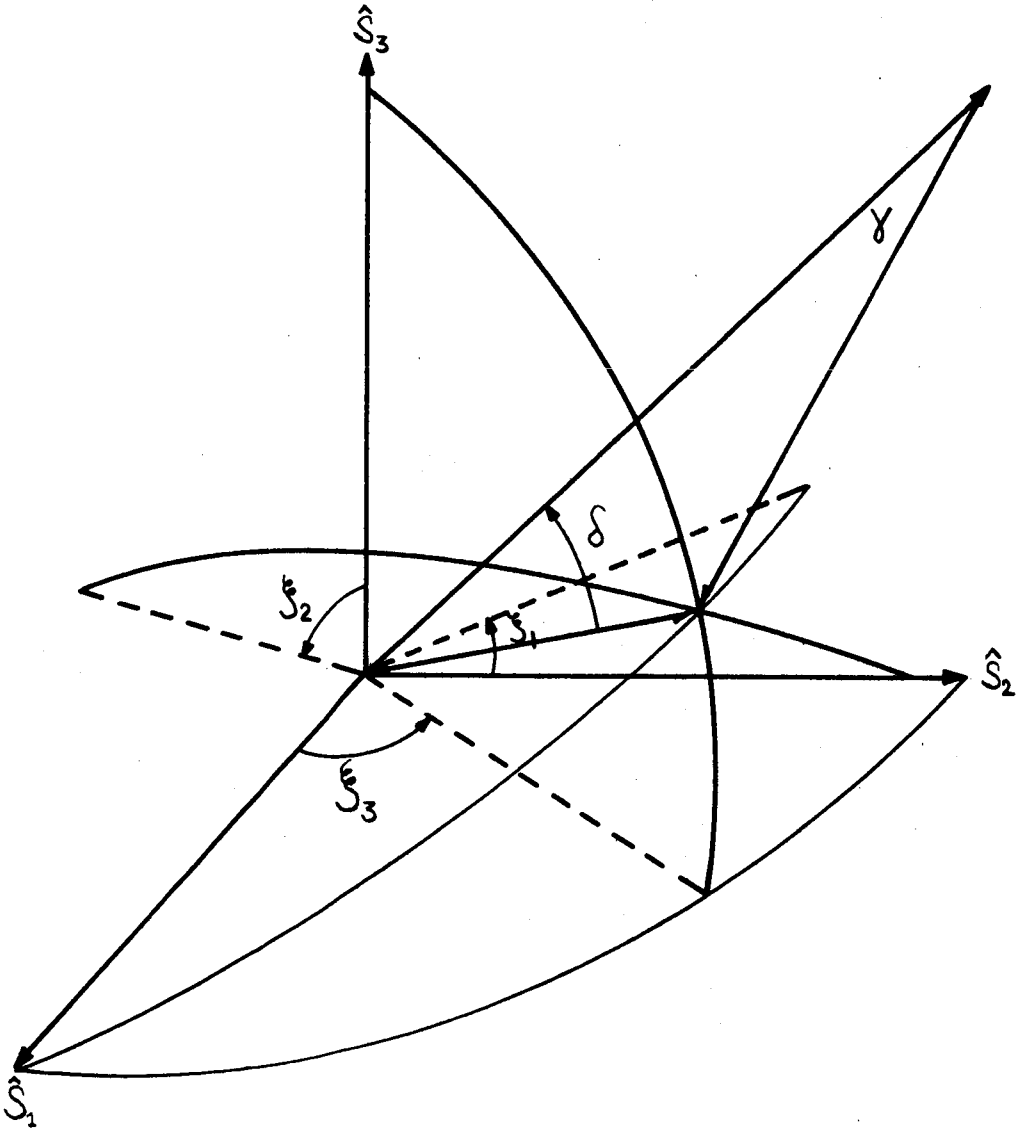

Figure B-2. Orientation of Vehicle to Earth Transmitter

$$\hat{Y} = \left[\frac{\vec{R}_E(t)}{\hat{S}_1\hat{S}_2\hat{S}_3} + \frac{\vec{V}_E(t)}{\hat{S}_1\hat{S}_2\hat{S}_3} \right] \qquad (B\text{-}13)$$

and Y may be written

$$Y = e\,\hat{S}_1 + f\,\hat{S}_2 + g\,\hat{S}_3 \qquad (B\text{-}14)$$

and the orientation angles ζ_1, ζ_2, and ζ_3 of the transmitter are thus given by

$$\begin{aligned} \zeta_1 &= \tan^{-1}[g/f] \\ \zeta_2 &= \tan^{-1}[e/g] \\ \zeta_3 &= \tan^{-1}[f/e] \end{aligned} \qquad (B\text{-}15)$$

The position and velocity vectors of the Earth and vehicle in the vehicle and Earth coordinate systems respectively are derived in Appendix A for a given trajectory. The coordinate systems are also discussed in Appendix A.

APPENDIX C

TRANSIT TIME AND ABERRATION CORRECTIONS*

I. INTRODUCTION

In Appendix B, the required line of sight of an Earth Station to vehicle or vehicle to Earth Station transmitter was derived as a function of trajectory data. A transit time correction was made in order to correct for the time required to transmit a signal from the Earth Station (or vehicle) to the vehicle (or Earth Station) owing to the relative velocity of the vehicle (or Earth Station) in the Earth Station (or vehicle) coordinate system. This correction is a ballistic correction and does not involve any special relativistic effects as all effects are referred to one coordinate system. However, in determining the required line of sight for the receiver, special relativistic effects must be considered, the reason being that a signal received in one coordinate system has been transmitted from another coordinate system moving with a relative velocity with respect to the first. This correction is called an aberration correction. The aberration correction may be made non-relativistically from a ballistic point of view. The received signal may be considered as having been retarded by a time Δt. Essentially, then, a transit time correction is being made. However, this approximation is only correct to first order in V/C.

II. RELATIVISTIC ABERRATION CORRECTION

The lead angle, α_{ab}, necessary to correct for aberration, is given by Ref. C-1:

$$\alpha_{ab} = \beta' - \beta \tag{C-1}$$

where

$$\sin\beta = \frac{\sin\beta' \left(1 - \frac{|\vec{V}_{rel}|^2}{C^2}\right)^{1/2}}{1 + \frac{|\vec{V}_{rel}|}{c}\cos\beta'} \tag{C-2}$$

$$\cos\beta' = \frac{\vec{R}_{obs_{rel}}(t) \cdot \vec{V}_{rel}(t)}{|\vec{R}_{obs}(t)|\ |\vec{V}_{rel}(t)|} \tag{C-3}$$

where

$\vec{R}_{obs_{rel}}(t)$ = the observed position of the vehicle (Earth Station) in the Earth Station (vehicle) coordinates.

* Based on notes prepared by S. Winsberg and G. Schuster

$\vec{V}_{rel}(t)$ = the velocity of the vehicle (Earth Station) in the Earth Station (vehicle) coordinates.

$|\vec{R}obs_{rel}(t)|$ = the measured range of the vehicle (Earth Station)

$\frac{\vec{R}obs(t)}{|\vec{R}obs(t)|}$ = the observed position vector of the vehicle (Earth Station)

$|\vec{V}rel_{(t)}| \cos\beta'$ = radial velocity of the vehicle (Earth Station) in the Earth Station (vehicle) coordinates measured from the doppler shift.

$\vec{V}rel(t)$ is calculated from the radial velocity and the trajectory data.

The receiver is pointed in the direction

$$\hat{X} = a_1 \hat{V} + b_1 \hat{E} + d_1 \hat{N}$$

or

$$= a_1 \hat{S}_1 + b_1 \hat{S}_2 + d_1 \hat{S}_3 \qquad \text{(C-4)}$$

where the azimuth and elevation angles S_1 and ϕ_1 of the receiver are known.

$$S_1 = \tan^{-1} \frac{d_1}{b_1} \qquad \text{(C-5)}$$

$$\phi_1 = \tan^{-1} \left[\frac{a_1}{(b_1^2 + d_1^2)^{1/2}} \right]$$

III TRANSIT TIME CORRECTION

Let Δt denote the time required to transmit the signal.

Let Γ denote the delay time between receipt of the signal and transmission of a second signal based on information received. (The delay time, Γ, is due to information processing.) Then, from Figure C-1 and Ref. C-1,

$$|\vec{R}| = \frac{|\vec{R}rel\ obs\ (t)| \sin\beta'}{\sin\beta} \qquad \text{(C-7)}$$

$$\sin\alpha_T = \frac{|\vec{V}rel(t)|}{C} [\sin\beta] \left[1 + \frac{\Gamma}{\Delta t}\right] \qquad \text{(C-8)}$$

$$\Delta t = \frac{\frac{|\vec{V}rel|\,|\vec{R}|\cos\beta}{C^2} + \frac{|V|_{rel}^2 \Gamma}{C^2} + \frac{1}{C}\sqrt{|R|^2\left(1 - \frac{|V|_{rel}^2}{C^2}\sin^2\beta\right) + |Vrel|\Gamma^2 + 2|V_{rel}|\Gamma|\vec{R}|\cos\beta}}{\left(1 - \frac{|Vrel|^2}{C^2}\right)} \qquad \text{(C-9)}$$

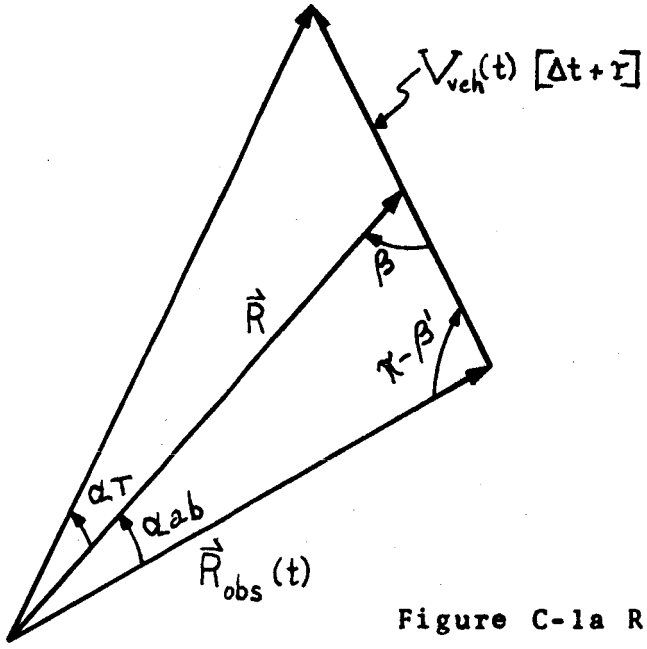

Figure C-1a Relativistic Diagram

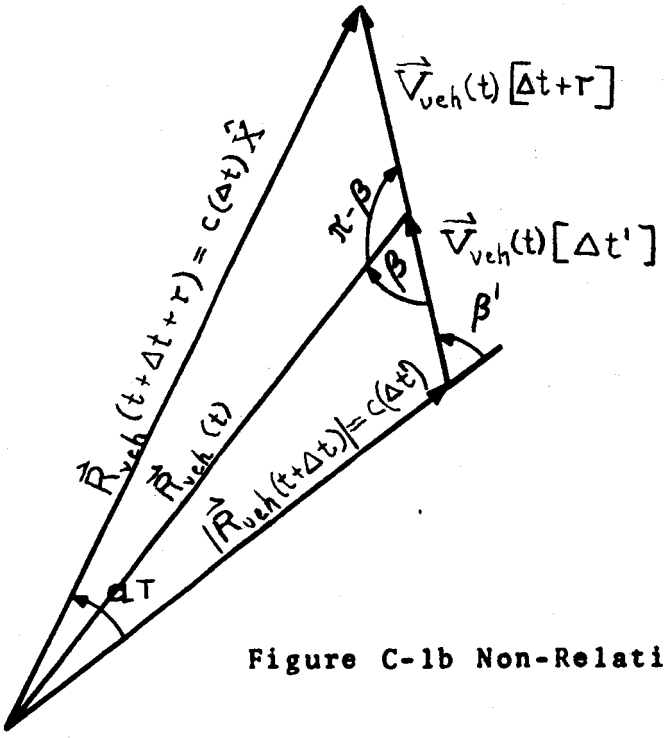

Figure C-1b Non-Relativistic Diagram

Figure C-1 Lead Angle Correction Due To Aberration and Transit Time Effects

IV TOTAL CORRECTION

The total lead angle, α, is given by

$$\alpha = \alpha_T + \alpha_{ab} \qquad \text{(C-10)}$$

The transmitter must be pointed in the direction of the unit vector $\hat{X}$, where

$$\hat{X} = \frac{\vec{R}}{c(\Delta t)} + \frac{\vec{V_{rel}}}{c}\left[1 + r/\Delta t\right] \qquad \text{(C-11)}$$

$$= a\,\hat{V} + b\,\hat{E} + d\,\hat{N}$$
or
$$= a\,\hat{S}_1 + b\,\hat{S}_2 + d\,\hat{S}_3 \qquad \text{(C-12)}$$

The azimuth and elevation angles of the transmitter, ξ and ϕ, are then given by (see Figure C-2):

$$\xi = \tan^{-1}\frac{d}{b} \qquad \text{(C-13)}$$

$$\phi = \tan^{-1}\left(\frac{a}{(b^2 + d^2)^{1/2}}\right) \qquad \text{(C-14)}$$

In the non-relativistic limit (that is, to order $\left|\frac{V_{rel}}{c}\right|$ the total lead angle $\alpha_{non\text{-}rel}$ is given by (from Figure C-1b):

$$\sin\alpha_{non\text{-}rel} = \frac{|\vec{V}_{rel}|}{c}\sin\beta'\left[1 + \frac{\Delta t'}{\Delta t} + \frac{r}{\Delta t}\right] \qquad \text{(C-15)}$$

where

$$\Delta t' = \frac{\left|R^{obs}_{rel}(t)\right|}{c} \qquad \text{(C-16)}$$

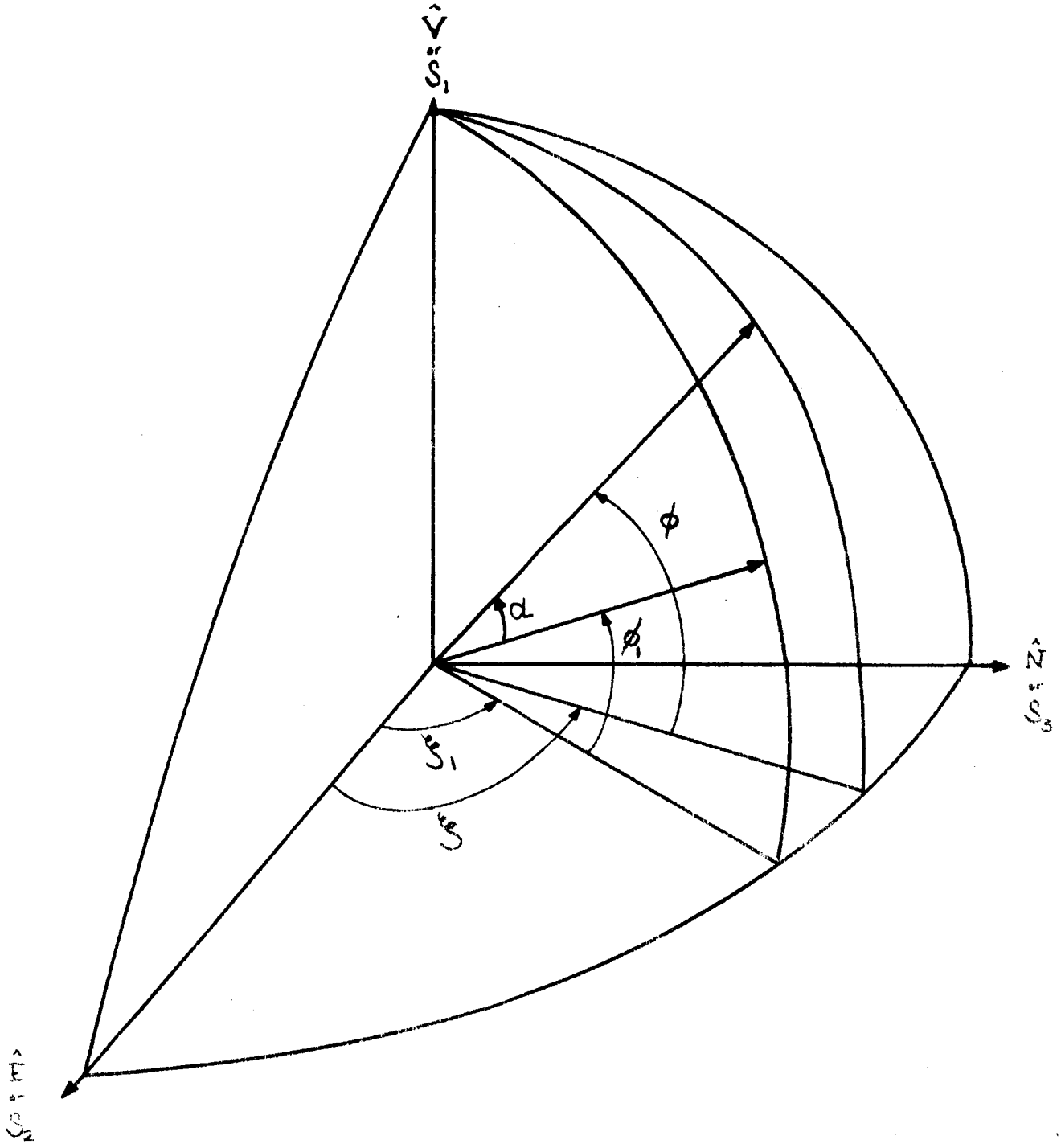

Figure C-2 Azimuth And Elevation Angles of Earth Station Vehicle Receiver and Transmitter

APPENDIX D

LEAD ANGLE, AZIMUTH AND ELEVATION RATES*

I INTRODUCTION

In this appendix $\vec{R}rel$ and $\vec{V}rel$ will denote the relative position and velocity of the vehicle to Earth Station, or vice versa. The Earth Station coordinates will be denoted as $\hat{V}$ $\hat{E}$ $\hat{N}$; and those of the vehicle as $\hat{S}_1$ $\hat{S}_2$ $\hat{S}_3$. Thus, all equations will be written to apply to transmission from the vehicle to the Earth Station, or from the Earth Station to the vehicle.

II RATE OF CHANGE OF THE LEAD ANGLE

From Appendix C, the lead angle, α, may be written as

$$\alpha = \alpha_{ab} + \alpha_T \tag{D-1}$$

where

$$\alpha_{ab} = \beta - \beta' \tag{D-2}$$

$$\sin\beta = \frac{\sin\beta' \left[1 - \frac{|Vrel|^2}{c^2}\right]^{1/2}}{1 + \frac{|Vrel|}{c}\cos\beta'} \tag{D-3}$$

$$\cos\beta' = \frac{\vec{R}obs_{rel}(t) \cdot \vec{V}rel(t)}{|\vec{R}obs(t)|\ |\vec{V}rel(t)|} \tag{D-4}$$

$$\sin\alpha_T = \frac{|\vec{V}rel(t)|}{c}[\sin\beta]\left[1 + \frac{r}{\Delta t}\right] \tag{D-5}$$

$$\Delta t = \frac{|\vec{V}rel|\,|R|\cos\beta}{c^2} + \frac{|Vrel|^2 r}{c^2} + \frac{1}{c}\sqrt{|R|^2\left[1 - \frac{|Vrel|^2\sin^2\beta}{c^2}\right] + |Vrel|^2 r^2 + 2|Vrel|r|\vec{R}|\cos} \tag{D-6}$$

$$|\vec{R}| = \frac{|\vec{R}rel\ obs\ (t)|\ \sin\beta'}{\sin\beta} \tag{D-7}$$

Quantities $\vec{R}rel$ obs (t), Vrel (t), and r, are defined in Appendix C as follows:

$\vec{R}obs$ rel (t) is the observed position of the vehicle (Earth) in Earth Station (vehicle) coordinates;

$\vec{V}rel$ is the relative velocity of the vehicle (Earth Station) in Earth Station (vehicle) coordinates.

* Based on notes prepared by S. Winsberg and G. Schuster

$\frac{|V_{rel}|}{c}$ However, the total lead angle, α, may be written to order as,

$$\alpha = \left[2 + \frac{r}{\Delta t} + \text{terms of order } \frac{|V_{rel}|^2}{c^2} \text{ or greater}\right]\left[\frac{|V_{rel}| \sin\beta'}{c}\right] \qquad \text{(D-8)}$$

where β' is defined in equation (4).

Therefore, when $\frac{r}{\Delta t} < 1$ to order $\frac{|V_{rel}|}{c}$:

$$\frac{d\alpha}{dt} = \frac{2}{c}\left\{\frac{d|V_{rel}|}{dt}\sin\beta' - \frac{|\vec{V}_{rel}|}{\sin\beta'}\left[\frac{|\vec{R}_{rel}||\vec{V}_{rel}|}{}\left(\frac{d\vec{R}_{rel}}{dt}\cdot\vec{V}_{rel} + \frac{d\vec{V}_{rel}}{dt}\cdot\vec{R}_{rel}\right) - \vec{R}_{rel}\cdot\vec{V}_{rel}\left(|V_{rel}|\frac{d|R_{rel}|}{dt} + |R_{rel}|\frac{d|V_{rel}|}{dt}\right)\right]\right\} \qquad \text{(D-9)}$$

$$= \frac{2}{c}\left\{\frac{d|V_{rel}|}{dt}\left(\sin\beta' + \frac{\cot\beta'}{\sec\beta'}\right) + \frac{\cot\beta'}{\sec\beta'}\left[\frac{|\vec{V}_{rel}|}{|R_{rel}|}\frac{d\vec{R}_{rel}}{dt}\right] - \frac{1}{\tan\beta'}\left[\frac{|V_{rel}|^2}{|R_{rel}|} + \frac{d\vec{V}_{rel}}{dt}\cdot\frac{\vec{R}_{rel}}{|\vec{R}_{rel}|}\right]\right\}$$

where

$$\frac{d\vec{R}_{rel}}{dt} = \vec{V}_{rel} \qquad \text{(D-10)}$$

$$\vec{R}_{rel} = \pm\left\{E_2(-\sigma)E(\alpha)\left\{\frac{K_1}{(1+\epsilon\cos\theta)}\begin{bmatrix}\cos(\theta-\theta_L)\\ \sin(\theta-\theta_L)\\ 0\end{bmatrix} - K_2 A \vec{R}_E'(t)\right\}\right\} \qquad \text{(D-11)}$$

$$|R_{rel}| = E_2(-\sigma)E_3(\alpha)\left\{\frac{K_1^2}{(1+\epsilon\cos\theta)^2} + A^2K_2^2|R_E'(t)|^2 + \frac{2K_2K_3A}{(1+\epsilon\cos\theta)}\left[R_E'(t)\cdot\begin{matrix}\cos(\theta-\theta_L)\\ \sin(\theta-\theta_L)\\ 0\end{matrix}\right]\right\} \qquad \text{(D-12)}$$

$$\vec{V}_{rel} = \pm\left\{E_2(-\sigma)E_3(\alpha)K_1\left\{\frac{|\vec{V}_{sv}|}{|\vec{R}_{sv}(t)|}\left[\hat{W}\times\vec{R}_{sv}(t)\cos\Gamma_{sv} + \vec{R}_{sv}(t)\sin\Gamma_{sv}\right] - \frac{|\vec{V}_E|}{|\vec{R}_E(t)|}\left(\hat{K}\times\vec{R}_E(t)\cos\Gamma_E + R_E\sin\Gamma_E\right)\right\}\right\} \qquad \text{(D-13)}$$

$$|\vec{V}_{rel}| = E_2(-\sigma)E_3(\alpha)K_1\left\{|V_{sv}|^2 + |V_E|^2 + v^2 + 2v(\hat{V}_E\cdot\hat{E}) + 2\vec{V}_v\cdot(\vec{V}_E + v\hat{L}\right] \qquad \text{D-14)}$$

$$\frac{d\theta}{dt} = \sqrt{\frac{GM_s}{a(1+\epsilon)^2}}\left(1+\epsilon\cos\theta\right)^2 \qquad \text{(D-15)}$$

All the above quantities are defined in Appendix A, as are K2 and K1 (constants of the motion).

Where there is a (±) sign, the plus sign is for Earth Station to vehicle transmission and the minus sign is for vehicle to Earth Station transmission.

III RATE OF CHANGE OF THE AZIMUTH AND ELEVATION ANGLES OF THE TRANSMITTER

From Appendix C, the azimuth angle of the transmitter, ξ, is given by

$$\xi = \tan^{-1}(d/b) \tag{D-16}$$

therefore,

$$\frac{d\xi}{dt} = \frac{1}{(1-a^2)}\left[b\,\frac{d(d)}{dt} - d\,\frac{d(b)}{dt}\right] \tag{D-17}$$

where

$$a^2 + b^2 + d^2 = 1 \tag{D-18}$$

$$b = \frac{1}{c(\Delta t)}\left\{\vec{R}_{rel}(t)\cdot\begin{bmatrix}\hat{E}\\ \hat{S}_2\end{bmatrix} + \left[\vec{V}_{rel}\right]\left[(\Delta t + \tau)\right]\cdot\begin{bmatrix}\hat{E}\\ \hat{S}_2\end{bmatrix}\right\} \tag{D-19}$$

Quantities Δt and τ are defined in Appendix C. Quantity $\hat{E}$, applies to Earth Station to vehicle transmission, and $\hat{S}_2$ to vehicle to Earth Station transmission.

$$d = \frac{1}{c(\Delta t)}\left\{\vec{R}_{rel}(t)\cdot\begin{bmatrix}\hat{N}\\ \hat{S}_3\end{bmatrix} + \left[\vec{V}_{rel}\right]\left[(\Delta t + \tau)\right]\cdot\begin{bmatrix}\hat{N}\\ \hat{S}_3\end{bmatrix}\right\} \tag{D-20}$$

$$\vec{R}_{rel}(t) = \vec{R}_{rel}(t-\Delta t) + \vec{V}_{rel}(t)\left[\Delta t'\right] \tag{D-21}$$

$\hat{N}$ applies to Earth to vehicle transmission, $\hat{S}_3$ applies to vehicle to Earth transmission.

From Appendix C, the elevation angle, ϕ, of the transmitter is given by

$$\phi = \tan^{-1}\left(\frac{a}{(b^2+d^2)^{1/2}}\right) \tag{D-22}$$

and

$$\frac{d\phi}{dt} = \left\{(b^2+d^2)^{1/2}\,\frac{d(a)}{dt} - \frac{a\left[\frac{d(b)}{dt} + \frac{d(d)}{dt}\right]}{\left[b^2+d^2\right]^{1/2}}\right\} \tag{D-23}$$

where

$$a = \frac{1}{c(\Delta t)} \left\{ \vec{R}_{rel}(t) \cdot \left[\begin{matrix} \hat{V} \\ \text{or} \\ \hat{S}_1 \end{matrix} \right] + \vec{V}_{rel}(t) \left[\Delta t + r \right] \cdot \left[\begin{matrix} \hat{V} \\ \text{or} \\ \hat{S}_1 \end{matrix} \right] \right\} \qquad \text{(D-24)}$$

and $\hat{V}$ applies to Earth to vehicle transmission,

$\hat{S}_1$ applies to vehicle to Earth transmission.

APPENDIX E

BIBLIOGRAPHY FOR APPENDICES

A-1. Clarke, V. C. Jr. et al: Design Parameters for Ballistic Interplanetary Trajectories, Part 1. One-way Transfers to Mars and Venus: Jet Propulsion Laboratory Report No. 32-77.

A-2. Battin, R. et al: A Recoverable Interplanetary Space Probe; MIT Instrumentation Laboratory Report R-235.

A-3. Battin, R.: "The Determination of Round-Trip Planetary Reconnaissance Trajectories"; Journal of the Aerospace Sciences, 26, 9, 545 (1959)

C-1. Joos, G.: Theoretical Physics; G. B. Stechert and Company; New York, 1934, pp 232-4